3-18-1996

Modeling the MTF and noise characteristics of an image chain for a synthetic image generation system

Frank Tantalo

Modeling the MTF and Noise Characteristics of an Image Chain for a Synthetic Image Generation System

by

Frank J. Tantalo

B.S. University of Notre Dame (1988)
M.S. University of Houston / Clear Lake (1992)

A thesis submitted in partial fulfillment of the
requirements for the degree of Master of Science
in the Center for Imaging Science in the College of Science
Rochester Institute of Technology

March 18, 1996

Signature of Author_____
Frank J. Tantalo

Accepted by Dana G. Marsh March 25, 1996
Coordinator, M.S. Degree Program Date

CENTER FOR IMAGING SCIENCE

COLLEGE OF SCIENCE

ROCHESTER INSTITUTE OF TECHNOLOGY

ROCHESTER, NEW YORK

CERTIFICATE OF APPROVAL

M.S.DEGREE THESIS

The M.S. Degree Thesis of Frank J. Tantalo
has been examined and approved by the
thesis committee as satisfactory for the
thesis requirement for the
Master of Science degree

Dr. John Schott, Thesis Advisor

Dr. Roger Easton

Dr Zoran Ninkov

March 25/96

Date

THESIS RELEASE PERMISSION

ROCHESTER INSTITUTE OF TECHNOLOGY

COLLEGE OF SCIENCE

Modeling the MTF and Noise Characteristics of an Image Chain

for a Synthetic Image Generation System

I, Frank J. Tantalo, hereby grant permission to the Wallace Memorial Library of RIT to reproduce my thesis in whole or in part. Any reproduction will not be for commercial use or profit.

Signature _____

Date 21 March 96

Acknowledgments

I would like to acknowledge those who helped me along my journey.

Dr. John Schott for helping me stay on track and providing quality guidance at school and in my career.

Dr. Roger Easton for his help and encouragement throughout my experience in the Imaging Science Program.

Dr. Zoran Ninkov for his useful information about detectors.

Mr. Scott Brown for helping my with my programming and basically teaching me UNIX.

Mr. Steve Schultz for getting me started with AVS and his helpfulness throughout my ordeal.

Mr. Tim Gallagher for his help in setting up and collecting data with the sensor equipment.

Capt. Steve Nessmiller for being a sanity check and encouraging classmate.

Major Harry Gross for his help in explaining the difficult concepts Steve and I couldn't decipher.

The graduate students in the Imaging Science program, helping make exams less painful.

My wife, Becky, for her belief in my ability to succeed and never-ending patience in my endeavor.

Abstract

This is an approach for modeling sensor degradation effects using an image chain applied to a synthetic radiance image. The sensor effects are applied in the frequency domain by cascading modulation transfer functions (MTF) and phase transfer functions (PTF) from the different stages in the acquisition portion of the image chain. The sensor simulation is intended to not only degrade an image to make it look real, but to do so in a manner that conserves the image's radiometry. Some common transfer functions steps include; effects from the atmosphere, optical diffraction, detector size, and scanning motion. The chain is modeled in a modular format that allows for simplified use. AVS was chosen for the operating platform because of its "drag and click" user interface. The sensor model includes the addition of noise from various stages and allows the user to include any noise type. The frequency representations of the images are calculated using the Fast Fourier Transform (FFT) and the optical transfer function (OTF) for the exit pupil function is calculated by an autocorrelation of a digital representation of the exit pupil. Analysis of the simulation image quality is conducted by comparing the empirical MTFs between a truth image and a simulated image. Also, a visual comparison between the image features is made for further validation.

Contents

List of Figures

List of Tables

1 Introduction

One of the tasks in the remote sensing community is to better understand the physical world in order to postulate sufficient explanations for known events. Often this is accomplished through the use of simulations where mathematical models are used to reconstruct the real world element-by-element. One such method is to model the radiometry of a scene given certain characteristics such as material type, time of day, weather conditions, etc. With this information, an accurate representation of the real world can be constructed which is radiometrically correct. This means that radiance values for different objects in the synthetic scene are similar to the radiance values that would be measured in an actual real-world scene. When imaged, these scenes should be degraded by the sensor package which is used to collect and display the image information. In some scene generation models, degradations such as diffraction caused by the sensor optics are not taken into account. The result is an image that is a perfect representation of the real world as if it were sampled with delta functions, i.e. "infinitesimally small pin holes" using a comb function. Because the sensor is composed of a finite number of non ideal delta functions, the finite detector averages the radiance over the scene at finite intervals. Not only is the data averaged over some finite element size, other effects also degrade the synthetic scene. They include optical diffraction, motion blur due to scanning and platform vibration, and blurring from atmospheric turbulence. Noise from various sources, such as the Poisson noise of the incoming photons and noise from the detector and electronics can also be introduced into the model. The intent of these models is to provide the capability to describe current or future sensor systems by utilizing specific system characteristics, i.e. fill factor, rms noise, pixel-to-pixel noise, etc.

This thesis describes two-dimensional electro-optical (EO) / infrared (IR) sensor model created to degrade a synthetically generated radiance image produced using the image generation (DIRSIG) model from RIT's Digital Imaging and Remote Sensing (DIRS) lab's . The sensor model uses linear systems theory to cascade the modulation transfer functions (MTF) and phase transfer functions

(PTF) of an EO/IR sensor system to produce realistically degraded images that preserve scene's radiometric information. The MTF describes the image contrast. Individual component MTFs can be multiplied to get a total system MTF. The phase information, often neglected in sensor models, is very important in reconstructing the original image. The following figure demonstrates the cascading approach used to model the sensor system.

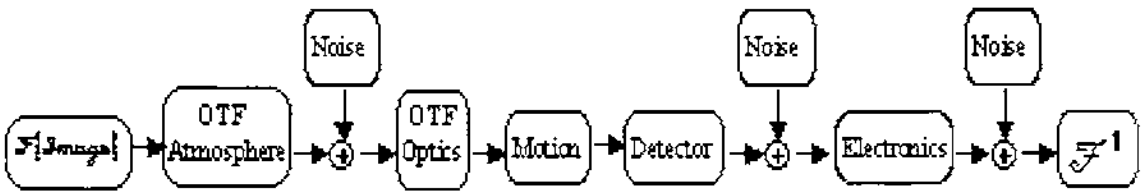

Figure 1.1: Block diagram of cascaded sensor sub-system MTF

This sensor system model derives the optical transfer function (OTF) by autocorrelating the 2-D exit pupil. Up until now, most sensor systems assume a circular exit pupil when constructing the optical diffraction MTF. This new method allows for a greater variety of apertures to be modeled in the system.

Section 2 of the thesis provides background information leading up to the development of this particular design including a literature search.

Section 3 is a work statement defining the thesis tasks.

Section 4 describes the theoretical approach for using linear systems for the various MTFs and how the sensor modules were implemented in AVS

Section 5 contains the results and analysis of the collected image data.

2 Background

The remote sensing community has always had a keen interest in modeling IR/thermal imaging sensor systems. The main interest has been focused on predicting sensor performance characteristics. This ability to predict the operation of a sensor system under various conditions provides a better understanding of the physical principles behind an imaging system. Much of this attention has been focused on predicting the characteristic MTF based on certain sensor sub-systems. Most of these sensor models are one dimensional and thus make several assumptions, e.g., that the optical system is circularly symmetrical with or without a circular obscuration. The reason is that most sensor packages contain circular optics; the analysis was worked out in 1956 (O'Neill). The sensor models investigated, such as the Night Vision Laboratory's (NVL's) FLIR92 system (Scott and D'Agostino, 1992), ATTIRE (Jaggi, 1992), the Ratches NVL model (1976), and Balik and Wan's (1976) simple model for an IR sensor, all include the standard equation or a simplified version, (see Appendix E.) All of these models assume radial symmetry and neglect noise sources in their models. In addition, these models are not intended to act as post-processing imaging tools such as the one I created. Another assumption is that the MTF and phase effects from atmospheric turbulence and aerosol scattering can be neglected.

The DIRSIG sensor model is a two-dimensional post-processing imaging tool used to apply MTFs and PTFs of a sensor to a radiance image. The sensor model does not assume radial symmetry, though it has the ability to use preset algorithms for well defined configurations. In addition, the model incorporates the noise characteristics from the detector and electronics directly into the post-processing calculations. Developed using many principles from the NVL FLIR92 and the Ratches model, the model has many of the same sub-systems effects. These sub-system effects are common to most sensor packages and are well known throughout the IR sensing community. The model transforms and manipulates an image in the Fourier domain using the filter theorem which, linear systems theory, states that the convolution of two functions in the spatial domain can be repre-

sented by the multiplication of their representations in the Fourier domain. Figure 2.1 is an example of a frequency representation of a detector element. Since the blurring effects that are simulated by a

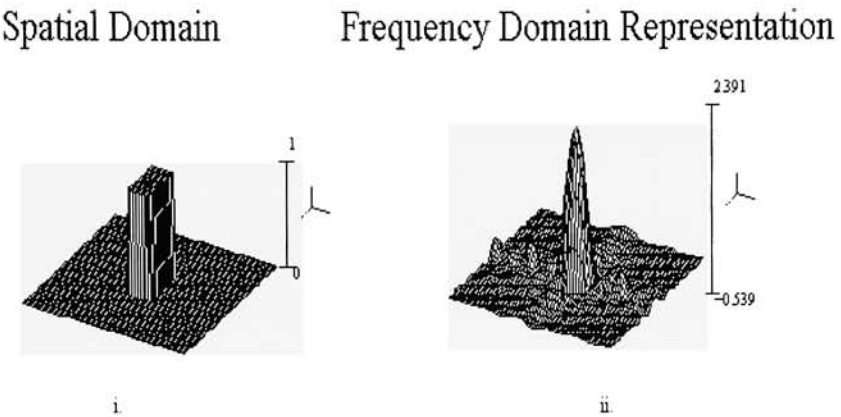

Figure 2.1: A 3-D spatial representation (i) and frequency representation (ii) of a detector element

sensor are a result of averaging in the spatial domain (NVSIM) (Horger, 1993), the individual sensor contributions are multiplied in the Fourier domain. By using multiplication instead of convolution, the image may be post-processed very quickly. Noise is an important quantity in image formation and for this model is modeled as additive in the spatial domain; the linearity of the Fourier Transform ensures the MTF is additive in the frequency domain as well. The noise will be created and applied in the spatial domain. The ability to add periodic noise to the system is an available option. Simple sinusoidal noise models and modified periodic noise can be constructed for use. The user is allowed to choose a stored noise file or input one that was created elsewhere. This model incorporates the MTF from atmospheric effects resulting from turbulence in the atmosphere and turbidity from levels of particulate matter in the atmosphere.

Although linear systems theory is the basis for applying the sensor effects, the modeled image and degradation process are not continuous, but rather are sampled spatially. Therefore, discrete mathematical analysis must be used. The disadvantages of this analysis is that if the Whitaker-

Shannon sampling theorem is not obeyed, i.e. the signals are sampled well within the Nyquist limit to prevent aliasing (Gonzalez and Woods, 1992) reconstruction is impossible. Another disadvantage in discrete systems is that ringing often occurs as a result of undersampling hard edges. A major advantage of a discrete system is that an image in digitized format can be stored and manipulated with a fair amount of ease. The only constraint is that the scaling of sampling intervals be consistent.

A majority of optical systems have circularly aperture functions, and some have circular obscurations. Though algorithms exist to calculate the OTF, they are not useful in the event that the user desires to use a non-symmetric aperture function or one that is not defined by a known set of equations. The autocorrelation function of the sampled aperture model is used to eliminate this problem. This utility separates this model from the others because the optical diffraction MTF is formed via the autocorrelation of the pupil function. In an incoherent system, the optical transform function (OTF) can be calculated through the autocorrelation of the pupil function (figure 2.2). The autocor-

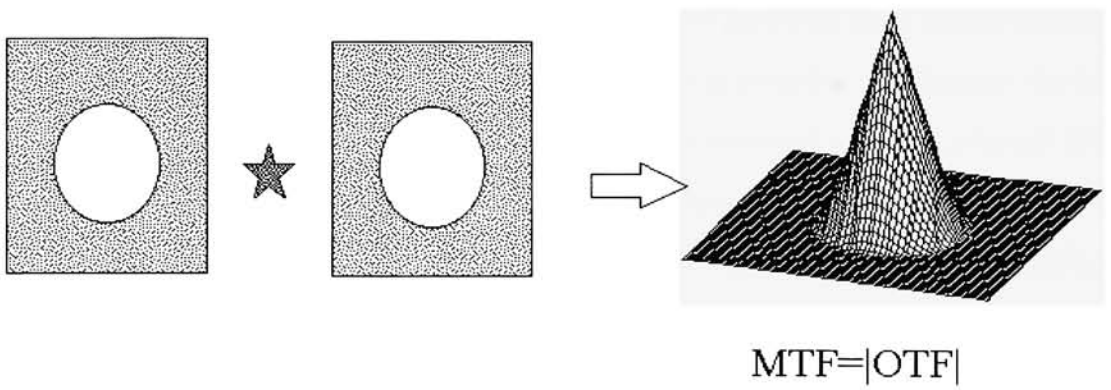

Figure 2.2: Autocorrelation of Pupil Function

relation may be expressed as the convolution of a function and a flipped complex conjugate copy (Gaskill, 1979). The convolution of two functions, $h(x, y)$ and $f(x, y)$, is defined in equation 2.1

$$f(x, y) * h(x, y) = \int f(\alpha, \beta)\, h(x - \alpha, y - \beta)\, d\alpha\, d\beta \tag{2.1}$$

and the normalized autocorrelation of a function f(x,y) is defined in equation 2.2

$$\gamma_F(\xi,\eta) = \frac{f(x,y) * f^*(-x,-y)}{\int \gamma_f(\xi,\eta)\, d\xi\, d\eta} \tag{2.2}$$

where:

$\gamma_f(\xi,\eta)$ is the autocorrelation of $f(x,y)$

$\gamma_F(\xi,\eta)$ is the normalized autocorrelation of $f(x,y)$

$f^*(-x,-y)$ is the flipped complex conjugate of the original function $f(x,y)$

This being the case, linear systems filter theory is used to generate the OTF for the pupil. The MTF and the PTF are then derived from the OTF.

where:

$$MTF(\xi,\eta) = \sqrt{Im\left\{\gamma_F(\xi,\eta)\right\}^2 + Re\left\{\gamma_F(\xi,\eta)\right\}^2} \tag{2.3}$$

$$PTF(\xi,\eta) = tan^{-1}\frac{Im\left\{\gamma_F(\xi,\eta)\right\}^2}{Re\left\{\gamma_F(\xi,\eta)\right\}^2} \tag{2.4}$$

This means that any size or shape of pupil function can be used to calculate an optical MTF.

The model also has the ability to mimic linear scanning or fixed focal plane systems depending on the input parameters selected. The model is assumed to be separable, which means that the x and y components of the effects that degrade the image can be treated separately (Gaskill, 1979). MTF effects are expected to be most prevalent in (but not limited to) the acrosstrack direction. The degradations incorporated in this model are determined by the imaging sensor platform. Line scanners and whiskbroom scanners sample at equal spacings measured in angular units in the crosstrack (scan) direction and sample at equal spatial intervals in the alongtrack (flight path) direction (figure 2.3a) while pushbroom scanners and 2-D framing cameras sample in spatial units as the sensing platform passes overhead (figure 2.3b.) These two different sampling scenarios are treated on a platform-by-platform basis. The user chooses the sensor platform type and configures the model appropriately, the platform specific corrections are then passed to each sub-system. In the case of the line scanner, crosstrack sampling is in angular units while the alongtrack motion of the sensor is in spatial units. The mixed sampling intervals require that, the image be transformed and corrected

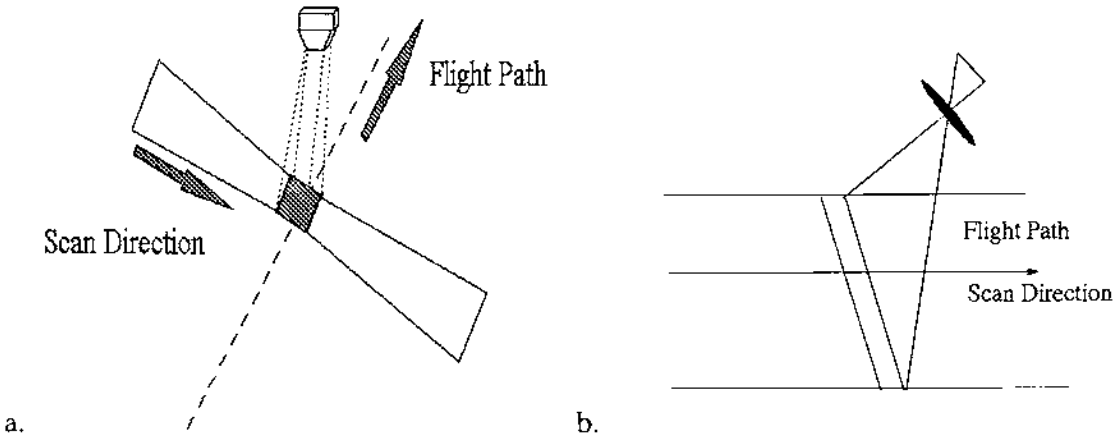

Figure 2.3: a. Line Scanner b. Pushbroom Scanner

on a line-by-line basis. This would provide a very accurate sensor model, but the computing power required is considerable. A trade-off that would save computation time and minimally affect the sensor correction is to apply the correction algorithm over the entire 2-D scene instead of line-by-line. A comparison of the two techniques might prove useful further along in the study or as a study itself. For the time being, the image correction scheme will be utilized over the entire 2-D image to save on computing time. In addition, the model will not incorporate the actual scanning effects due to image overlap or zigzagging lines (Salacain, 1995); these are thought of as sensor geometry problems and are outside the scope of this post-processing package . The model incorporates noise via specific detectivity (D*) values based on the detector material and wavelength. The sensor model incorporates figures of merits that relay to the user how well the sensor is operating. Such figures include signal-to noise ratio (SNR), and noise equivalent temperature difference (NETD).

Linear systems theory was used to construct mathematical representations of the effects found in a sensor's imaging chain. These effects can be "linked" together to form various imaging chains that could represent current or future systems. This sensor model will enhance the capability of the DIRSIG model to accurately produce a more "real" image.

2.1 Literature Review

The literature was searched to identify the existing types of sensor models and to learn how to model various sensor system effects. Many articles pertaining to sensor modeling and design were found in the proceedings of SPIE conferences. Many models discussed in the articles have incorporated simple assumptions into their simulations and evolved over many iterations. This sensor model draws mainly on Ratches' models (1976) and its FLIR92 derivative (Scott, 1992). The Ratches model simulates simple linear scanning systems, while the FLIR92 simulate focal plane array systems. The advantages and disadvantages are discussed in the following section.

2.1.1 Ratches Model

The Ratches model (Ratches, 1976) is an IR sensor system performance and evaluation model. Based on linear filter theory, the model cascades individual sub-system MTFs to calculate a total system MTF. The sub-system MTFs address the scanning component of the degradation and thus are only one dimensional. This paper addresses the general types of MTF effects including equations that model the assumption that the aperture is circular. However, it does not account for other shapes of the exit pupil. The model does not address sampling or aliasing effects. This is very important that the integrity of the radiance field be preserved. This model does not degrade an image; it was designed to evaluate the performance of sensor types and to assess the possibility for detection in a scene, not for implementing the sensor effects. The model also has the capability for calculating SNR and figures of merit such as noise equivalent temperature, minimum resolvable temperature, and minimum detectable temperature.

The Ratches model does not include additive noise. Rather, it calculates detector noise characteristics such as noise equivalent temperature difference. Noise should be included in the model, whether it is Poisson noise from the photons, variability in pixel sensitivities, or gaussian detector noise. This allows for a more realistic representation of a sensor system. The Ratches model does

not address phase effects from possible filter sources such as sensor electronics. This is common among several models and it unjustly neglects the important role that phase manipulation/distortion plays in modeling a system. The Ratches model is however, capable of determining an accurate estimate of the system MTF even without additive noise and phase effects.

2.1.2 FLIR92 Model

The FLIR92 sensor model was developed by the US Army Night Vision and Electronic Sensors Directorate for use as a thermal imaging performance and evaluation tool (Scott, 1992). FLIR92 is capable of modeling parallel scan, serial scan, and staring thermal imaging systems (figure 2.4). It

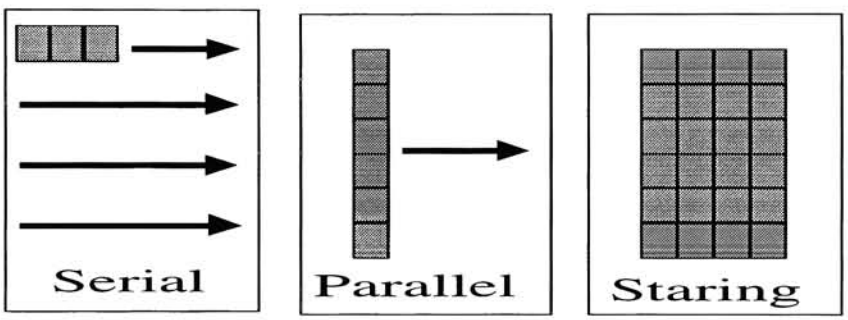

Figure 2.4: Scanning Schemes

was designed to calculate the total system MTF and noise attributes such as minimum detectable temperature difference (MDTD) and noise equivalent temperature difference (NETD), but the sensor degradations cannot be applied to an actual image. This model computes a two-dimensional numerical representation of the total MTF in the form of horizontal and vertical components. Subsystem MTFs, other than the detector, are assumed to be radially symmetric thus making the MTF calculations much simpler and faster. One of the assumptions is that FLIR92 uses a circularly symmetric aperture for the MTF of diffraction-limited optics. Because the FLIR92 has its origins in the Ratches model, the same equation is used for those calculations.

The FLIR92 model does not calculate an atmospheric MTF, nor does it consider any phase ef-

fects. Phase effects should not be overlooked because it is the phase information that contains all the edge information. The FLIR92 model incorporates a special 3-D noise model into its performance evaluation. The noise model seems to quantify different noise effects caused by the MTF filters. It does not address the actual source of noise, whether it be fixed pattern or random. The DIRS model will model these types of noise as well as the other possible sources such as pre-amplifier noise and pixel-to-pixel variations in detector response.

Other advantages that the FLIR92 model does have is the portability to different computing environments, such as a UNIX and PC windows. Overall, FLIR92 is a well organized software package that includes most of the filters necessary in order to evaluate the performance of a sensor.

2.1.3 ATTIRE Sensor Model

The Analytical Tools for Thermal Infrared Engineering (ATTIRE) model was written to be a tool to analyze design trade-offs (Jaggi, 1992). It has the capability to cascade the basic sub-system MTFs to create a total system MTF. The numerical system MTF is converted into figures of merit which are used to predict the performance of the sensor. ATTIRE does not have the capability to process and manipulate images to demonstrate the MTF effects. The ATTIRE tool is not very user friendly and was found to be difficult to operate.

2.1.4 NVSIM Model

NVSIM is a two-dimensional IR sensor model that degrades images in the spatial domain rather than the frequency domain (Horger, 1993). By invoking a series of convolutions with the impulse responses of the system, an input image is degraded to appear as though it suffered from sensor effects. The NVSIM program runs on a UNIX platform but, the image processing is slow. This tool is also available from the Night Vision Laboratory (NVL) and could be a useful tool for evaluating output reported from the FLIR92 model.

3 Statement of Work

A computer model was created to demonstrate the functional capabilities of a sensor system model. The model incorporates the following sensor sub-system effects:

1. Degradations due to atmospheric turbulence
2. Degradations due to turbidity from particles in the atmosphere
3. Optical diffraction effects based on the autocorrelation of the pupil function
4. Sampling and quantization noise
5. Detector noise (pattern and random)
6. Detector fill factor
9. Scanning in the along track and crosstrack directions
10. Jitter
11. Motion due to linear motion of the platform
12. Motion due to vibration of the sensor
13. Electronic pre-filtering and post-filtering
14. CCD charge transfer efficiency
15. Electronics noise

The model is written in C to run in AVS. The program allows sensor effects to be examined more closely. The user will be allowed to specify the resolution of the image by aggregating pixels in an oversampled DIRSIG image. The sampling information is stored in the header file attached to the input image.

The model demonstrates the functional sensor capabilities of the overall system. The input is a DIRSIG radiance image that is transformed into the Fourier domain where the effects of the MTF and phase are applied.

Task 1: Modeling the Inframetrics IR Camera

The MTF from a degraded DIRSIG radiance image of an RIT dormitory will be compared to that from an actual sensor image taken with the Inframetrics IR camera. The model should be valid in the 8 to 12μm region.

Task 2: Modeling the Kodak IR Camera

The MTF from a degraded DIRSIG radiance image of an RIT dormitory is compared to that from an actual sensor image taken with the Kodak IR camera.

Task 3: Combining the Enhanced Sensor Model with the Camera Model

Before and after image synthetic images will be generated showing the improvements of the Salacain Camera model upgrade and this model (Salacain, 1995).

4 Sensor Model Theory & Application

Each component of the sensor model is a spatial averager where the input image radiance field is "smoothed" as it travels through each step in the sensor chain. This model cascades those spatial averaging effects to form a sensor imaging chain. The modulation transfer functions and phase transfer functions MTF and phase of these spatial averagers are applied to the magnitude and phase components of the input image. The model uses the Fast Fourier Transform in converting the input image from the spatial representation and in reconstructing the image from the frequency domain. The following sections contain the sub-system equations that are implemented in Advanced Visual Systems (AVS) model.

A library of sensor sub-system modules were written in 'C' to run in AVS. The AVS environment allows the user to select and manipulate functions through the use of a graphical user interface (GUI). The individual modules are located in scrolling library where they are displayed for use

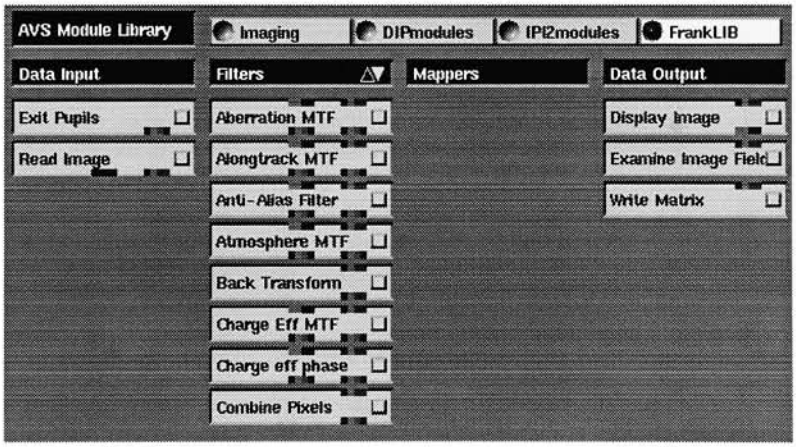

Figure 4.1: AVS Module Library

(figure 4.1). The modular functions are implemented by dragging the function into the workspace from the library using the mouse. The functions are selected based on the sub-system found in each sensor, i.e. a linescanner, pushbroom, or staring array. Sensors of the same type may have simi-

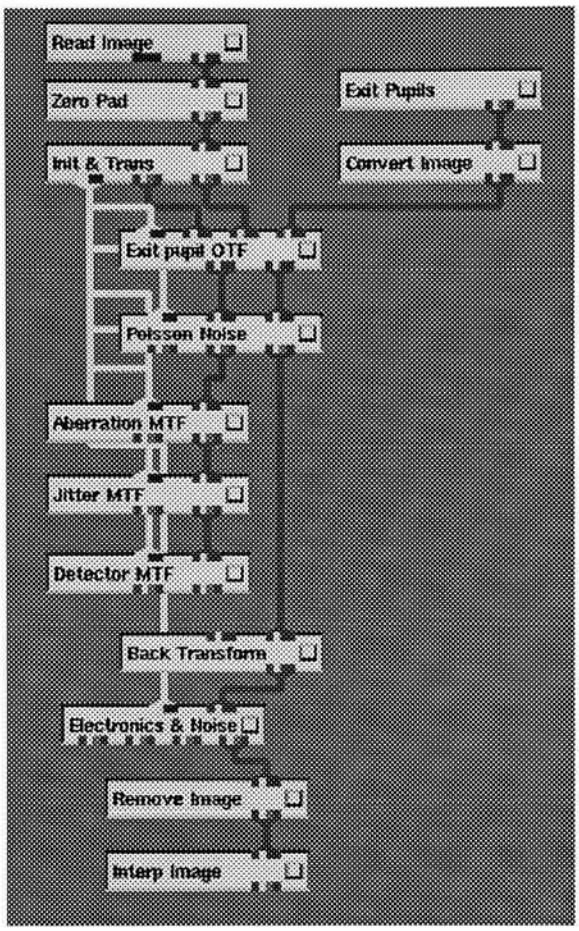

Figure 4.2: AVS Network

lar configurations but will differ from sensors of a different type. This requires various modules to simulate the effects from each sensor type. The modules are connected through input and output ports that require similar data structures (figure 4.2.) Inputs given to the modules consists of push buttons and toggle buttons to choose selections, and type-ins for real and integer values. The AVS environment is an excellent training tool that can be used by the novice or the trained professional.

The following subsections describe the theory involved in each step along the imaging chain and how it was implemented in AVS. An example imaging chain is modeled in the AVS environment for each of the subsections.

4.1 Synthetic Image Transformation

The input image carries a DIRSIG header which contains some scene information, such as sensor focal length, image size, field-of-view (FOV), atmospheric conditions, and radiance tables. As mentioned in section 2 on page 6, each type of sensor platform influences the image sampling mechanism and determines how effects (such as noise) are applied in the chain. The sampling scheme used in this model uses angular sampling intervals measured in milliradians (mrad) to determine the frequency sampling interval in cycle/mrad. The ratio of the scene FOV to the number of pixels determines Δx, the spatial sampling interval.

$$\Delta x = FOV \left(\frac{\pi}{180}\right) \frac{1}{N} \tag{4.1}$$

This sampling assumption is valid for the three acquisition schemes; only the geometry of the scene collection varies for each sensor type (Salacain, 1995). The Nyquist frequency can be derived from this sampling interval and then be used to calculate the frequency sampling interval.

$$\xi_N yq = \frac{1}{2\Delta x} \tag{4.2}$$

$$\Delta\xi = \frac{2\xi_{Nyq}}{N} \tag{4.3}$$

where:

Δx is the sampling interval,

$\Delta\xi$ is the frequency interval,

x_{Nyq} is the Nyquist frequency, and

N is the number of image dimensions in pixels.

The degradations will be applied to the model with respect to an image accounting for either spatial or angular sampling, but not both. The sampling interval Δx and the Nyquist frequency x_{Nyq} are passed to module subroutines as scale factors which allows for direct multiplication of the transfer functions with the specific sensor effect without interpolation (in most cases).

The spectrum of the synthetic image is created using the 2-D Fourier transform

$$\Im\{a(x,y)\} = A(\xi,\eta) \tag{4.4}$$

The Fourier transform produces complex valued output. The modulus $|A(\xi,\eta)|$ and the phase Φ of the transfer function are separated:

$$|A(\xi,\eta)| = \sqrt{Im\left\{A(\xi,\eta)\right\}^2 + Re\left\{A(\xi,\eta)\right\}^2} \tag{4.5}$$

$$\Phi\left[A(\xi,\eta)\right] = tan^{-1}\frac{Im\left\{A(\xi,\eta)\right\}^2}{Re\left\{A(\xi,\eta)\right\}^2} \tag{4.6}$$

so that,

$$A(\xi,\eta) = |A(\xi,\eta)|\, e^{i\Phi[A(\xi,\eta)]} \tag{4.7}$$

The image transformation and dissemination of input parameters to the rest of the chain is carried out by the initialization module called "Init & Trans". The control panel for the initialization module is shown in figure 4.3. This module is used to pass parameters to other sub-systems at once so the user need not update modules for each change. The module has one input port located on top for the input image and three output ports located on the bottom of the module. The real-valued input image is Fourier transformed. The port on the bottom left passes data initialization structure to other modules in the system, and the two ports on the right are for passing the magnitude and phase images respectively.

The major input parameters used by the downstream modules, such as the size of the detector element [μm], the focal length of the system [mm], the altitude or distance from the object [m], the F number, the x-fill and y-fill factors for the detector element, and the velocity of the platform or object [m/s] are provided by the user. The user can select the platform type by depressing the radio button from the choices shown in figure 4.4.

The platform-specific characteristics are edited when a particular platform is selected. In addition to image and data structure as output, the module calculates and displays the horizontal and vertical instantaneous fields of view and calculates and displays the $\Delta\xi$ and $\Delta\eta$ [cycles/mrad].

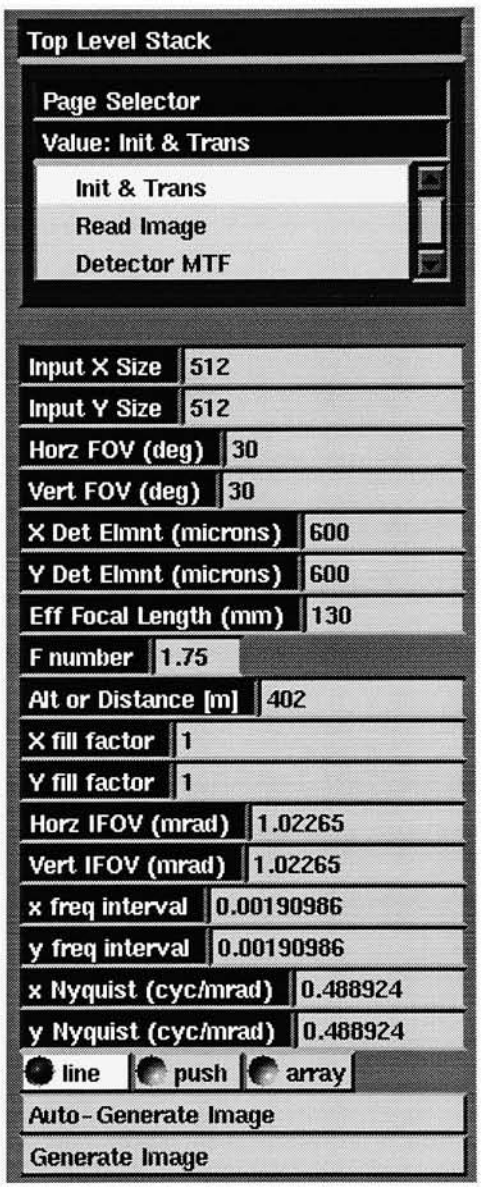

Figure 4.3: Initialization Module Control Panel

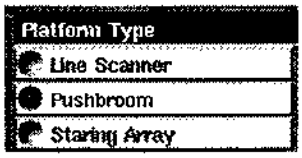

Figure 4.4: Collection Mode Selection

An example of input and output data can be seen in the initialization control module. The input scene field of view is 30 degrees in both the horizontal and vertical directions and instantaneous

Figure 4.5: FOV and Calculated IFOV

field-of-view (IFOV) is calculated by dividing the scene FOV by the number of samples in both directions. The resulting sample spacing directions are shown in figure 4.5.

The spatial resolution is a very important determinant of the quality of the final image. The DIRSIG image can be sampled at any desired interval. The user should be aware that the detector pitch should not be too large otherwise aliasing will result. The DIRSIG model has the inherent capability to oversample because the scene is being generated by a raytrace. This sensor model is capable of handling oversampled input images. The amount of over or undersampling is determined in the main DIRSIG simulation. The sensor model calculates the sampling ratio between the detector IFOV and the DIRSIG spatial sampling interval in the detector module so that aggregation of the pixels can be accomplished to simulate the actual sensor output (figure 4.6.) The user also can aggregate the output pixels in the sensor model to any desired resolution to simulate different aggregation modes. The user is advised to construct images that have sample spacing of $\Delta x = \frac{1}{3}$ or $\frac{1}{4}$ the size of the detector pixel pitch.

The detector section shows an example of the detector MTF being applied to the oversam-

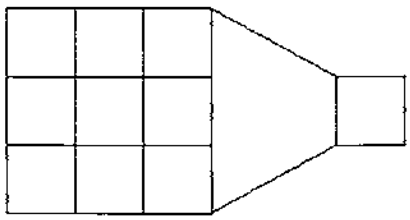

Figure 4.6: Aggregation of 3x3 pixels to single output pixel

pled frequency spectrum. The aggregation mode itself equivalent to selecting every other pixel and line by the amount of the aggregation and convolving with an anti-aliasing kernel. However, an anti-aliasing module was built for those users who wish to incorporate the module in their imaging chain.

4.2 Atmosphere

Image degradation by the atmosphere is divided into two categories: turbulence MTF and turbidity MTF. The turbulence MTF is caused by air flow and different indices of refraction in thermal layers of the atmosphere. The turbidity MTF results from adjaceny effects and concentration levels of pollutants in the atmosphere.This thesis addresses these two categories as well as horizontal and vertical viewing through the atmosphere. The atmospheric effects vary with view angle. The horizontal viewing path assumes a homogeneous medium at ground level. This is useful in a FLIR-type sensor system. The MTF associated with horizontal viewing depends on aerosol scattering and absorption coefficients. (Sadot and Kopeika, 1992b)

Vertical viewing must account for inhomogenous layering of the atmosphere. The concentration profile of particulate matter in the atmospheric layers must be determined from the ground layer on up; this is denoted by C_n^2 which is a function of altitude, temperature and pressure. It is very difficult to accurately model this profile in an MTF. It would be better to incorporate it into a raytracing algorithm utilizing the same principles as LOWTRAN/MODTRAN, treat each layer as a lens, and trace the ray in the same fashion as in geometrical optics. In this thesis, a C_n^2 is not modeled, but the effect is approximated by a Gaussian blur function (figure 4.7a). This defines the point spread function (PSF) of image blur due to the atmosphere. The value used to define the quantity is the full-width of the Gaussian curve at the half maximum (FWHM.)

The Fourier transform of the Gaussian PSF yields the Gaussian MTF of the turbulent atmosphere (figure 4.7b). The relationship is:

$$\Im\left\{e^{-\frac{\pi x^2}{b^2}}\right\} = |b|\, e^{-\pi(\xi b)^2} \tag{4.8}$$

where the width parameter, b, in the frequency domain:

$$b = \frac{1}{\sqrt{2 \cdot \pi} \cdot \sigma} \tag{4.9}$$

In addition to the MTF from the turbulent air cells, turbidity (adjacency effects) are modeled

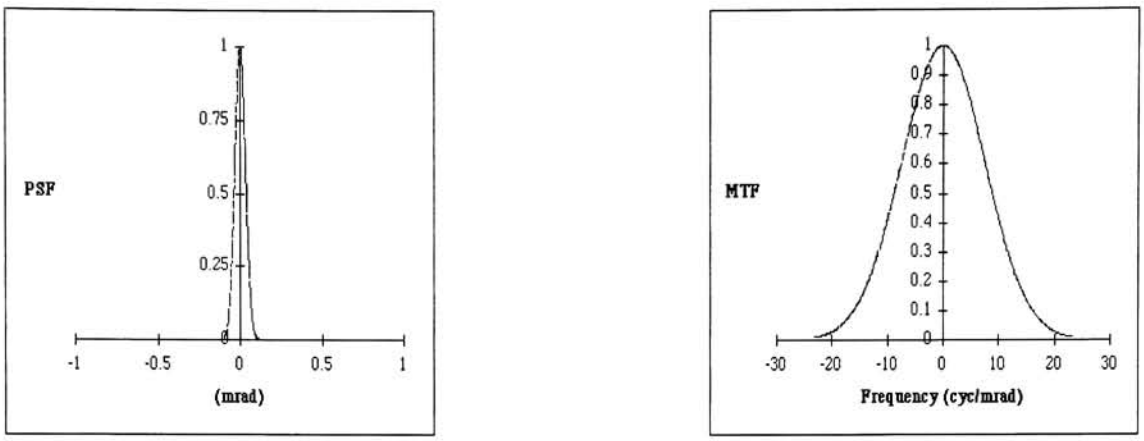

Figure 4.7: a. Gaussian Blur Spot (PSF) b. Atmospheric Turbulence MTF

based on results of Kaufman (1982) and Pearce (1977). The extrapolation of data from mathematical models and atmospheric measurements led to their conclusion that turbidity levels could be modeled as a function of concentration levels.

a.

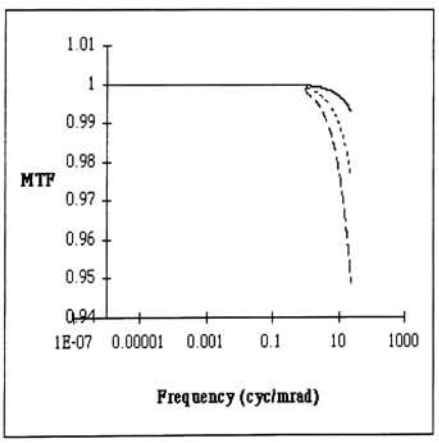

b.

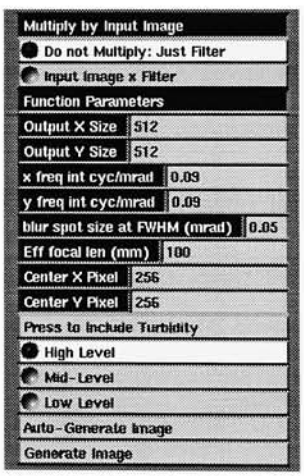

Figure 4.8: a. Turbidity levels b. Atmospheric MTF Control Panel

Three turbidity MTF curves from the study were incorporated in the model, (figure 4.8a). The three curves represent MTFs due to low, moderate and high concentrations of pollutants in the at-

mosphere and can be controlled from the atmospheric MTF control panel (figure 4.8b). The MTFs for these levels of turbidity are combined with the Gaussian MTF due to turbulence to generate an overall atmospheric MTF. At close range on a clear day, the atmospheric MTF is treated as negligible because the PSF of the blur spot is very small. This is because the sensor system is viewing downward and the diffraction is less than that of a system looking up (figure 4.9a). On a clear day, the effect of the atmosphere on the MTF is negligible for close range horizontal viewing.

Figure 4.9: a. PSF looking down vs. PSF looking up b. 2-D Atmospheric MTF output

An example of a 2-D atmospheric MTF is shown in figure 4.9b. The atmospheric module accepts two inputs; a data structure from the initialization module for the calculation of the MTF, and one frequency image that is modulated by the MTF. The frequency image is either passed to the module by a previous MTF module or by the initialization module. This module has two outputs; One is the modified image magnitude and the other is a debug image displaying the actual MTF applied to the input image.

4.3 Optics

4.3.1 Diffraction-Limited System

The optical transfer function for an incoherent system is determined by the shape of the aperture. Most sensor models (e.g. FLIR92 and ATTIRE) assume that the optical system is circular (figure 4.10). The equations used by these models were based upon the relation between the autocorrelation

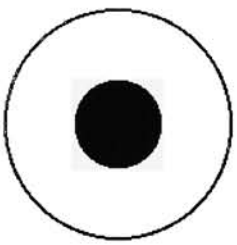

Figure 4.10: Circular obscuration in circular aperture

of the pupil function and the frequency response of the system. These equations are valid for a circular exit pupil with a circular obstruction. These equations can be found in Appendix E. These equations are not valid if the obscuration is not circular or has an additional obscuration (e.g., due to lens mount as in the spiderweb mount shown in figure 4.11.) An asymmetric aperture cannot be modeled in this way.

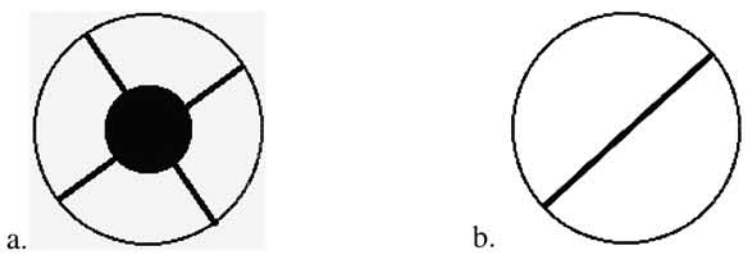

Figure 4.11: a. Aperture obscuration with spiderweb mount b. Shutter Door Obscuration

Phase relationships vary over time for two distinct points in an incoherent illumination system. This means that all wavelengths must be present, i.e. a white spectrum. If the phase difference for points always has the same value then the light is said to be coherent. A properly scaled 2-D autocorrelation of the pupil function can be used to model the optical transfer function (OTF) for an incoherent system. The OTF is the Fourier transform of the point spread function, $h[x, y]$, of an incoherent illumination system (Gaskill, 1979).

$$\mathcal{H}[\xi, \eta] = \Im \{h[x, y]\} \tag{4.10}$$

where:

$h[x, y]$ is the point spread function of the incoherent illumination system,

$\mathcal{H}[\xi, \eta]$ is the optical transfer function (OTF)

The Fourier transform of the point spread function is also equal to the normalized complex autocorrelation of the coherent transfer function $H[\xi, \eta]$ (Gaskill, 1979).

$$\mathcal{H}[\xi, \eta] = \frac{\gamma_H[\xi, \eta]}{\gamma_H[0, 0]} \tag{4.11}$$

where:

$\gamma_H[\xi, \eta]$ is the complex autocorrelation of $H[\xi, \eta]$ and has the form:

$$\gamma_H[\xi, \eta] = H[\xi, \eta] \star H^*[\xi, \eta] \tag{4.12}$$

where:

the '$\star$' is the symbol used to denote the correlation function.

The a pupil function p[x,y] can be used as the coherent transfer function using a change in variables for x and y (Gaskill, 1979).

$$x = -\lambda z\xi \; and \; y = -\lambda z\eta \tag{4.13}$$

$$p[x, y] = p[-\lambda z\xi, -\lambda z\eta] \tag{4.14}$$

where:

λ is the wavelength of the light source,

z is the distance from lens to image plane (effective focal length)

Then the autocorrelation of the pupil function is defined in equation 4.15 and the OTF of the diffraction-limited system in terms of frequency is equation 4.16.

$$\gamma_P = p(-\lambda z\xi, -\lambda z\eta) \star p^*(-\lambda z\xi, -\lambda z\eta) \tag{4.15}$$

$$\mathcal{H}[\xi, \eta] = \frac{\gamma_P[\frac{x}{\lambda z}, \frac{y}{\lambda z}]}{\gamma_P[0, 0]} \tag{4.16}$$

The modulus must be scaled so that the frequency sampling intervals match. The cutoff frequency of the optical MTF can be calculated by using the effective focal length for the distance from the lens to the image plane (equation 4.17).

$$\xi_{cutoff} = \frac{x}{\lambda f_e} \tag{4.17}$$

where:

f_e is the effective focal length of the sensor,

x is the half width of the aperture,

λ is the wavelength of the IR image,

ξ_{cutoff} is the cutoff frequency in cycles/mm,

If the distance to the film plane, z is the effective focal length, then cutoff frequency can be expressed in cycles/mrad.

$$\xi_{cutoff} = \frac{x}{\lambda f_e} f_e \tag{4.18}$$

$$\xi_{cutoff} = \frac{x}{\lambda} \tag{4.19}$$

4.3.2 Generation of Exit Pupil and Calculation of MTF

The module "Exit Pupils" is used to generate four types of circular apertures (figure 4.12).

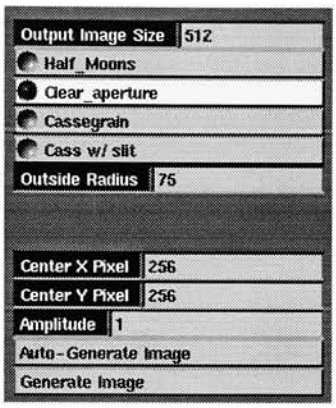

Figure 4.12: Exit Pupil Construction Panel

Each selection allows the user to specify the x and y dimensions of the image as well as the radius or slit width of the aperture. All images of the aperture function are bipolar: $1 \Rightarrow$ transparent and $0 \Rightarrow$ opaque. The following figure shows output below the specified parameters:

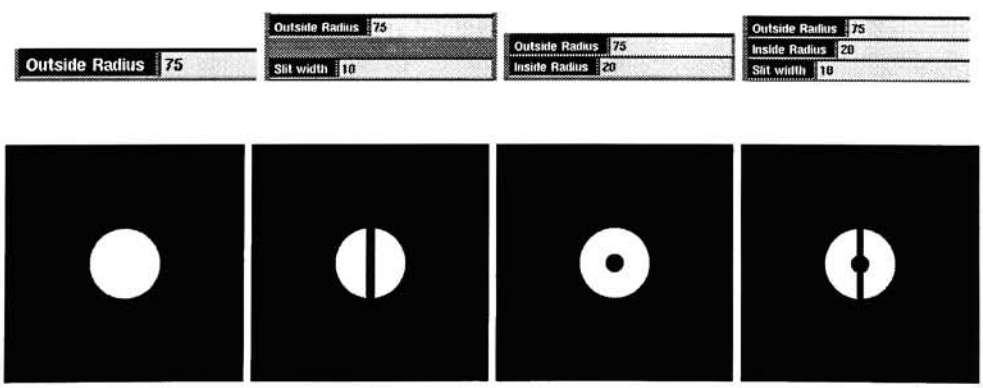

Figure 4.13: Clear, "Half-Moon", Cassegrain, and Hinged apertures

The OTF of the exit pupil is constructed using the "Exit Pupil MTF" module. It has four input portsand two output ports. The module accepts the data array structure from the initialization module, and outputs the input image frequency magnitude, input image frequency phase, and the exit pupil function respectively. The output ports pass along the modulus and phase components of the

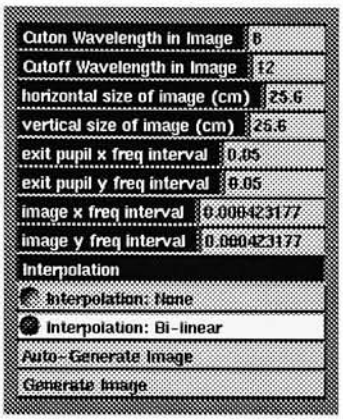

Figure 4.14: Exit Pupil OTF Control Panel

input frequency image after passing through the exit pupil OTF. The control panel shown in figure 4.14 needs the total exit pupil function size in centimeters, (not just the diameter of the exit pupil) and the spectral bandpass limits from the imaging sensor. The user has the option to calculate just the autocorrelation of an aperture or to interpolate and combine the aperture OTF with the input images. The module displays the x and y image frequency intervals (cycles/mrad) passed by the initialization module. The module also calculates and displays the exit pupil $\Delta\xi$ and $\Delta\eta$ intervals in cycles/mrad. The following figures show the 2-D MTF and the 1-D slice through the center of the MTF.

Each of the following exit pupil functions,shown in figures 4.15 through 4.18 are 512x512 with aperture diameters of 150 pixels. The image size of 25.6 cm for both directions is set in the control panel along with the spectral bandpass wavelengths. The module uses an average wavelength value ($10\mu m$ in this case) for determining the cutoff frequencies.

A sample calculation of the cutoff frequency is shown below.

$$\xi_{cutoff} = \frac{12.8cm}{10\mu m} \tag{4.20}$$

$$\xi_{cutoff} = 12\frac{cycles}{mrad} \tag{4.21}$$

The unobstructed aperture is very common in and the MTF looks like a low-pass filter attenuating the higher frequencies of the image.

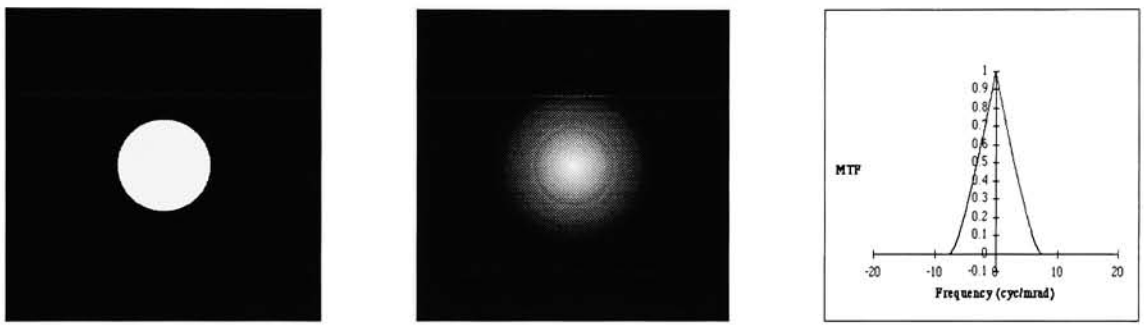

Figure 4.15: Clear Exit Pupil with MTF

The cassegrain aperture is a popular optical design and is found in many telescopes. The corresponding diffraction-limited MTF is also a low-pass filter, but has a sharper attenuation curve for the the low frequency signals than that of the clear aperture MTF.

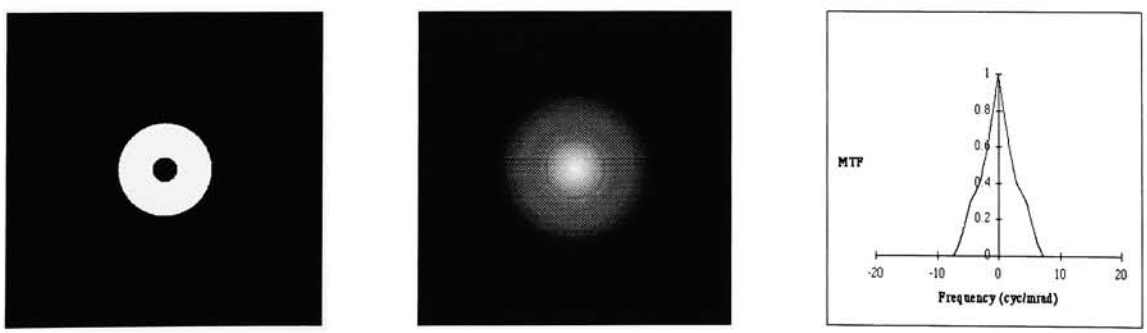

Figure 4.16: Cassegrain Exit Pupil with MTF

The 'Half-Moon' aperture is uncommon and the MTF is asymmetrical with the vertical resembling like that of the clear aperture MTF and the horizontal MTF resembles a 'hipped' appearance. The overall MTF is a low-pass filter with the horizontal MTF attenuating lower frequencies more severly than the vertical MTF.

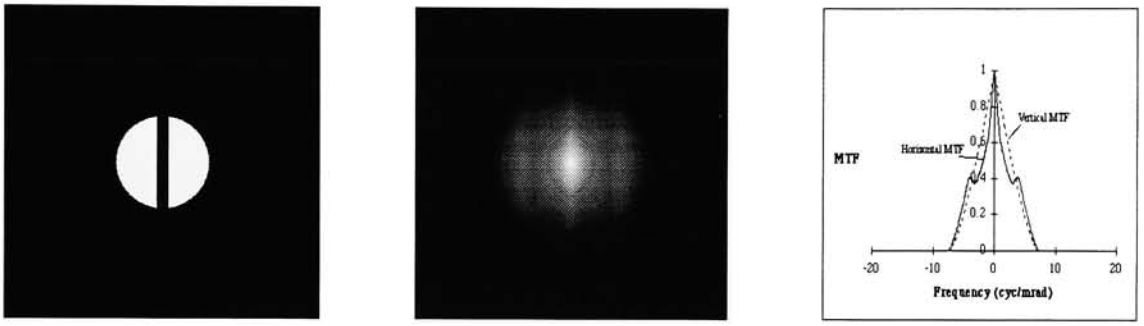

Figure 4.17: "Half-Moon" Exit Pupil with MTF

The cassegrain with the slit aperture is an uncommon design. The resulting MTF attenuates many of the low frequency signals more than the normal cassegrain design and actually has an asymmetrical MTF.

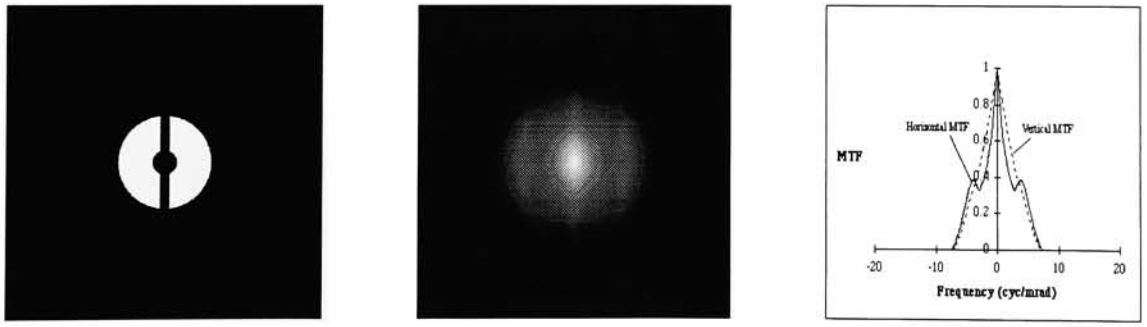

Figure 4.18: Cassegrain with slit Exit Pupil and MTFs

4.3.3 Gaussian Correction MTF

A Gaussian correction factor was added to the simulation to compensate for additional MTFs that were not modeled. The Gaussian MTF model control parameters, σ_x and σ_y allow for an asymmetric MTF corresponding to a asymmetric PSF.

$$MTF_{Guassian}(\xi, \eta) = e^{-2\pi^2(\sigma_x^2\xi^2 + \sigma_y^2\eta^2)} \tag{4.22}$$

where, σ_x and σ_y are standard deviations of the PSF in mrad

The user can multiply the input image by the calculated MTF or just generate an MTF using the PSF type-in selection (figure 4.19).

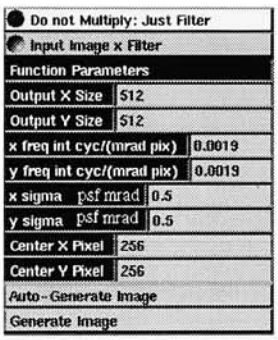

Figure 4.19: Guassian MTF Control Panel

The blur spot size is a type-in and accepts the PSF in mrad for both the horizontal and vertical directions.

a. 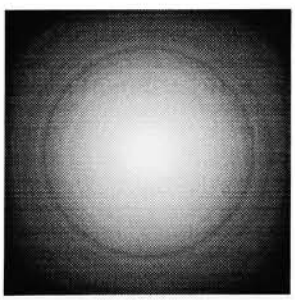

b. 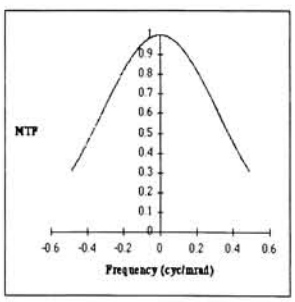

Figure 4.20: a. Example Guassian MTF and b. 1-D MTF Slice

4.3.4 Poisson Noise from Photon Activity

For each unit area in an illuminated source, the arrival rate of photons will fluctuate over time and this can be modeled with a Poisson distribution, where the density distributiion is given in equation 4.23 (Frieden, 1991). The Poisson noise in this model is upon a local brightness and added to the source before the sensor effects degrade the image. The DIRSIG input image is the radiance source and the noise is calculated by using a weighting function to determine a localized average for generating a statisitcal mean.

$$P_n = \frac{e^{-\mu}\mu^n}{n!} \tag{4.23}$$

where:

μ is the mean and variance of the distribution,

n is the number of photon arrivals

For illustration purposes, consider a radiance target that conists of two panels with different levels of illumination and a weighting function is used to calculate a localized brightness while taking into account adjaceny effects from bright sources (figure 4.21a). The user enters the pixel width (standard deviation) for the weighting function in the Poisson control panel (figure 4.21b).

a.

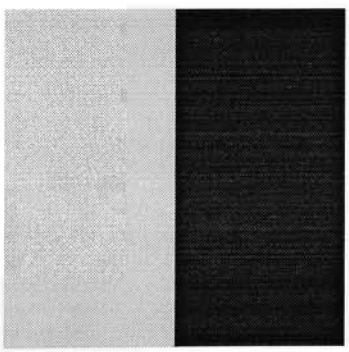

b.

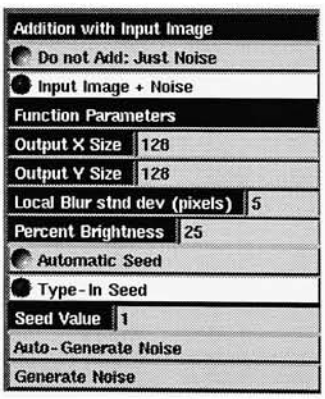

Figure 4.21: Poisson Noise Control Panel

The calculated average brightness for each pixel is modified by a percentage factor which produces a statistical noise mean used by the Numerical Recipe's Poisson noise generator. Each pixel will have a mean, μ, based on its local brightness. The distribution of the noise over the image is not

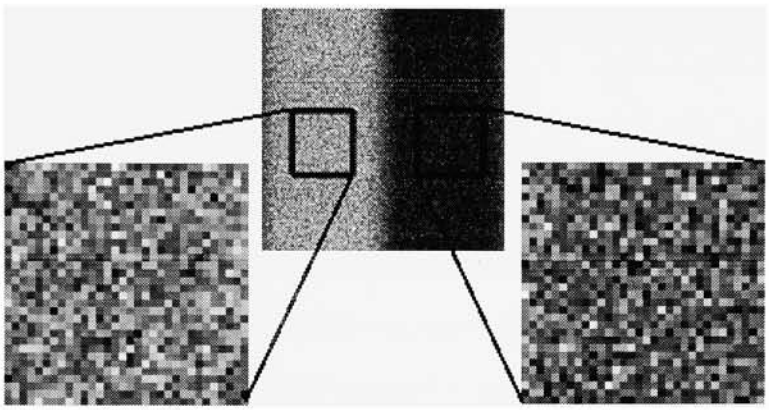

Figure 4.22: Example of Simulated Poisson Noise

Poisson unless the source is unitformly illuminated. For the test targets, the uniform sides will produce a noise image that has a Poisson distrubution for each side (figure 4.22). The histograms from each side of the noise image reflect a Poisson distribution verifying that the noise generator works (figure 4.23a and b). The mean and variance for the left side noise is 49.79 and 49.98 respectively and the right side noise has a mean of 12.54 and a variance of 13.10.

a.

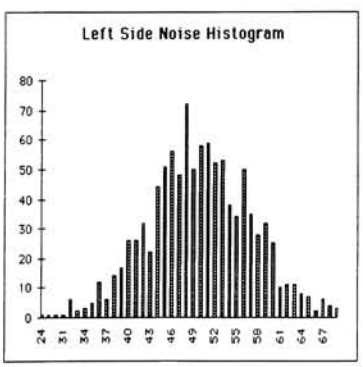

b.

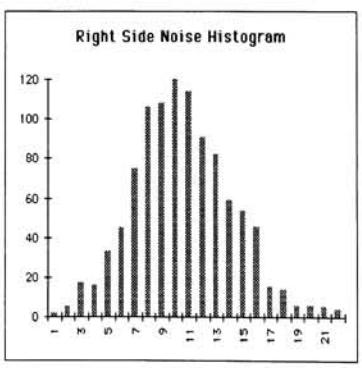

Figure 4.23: a. Leftside Histogram and b. Rightside Histogram

4.4 Motion of Platform

The MTF due to platform motion was adapted from the FLIR92 model. In the DIRS model, the assumption of separability is used to construct equations with the crosstrack and alongtrack motion of the sensor. The individual scanning MTFs and the linear motion MTF are computed below.

4.4.1 Crosstrack Scanning

Line scanners (Section 2) are modeled as separable one-dimensional operations. Scanning occurs only in the crosstrack direction where the MTF due to the scanning mirror is assumed to be negligible. The electronics package associated with the sensor system processes the information faster than the scan mirror rate allowing for "static pictures" of each footprint. Because the readout from each footprint is not dependent on the signal before or after, there is no blurring caused by crosstrack scanning motion. However there is an MTF associated with the electronics that causes a horizontal blur. This MTF is discussed in the "Electronics & Noise" module section.

4.4.2 Alongtrack Scanning

The second form of motion blur is the alongtrack blur. This blur is most common in pushbroom sensors. The blurring has the form of convolving (averaging) with a rect function:

$$h(y) = \frac{1}{l} Rect\left(\frac{y}{l}\right) \tag{4.24}$$

where:

l is the product of the dwell time and sensor velocity.

$$l = dwell\,time \times velocity \tag{4.25}$$

The averaging only occurs in the y-direction because that is the direction of motion. The MTF associated with this averaging can be calculated by Fourier transforming equation 4.24 to obtain:

$$MTF_{alongtrack}(\xi, \eta) = Sinc(t_i v_a \eta) \tag{4.26}$$

where:

v_a is the alongtrack scanning velocity (mrad/sec),

t_i is the scan integration time for one sample (sec), and

η is the angular frequency in cycles/mrad

The AVS imaging chain model implements the motion blur theory by retrieving the necessary information from the initialization module needed to calculate the motion blur MTF. These include the forward velocity of the platform, the integration time, the effective focal length, and the distance to target. The alongtrack blur model has input ports, for the data structure and the modified Fourier magnitude image. The outputs are the sub-system MTF and the processed MTF image. The module provides options for multiplying the input image by the motion MTF and calculating the motion MTF alone (figure 4.24). If the input image is not multiplied by the calculated MTF, the two output image ports pass along the same motion MTF by default. The specified inputs are processed to calculate the scale value for the velocity of the image on the focal plane to get the motion blur width.

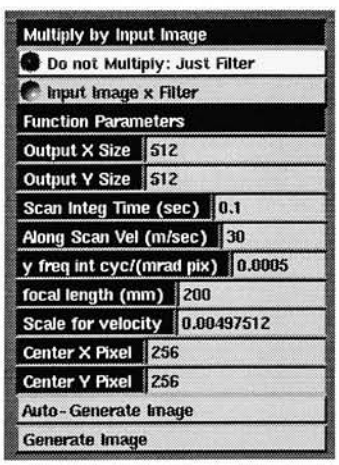

Figure 4.24: Alongtrack Motion Control Panel

The scale factor is:

$$\begin{aligned} scale &= \frac{f_{eff}}{distance} \\ &= \frac{0.200m}{402m} = 0.000497512 \end{aligned} \tag{4.27}$$

where the effective focal length, f_{eff}, is 200mm and the distance to the target is 402 m.

The width parameter of the sinc function is calculated in cycles/mrad as:

$$\begin{aligned} b &= \frac{f_{eff}}{vel\,\tau\,scale\,1000} \\ &= \frac{200}{30 \cdot 0.1 \cdot 0.000497512 \cdot 1000} = 134\frac{cycles}{mrad} \end{aligned} \tag{4.28}$$

where:

b is the width parameter of the sinc in cycles/mrad

vel is the velocity of the platform (m/sec)

τ is the scan integration time (sec)

This example indicates that the loss due to motion blur will probably be very small because the sinc function MTF is very wide. Figures 4.25a and b show the 2-D MTF and the calculated 1-D slice through the center in the vertical direction of the motion MTF.

a.

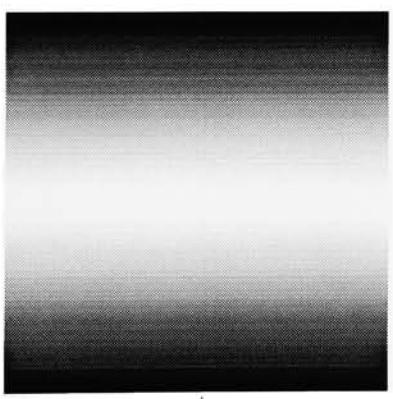

b.

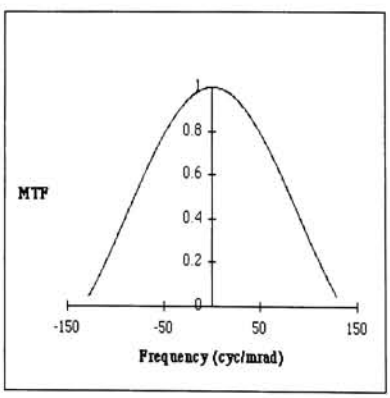

Figure 4.25: a. 2-D MTF output and b. 1-D MTF from Alongtrack Motion example

4.4.3 Relative Linear Motion

Staring arrays often may experience two-directional linear motion when an image passes through the focal plane while the sensor is integrating. However if the object has some velocity, then the relative velocity must be used in the x and y directions. The relative velocity is determined by subtracting the motion of the image from the scanner and is referred to as the "velocity" of the image with respect to the sensing platform.

$$V_{rel} = V_{scanner} - V_{image} \tag{4.29}$$

where:

$V_{scanner}$ is the velocity of the scanner wrt the origin in 2 dimensions,

V_{image} is the velocity of the image wrt the origin in 2 dimensions,

V_{rel} is the relative velocity of the image to the scanner in 2 dimensions

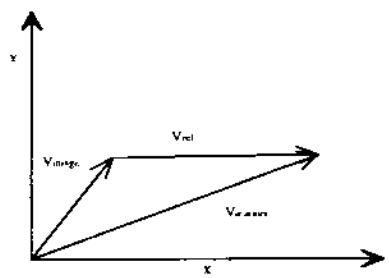

Figure 4.26: Relative velocity diagram

The result is a 2-D uniform averager function much like the alongtrack Rect function (Section 4.4.2):

$$h(x,y) = \frac{1}{u_{rel}} Rect\left(\frac{x}{u_{rel}t_i}\right) \frac{1}{v_{rel}} Rect\left(\frac{y}{v_{rel}t_i}\right) \tag{4.30}$$

where:

u_{rel} is the relative velocity in the x-direction (mrad/sec)

v_{rel} is the relative velocity in the y-direction (mrad/sec)

t_i is the detector integration time (sec)

The Fourier transform of equation 4.30 provides the appropriate MTF for relative motion.

$$MTF_{linearmotion}(\xi,\eta) = Sinc(t_i v_{rel}\xi)Sinc(t_i u_{rel}\eta) \tag{4.31}$$

The AVS imaging chain model implements the motion blur by retrieving the information from the initialization module needed to calculate the motion blur MTF. These include: the velocity of the platform and target, the integration time, the effective focal length, and the distance to target. The alongtrack blur model has two input ports, one for the data structure and one input for the modified magnitude frequency image. The module does not account for the speed of the target image towards or away from the platform (i.e. the z velocity parameter). The output ports are for the subsystem MTF and the processed MTF image. The module provides the options of multiplying the input image by the motion MTF or calculating the motion MTF alone (figure 4.27). If the input image is not multiplied by the calculated MTF, the two outputs pass along the same motion MTF by default. The scale factor for the velocity on the focal plane is calculated in the same fashion as described in the alongtrack motion section. Equations 4.32 thru 4.35 show the equations used in the application of the relative motion blur.

The velocity in the horizontal (x direction):

$$\begin{aligned} x_{velocity} &= platform_{velocity} - image_{velocity} \\ &= 30 - 5 = 25\frac{m}{sec} \end{aligned} \tag{4.32}$$

The velocity in the acrosstrack (y direction):

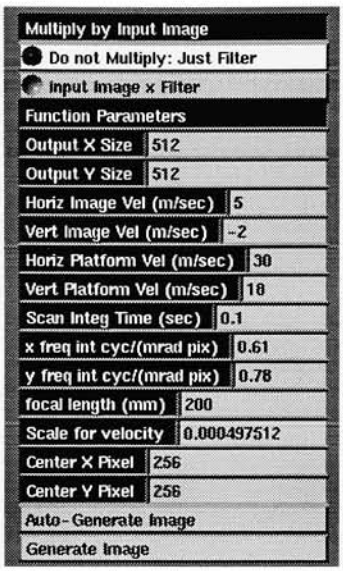

Figure 4.27: Relative Motion Control Panel

$$\begin{aligned} y_{velocity} &= platform_{velocity} - image_{velocity} \\ &= 18 - (-2) = 20\frac{m}{sec} \end{aligned} \tag{4.33}$$

The widths of the sinc functions are calculated in cycles/mrad as:

$$\begin{aligned} b_\xi &= \frac{f_{eff}}{x_{vel}\,\tau\,scale\,1000} \\ &= \frac{200}{25 \cdot 0.1 \cdot 0.000497512 \cdot 1000} = 160\frac{cycles}{mrad} \end{aligned} \tag{4.34}$$

$$\begin{aligned} b_\eta &= \frac{f_{eff}}{x_{vel}\,\tau\,scale\,1000} \\ &= \frac{200}{20 \cdot 0.1 \cdot 0.000497512 \cdot 1000} = 201\frac{cycles}{mrad} \end{aligned} \tag{4.35}$$

where:

b_ξ is the width of the sinc in the ξ direction (cycles/mrad)

b_η is the width of the sinc in the η direction (cycles/mrad)

f_{eff} is the effective focal length (mm)

x_{vel} is the x velocity of the platform (m/sec)

y_{vel} is the y velocity of the platform (m/sec)

τ is the scan integration time (sec)

scale is the calculated scale factor (unitless)

If the user selects the velocity components for the image and platform such that they equate to zero relative velocity, the MTF in that direction is automatically set to 1.0.

a. 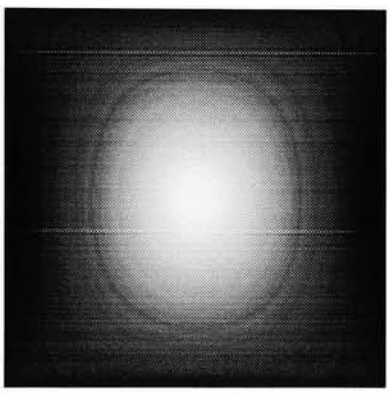

b. 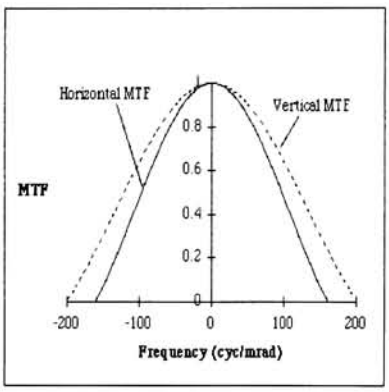

Figure 4.28: a. 2-D MTF output and b. $\xi\&\eta$ 1-D MTFs from the Relative Motion example

4.4.4 Jitter

Line-of-sight (LOS) jitter causes a blurring effect due to all vibration sources related to the sensor. The LOS jitter is modeled to have a Gaussian PSF and it is desirable to limit the LOS $\sigma^2_{LOS} < 20\,\mu rad$ blur spot for aircrafts and space based platforms (Pinsky, 1991). In the DIRSIG model, the user specifies the LOS jitter variance. Typical values range from 20 - 60 μrad. All vibration sources are grouped into one equation:

$$MTF_{jitter}(\xi,\eta) = e^{-2\pi^2\sigma^2_{LOS}(\xi^2+\eta^2)} \tag{4.36}$$

where the σ^2_{LOS} is the variance of the total vibration from all sources. (μrad)

The jitter module has two input: one for the data structure and one for the modified frequency image. The output ports are for the sub-system MTF and the processed MTF image. The user has the choice of multiplying the input image by the jitter MTF or calculate the jitter MTF only (figure 4.29).

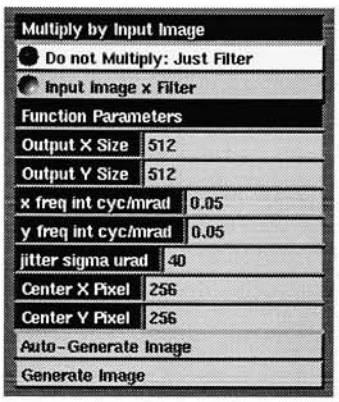

Figure 4.29: Jitter MTF Control Panel

If the input image is not multiplied with the MTF, both ports pass the jitter MTF by default. The user specifies the size of the jitter blur spot in μrad. The example (figure 4.30) uses a blur spot size of 40 μrad which has almost a negligible impact on the image.

a.

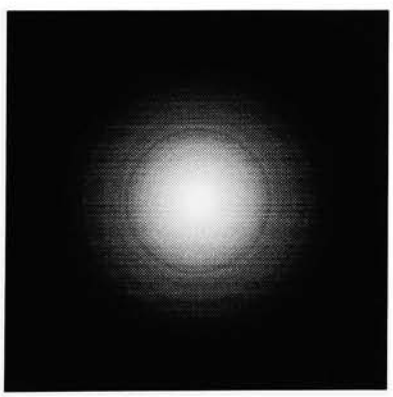

b.

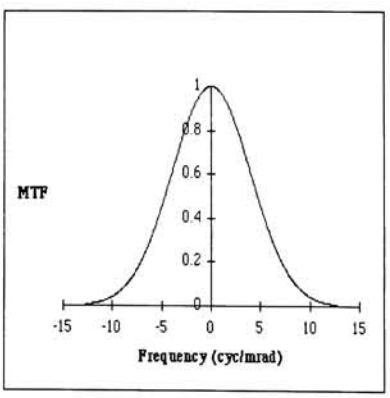

Figure 4.30: a. 2-D MTF output and b. ξ & η 1-D MTFs from the Jitter example

4.5 Detector

When the camera model samples a scene, the detector element in the sensor system averages the input signal over the detector size in both the x and y directions. This is equivalent to convolution of original 2-D image with a 2-D Rect function, followed by sampling at infinite intervals (Dudzik, 1993).

$$f_s(x,y) = \left[f(x,y) ** \left| \frac{1}{bd} \right| Rect\left(\frac{x}{b}, \frac{y}{d} \right) \right] \left| \frac{1}{\Delta x \Delta y} \right| Comb\left(\frac{x}{\Delta x}, \frac{y}{\Delta y} \right) \tag{4.37}$$

where:

b and **d** are the horizontal and vertical widths of the Rect, respectively

Δx and Δy are the x-direction and y-direction sampling intervals, respectively

$f(x,y)$ is the input image,

$f_s(x,y)$ is the sampled image

If the input spectrum is band limited at the Nyquist frequency and if the averaged signal is sampled sufficiently to avoid aliasing, (i.e. $\Delta x \leq \frac{1}{2\xi_{max}}$ and $\Delta y \leq \frac{1}{2\eta_{max}}$), then the Fourier Transform of the sampled signal results in an unaliased spectrum, equation 4.38.

$$F_s[\xi,\eta] = F[\xi,\eta] Sinc[\xi b, \eta d] ** Comb\left(\frac{\xi}{2\xi_{max}}, \frac{\eta}{2\eta_{max}} \right) \tag{4.38}$$

where:

$F_s[\xi,\eta]$ is the sampled signal frequency spectrum,

$F[\xi,\eta]$ is the input signal frequency spectrum,

$S[\xi,\eta]$ is the transfer function of the spatial averager

In the case of DIRSIG, the image is indeed band limited and many of the scenes are oversampled, resulting in equation 4.39.

$$f_d(x,y) = f(x,y) ** \left| \frac{1}{bd} \right| Rect\left(\frac{x}{b}, \frac{y}{d} \right) \tag{4.39}$$

where f_d is the input image with detector effects.

The prcoess can be performed in the frequency domain to avoid tedious convolutions in the

spatial domain:

$$F\{f_d(x,y)\} = \left[F(\xi,\eta)\, F\left\{\left|\frac{1}{bd}\right| Rect\left(\frac{x}{b},\frac{y}{d}\right)\right\}\right] \tag{4.40}$$

When the detector MTF in a sensor system is being modeled, the number and arrangement of individual detectors is not considered. The number and position of detectors is required when the camera model when the original scene is sampled (Salacain, 1995). In the DIRSIG simulation, the scene can be oversampled as described in section 4.1 page 18 and then aggregated of passing through this detector MTF module.

The detector MTF module has two input ports, one for the data structure and one input for the modified frequency image. The output ports are the sub-system MTF and the processed MTF image. The user specifies the size of the detector pitch in microns, the detector element fill factor in the x & y directions, and the effective focal length in millimeters in this module or can set the same parameters in the initialization module. The DIRSIG sensor model calculates the detector instan-

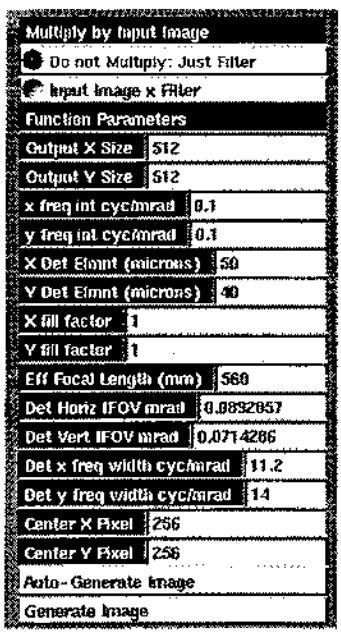

Figure 4.31: Detector MTF Control Panel

taneous field-of-view (IFOV) to describe the vertical and horizontal size of the detector element in angular terms. The IFOV for the detector is calculated by dividing the linear dimensions of the detector element by the effective focal length of the system. The small-angle approximation is used to calculate the IFOV in mrad. Equations 4.41 and 4.42 show sample calculations.

$$\begin{aligned} IFOV_e &= \frac{\delta_v}{f_e} \\ &= \frac{50\,\mu m}{560\,mm} = 0.0893\,mrad \end{aligned} \tag{4.41}$$

$$\begin{aligned} IFOV_a &= \frac{\delta_h}{f_e} \\ &= \frac{40\,\mu m}{560\,mm} = 0.0714\,mrad \end{aligned} \tag{4.42}$$

where:

f_e is the effective focal length

δ_v and δ_h are the detector vertical and horizontal element size respectively(μm)

$IFOV_a$ and $IFOV_e$ are the azimuth and elevation instantaneous field of view respectively (mrad)

The MTF of the detector element is proportional to the Fourier transform of the angular field of view of the detector.

$$s(x,y) = \left|\frac{1}{IFOV_a IFOV_e}\right| Rect\left[\frac{x}{IFOV_a}, \frac{y}{IFOV_e}\right] \tag{4.43}$$

$$MTF(\xi,\eta) = Sinc(IFOV_a\,\xi, IFOV_e\,\eta) \tag{4.44}$$

The width of MTF of the detector is the half-width distance to the first zero in the Sinc function. This is found by computing the reciprocal of the IFOV in both directions:

$$\begin{aligned} Sinc\,width_\xi &= \frac{1}{IFOV_a} \\ &= \frac{1}{0.0893\,mrad} = 11.2\frac{cycles}{mrad} \end{aligned} \tag{4.45}$$

$$\begin{aligned} Sinc\,width_\eta &= \frac{1}{IFOV_e} \\ &= \frac{1}{0.0714\,mrad} = 14.0\frac{cycles}{mrad} \end{aligned} \tag{4.46}$$

(4.47)

An example output of the detector MTF module is shown in Figure 4.32. The 1-D MTF slices are shown in the ξ and η (dotted) directions.

a.

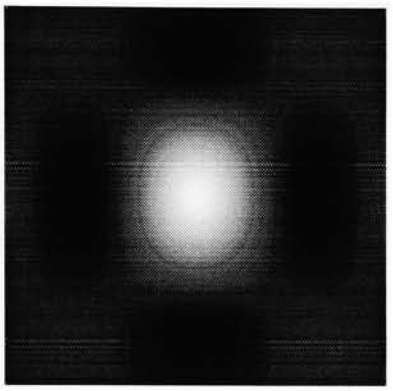

b.

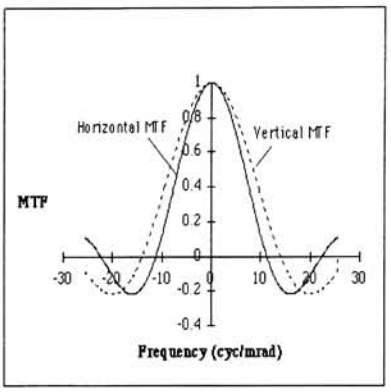

Figure 4.32: a. 2-D MTF and b. Horizontal and Vertical (dotted) 1-D Slices of the MTF

In some detectors, part of the element area is not able to register photo-electrons. This results in the detector having an effective area. The AVS module models this characteristic in the vertical and horizontal detector directions. The Figure 4.33a illustrates the concept.

a.

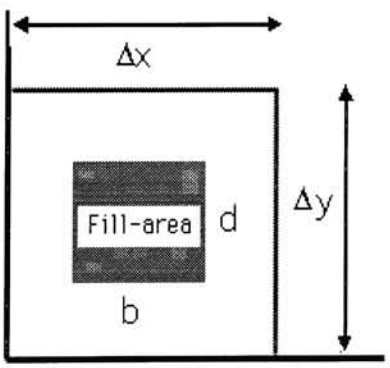

b.

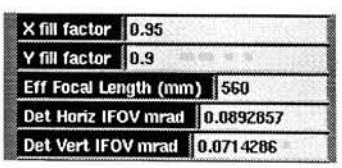

Figure 4.33: a. Detector Fill Factor MTF and b. Detector Dimensions with Fill Factor

The resulting MTF has the following form:

$$MTF(\xi, \eta) = Sinc(IFOV_a \Psi_h \xi, IFOV_e \Psi_v \eta) \tag{4.48}$$

where:

Ψ_h is the average fill factor in the horizontal direction $= \frac{d}{\Delta x}$

Ψ_v is the average fill factor in the vertical direction $= \frac{b}{\Delta x}$

Applying the fill factors, the change in the IFOV in each direction results in the width of the 2-D Sinc function getting wider in both directions:

$$\begin{aligned} Sinc\ width_\xi &= \frac{1}{IFOV_a \cdot \Psi_x} \qquad (4.49) \\ &= \frac{1}{0.0893 \times 0.95} = 11.8 \frac{cycles}{mrad} \\ Sinc\ width_\eta &= \frac{1}{IFOV_e \cdot \Psi_y} \qquad (4.50) \\ &= \frac{1}{0.0714 \times 0.90} = 15.56 \frac{cycles}{mrad} \end{aligned}$$

Example output from the detector MTF module is shown in figure 4.34. 1-D MTF slices are shown in the ξ and η directions. The smaller effective area results in a "better" detector MTF because

a. 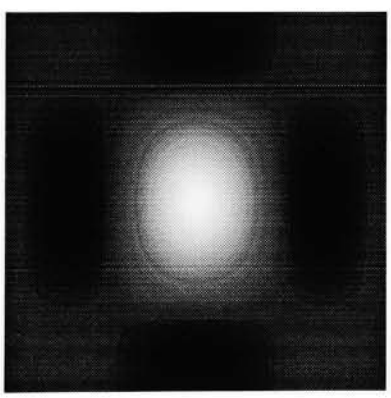

b. 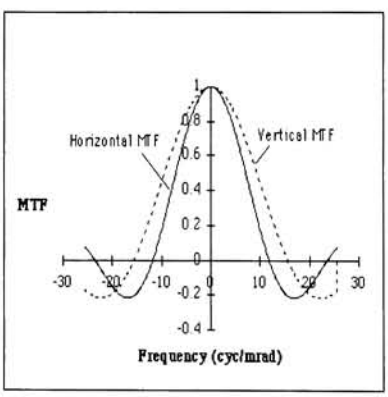

Figure 4.34: a. 2-D MTF and b. Horizontal and Vertical (dotted) 1-D Slices of the MTF

the attenuation is "pushed" towards higher frequencies. However, this gain in MTF performance is traded for a decrease in overall performance because the detector area, and the number of detected photons decrease.

4.6 Detector Noise

The detector noise model is computed as a noise-equivalent radiance and is based on the specific detectivity $D^*(\lambda)$ of the material type. The detector noise is modeled in the AVS module "Electronics and Noise". The detector noise model inputs are the detector material and pasband. Other variables provided by the user include: the detector time constant, transmission of the filter, and the transmission of the optics (figure 4.35). The results of the noise calculations are provided to the user as a detector NETD.

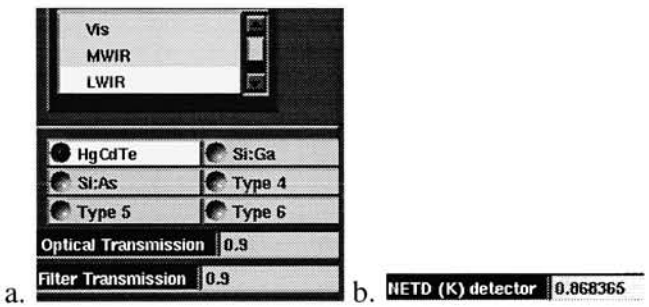

Figure 4.35: a. Detector Input Parameters and b. Example Output Noise expressed as NETD

The AVS model allows for selection of different material types based on the cuton and cutoff wavelengths. If the material type is not defined, the user may include a parameter D^* that is used to calculate the noise (figure 4.36). The noise in the AVS model is expressed in noise-equivalent radi-

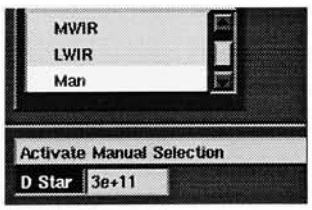

Figure 4.36: Manual D^* Entry

ance (NER equation 4.51). The NER is a function of the noise-equivalent power, effective detector

area, and the optical throughput.

$$NER = \frac{NEP}{A_{eff}} G\# \tag{4.51}$$

where:

NEP is the noise equivalent power (W/sr),

A_{eff} is the effective detector area, and

$G\#$ is the optical throughput

As the fill factor decreases (Section 4.5) the NER increases and has having a considerable effect on the overall detector performance (Section 4.10). The NEP is a function of the material D^*, detector area, and the bandwidth:

$$NEP = \frac{\sqrt{A_{eff}}\sqrt{\Delta f}}{D^*} \tag{4.52}$$

where:

A_{eff} is the detector area,

D^* is the integrated specific detectivity

The detector bandwidth, Δf, used in equation 4.52 is equal to $\frac{1}{2t_d}$, where t_d is the detector time constant.

Since $D^*(\lambda)$ is a function of wavelength and DIRSIG generates a scene within a wavelength region, the integrated D^* value is used in the above equation 4.52; where:

$$D^* = \frac{\int_{\lambda_1}^{\lambda_2} D^*(\lambda) M(\lambda, T)\, d\lambda}{\int_{\lambda_1}^{\lambda_2} M(\lambda, T)\, d\lambda} \tag{4.53}$$

$D^*(\lambda)$ is the wavelength dependent specific detectivity,

$M(\lambda, T)$ is the spectral exitance of a blackbody at a given temperature,

λ_1 and λ_2 are the cuton and cutoff wavelengths for the DIRSIG scene, respectively

The optical throughput is:

$$G\# = \frac{1 + 4F\#^2}{\tau_f \tau_o \pi} \tag{4.54}$$

where:

$F\#$ is the F-number of the system.

τ_f is the transmission of the filter, and

τ_o is the transmission of the optics

For the input parameters provided in figure 4.35, $G\#$ is computed to be:

$$G\# = \frac{1 + 4 \cdot 1.75^2}{0.9 \cdot 0.9 \cdot \pi} = 5.20692$$

Sample output from the AVS module is provided:

Figure 4.37: Example $G\#$ output

The calculated NER is used as the standard deviation for the noise image. The result is an uncorrelated pixel-to-pixel Gaussian white-noise distribution over the image.

4.7 Quantization Noise - Theory & Practice

Quantization is the process of assigning a discrete value for each continuous input amplitude. The number of available levels is 2^m, for m bits per pixel. The quantization adds noise to the signal which depends on the number of bits per pixel and dynamic range. The theoretical output quantization noise varies with the image input noise variance (Kennedy, 1990):

$$\sigma_{out}^2 = \sigma_{in}^2 \left[1 + \frac{q^2}{12\sigma_{in}^2} \right] = \sigma_{in}^2 + \frac{q^2}{12} \tag{4.55}$$

where:

q is the number of bits per pixel,

σ_{in}^2 is the noise input variance,

σ_{out}^2 is the noise output variance

An RMS quantization error is calculated:

$$\epsilon_{rms} = \sqrt{\sum (actual - quantized)^2} \tag{4.56}$$

The ϵ_{rms} describes the mean value of the quantized noise, while the second term in equation 4.55 is the variance contribution to the noise in the image. The user selects the quantization level using a radio button in "Electronics & Noise" module (figure 4.38). The quantization error (equation 4.56) is an output to the user.

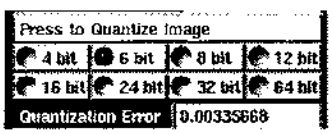

Figure 4.38: Image Quantization Selector

4.8 Charge Transfer Efficiency MTF & PTF

For a CCD to ouput its values, it must measure the number absorbed of photons at each detector element "well". This is done by "reading" the electron count "across" a horizontal path, then "down" a vertical path. As the electrons in each well are transferred from cell to cell, some either are lost or not transferred. This would result in electron loss and image degradation if the array transfer efficiency is poor. Because the transfer process is horizontal, its horizontal MTF and PTF components would dominate the filter. The MTF and PTF due to the CCD charge transfer efficiency in the horizontal is are described below (LeBlanc and Contini, 1990):

$$MTF_{cte}(\xi,\eta) = e^{(-N(1-\varepsilon))\left[1-\cos\left(\frac{2\pi\xi}{\xi_{Nyq}}\right)\right]} \tag{4.57}$$

$$PTF_{cte}(\xi,\eta) = -N(1-\varepsilon)\left[\frac{2\pi\xi}{\xi_{Nyq}} - \sin\left(\frac{2\pi\xi}{\xi_{Nyq}}\right)\right] \tag{4.58}$$

where:

ε is the charge transfer efficiency per pixel,

N is the number of charge transfers,

ξ_{Nyq} is the Nyquist frequency

The same module is applied in the staring array case because the array reads out the charge from each detector across the image. The flow of charge down the columnt is not modeled

a.

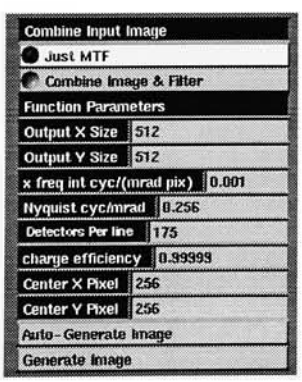

b.

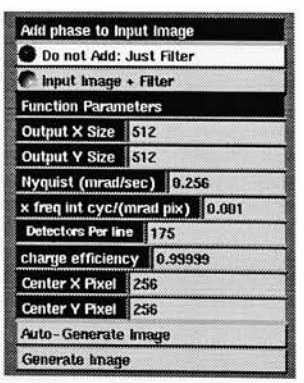

Figure 4.39: CTE a. MTF and b. PTF control panels

The CTE equations are implemented in the "Charge Eff MTF" and "Charge Eff PTF" modules and were designed for the pushbroom and staring array camera. This imaging chain package has two input ports: for the data structure and for the modified frequency image. The output ports are for the sub-system MTF and the processed image. In the MTF module, the user has the choice of multiplying the Fourier magnitude image by the CTE MTF or just calculate the CTE MTF (figure 4.39a). For the PTF module the user has the choice of adding the Fourier phase image by the CTE PTF or just calculate the CTE PTF (figure 4.39b). The user specifies the number of elements in the array by filling in the location "Detectors per line" with the number of samples in the array and by also defining the charge transfer efficiency per pixel. Sample 2-D MTF and PTF outputs from these modules are shown in figure 4.40a-d:

a.

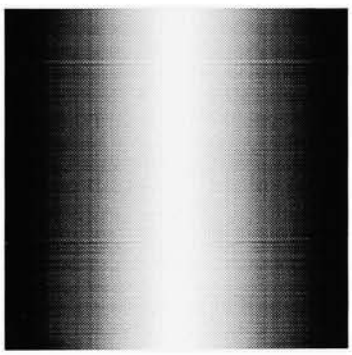

b.

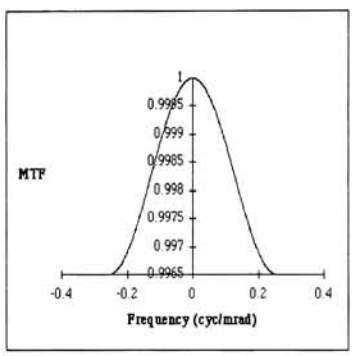

c.

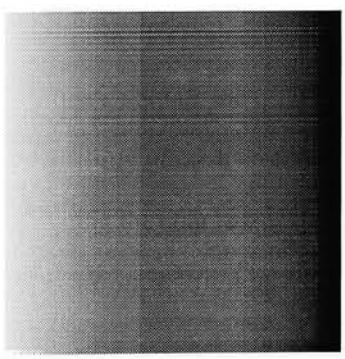

d.

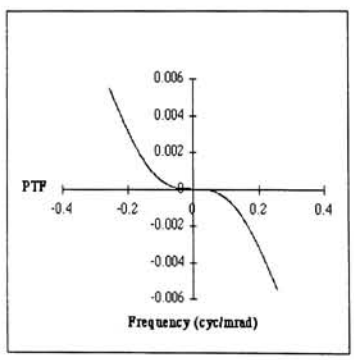

Figure 4.40: a. 2-D CTE MTF b. 1-D Slice through the center of the MTF c. 2-D CTE PTF d. 1-D Slice through the center of the PTF

4.9 Electronics

In image chain analysis, dealing with the application of sub-system MTFs, the noise due to the electronics ismost often neglected. However, the effect of the electronics package is very important. It can boost or block certain frequency components. If the signal-to-noise ratio (SNR) is too low, a pre-amplifier can boost the signal (and also input some noise) to within acceptable SNR levels. The package is responsible for converting the radiance values to voltage. These effects are crucial to accurately modeling the imaging system.

The electronics package in the AVS modules is called "Electronics & Noise" and houses all the electronic and noise-related effects that an input image encounters in the imaging chain. The input image is reconstructed prior to this stage and pixel aggregation is performed before the image is further processed. The image then is zero-padded to a size that is a multiple of 2^n to allow processing by the FFT. An electronics lowpass filter is applied in the Fourier domain. The input image is processed for detector noise, pre-amplifier low-pass MTF, and electronic noise in the system. The detector noise was discussed in Section 4.6.

4.9.1 Detector Noise Variability

For the linescanner mode the detector noise is applied as a the Gaussian noise distribution. If a pushbroom or framing camera platform is used, the noise from the individual detectors will differ even if made from the same material. The sensor model will vary the Gaussian noise statistics for each detector in the direction of collection. This allows for detector variability but keeps the noise statistics constant for each column of the image. The noise of the framing array detector noise is handled in the same fashion, but the noise statistics are recomputed for every element in the array. The noise is added over the entire image, even the zero-padded part. This is acceptable because the array size for the desired pushbroom or framing camera should be the size of the aggregated image.

a. 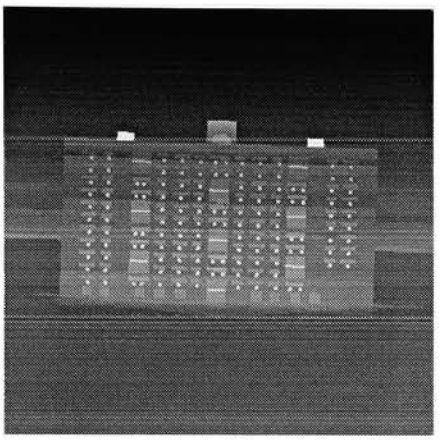 b. 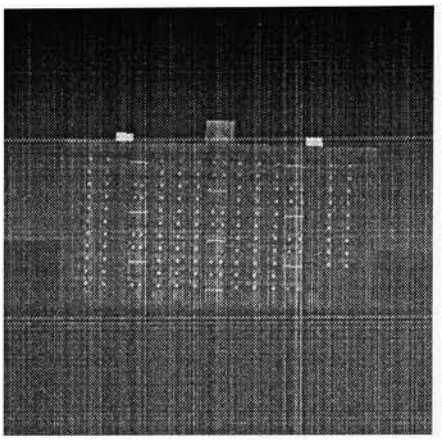

Figure 4.41: a. Normal Image b. Banding in an Pushbroom Sensor

In addition to noise among detectors, the conversion from radiance to voltages will exhibit a mean gain and mean bias for each detector. This results in banding in the collection direction, (figure 4.41). The model computes image gain and bias terms by multiplying the mean value of the image by a percent gain and adding a percentage bias to the result. The gain and bias base values are modified for each detector in the pushbroom array resulting in constant statistics for each element in the collection direction. The gain and bias conversions are applied to the input image as shown in equation 4.59. The gain and bias are input parameters are found on the control panel (figure 4.42).

$$Output = Input \cdot (gain \cdot Image_{mean}) + (bias \cdot Image_{mean}) \tag{4.59}$$

where:

Output is the output radiance value

Input is the input radiance value

gain is conversion gain error

bias is the conversion bias error

$Image_{mean}$ is the image mean value

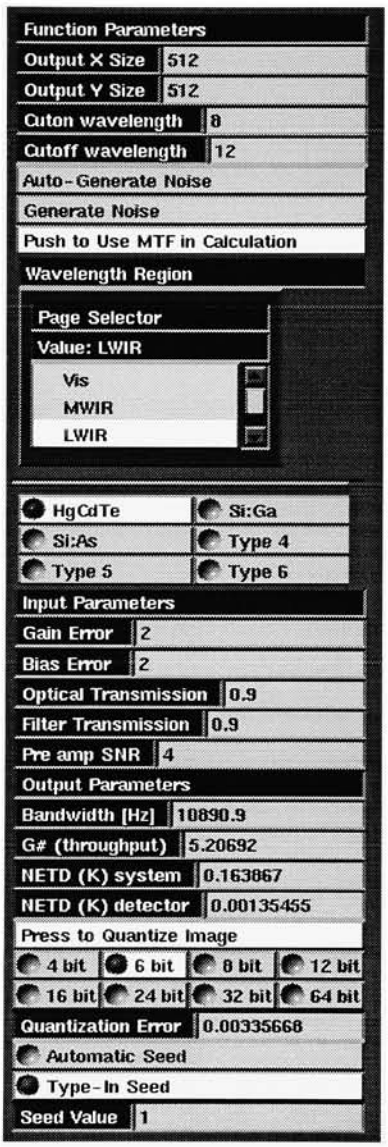

Figure 4.42: Electronics Control Panel

4.9.2 Pre-amplifier

Various types of amplifying filters can be used to enhance the SNR. The DIRSIG sensor model uses a lowpass filter based on the $3dB$ point $\frac{1}{2\pi\tau}$,using the detector time constant τ, and the mirror scan rate.

$$MTF(\xi,\eta) = \frac{1}{\sqrt{1+\frac{\xi vel}{f_{3dB}}}} \tag{4.60}$$

where:

ξ is the horizontal frequency (cycles/mrad),

vel is the scan velocity (mrad/sec)

The sensor model applies the lowpass amplifier MTF to the image after the detector noise is applied and before the amplifier noise is added. The detector noise is part of the input signal sent to the amplifier and is smoothed along with the rest of the input image.

4.9.3 Electronic Amplifier Noise

The DIRSIG sensor model electronics package allows the user to apply a pre-amplifier MTF after adding the detector noise to the signal. Once the electronics MTF is applied, the amplifier noise is introduced as an SNR. The noise is distributed over the image based on the quality of the electronics which is characterized by the SNR. This allows for a robust description of the noise that is added to the system. The noise representation will be displayed to the user in a format that can easily be understood. For this reason, the noise equivalent temperature difference (NETD) was chosen to display the amount of noise added to the image, (Section 4.10). The system noise and the detector noise are displayed, allowing for the user to view how much noise is introduced by the electronics package (figure 4.43).

The AVS module allows the user to specify an SNR from the amplifier that closely approximates the estimated noise contribution. The amplifier noise expressed in NETD is combined with the detector noise. The SNR for the DIRSIG sensor system is an input variable. This allows the

Figure 4.43: NETD for the System and Detector

user to modify a specific design or make adaptations to correctly model an existing system. Do not confuse the SNR with an MTF modification of the original system. Most of the SNR comes from the pre-amplifier, and if a poor pre- amp is used, most likely a poor quality image will be the result. A quick estimation of the SNR ratio for the pre-amp or the manufacturers own specifications can be used.

This model used the relationship:

$$\text{Mean pixel Noise} = \frac{\text{Mean Radiance of Input Image}}{\text{SNR}} \tag{4.61}$$

This noise is applied to simulate the electronics noise. The SNR parameter is easily adjusted for matching amplifier performance. The expression used to compute the system noise:

$$NETD_{sys} = \sqrt{(NETD_{amp}^2 + NETD_{det}^2)} \tag{4.62}$$

where:

$NETD_{sys}$ is the system noise,

$NETD_{amp}^2$ is the amplifier contribution to the noise, and

$NETD_{det}^2$ is the detector contribution to the noise

4.10 Noise Equivalent Temperature Difference in AVS

This figure calculates the temperature variance over the entire image in terms of temperature noise. It relates the detector and system NETD contributions to the image as a result of the pixel-to-pixel detector noise and the uniformly distributed amplifier noise.

The NETD is calculated by dividing the mean value of the output image by the change in radi-

ance with respect to temperature for the given spectrum.

$$\text{NETD} = \frac{\text{Mean NER}}{\Delta L/\Delta T} \tag{4.63}$$

where ΔL is:

$$\Delta L = L(T_2) - L(T_1) \tag{4.64}$$

The radiance:

$$L(T) = \int_{\lambda_1}^{\lambda_2} \frac{M(\lambda, T)}{\pi}\, d\lambda \tag{4.65}$$

The irradiance is determined from the Planck Law:

$$M(\lambda, T) = \frac{c_1}{\lambda^5 \left(e^{\frac{c_2}{\lambda T}} - 1\right)} \tag{4.66}$$

where:

$c_1 = 3.7405 \times 10^8$ W m^3

$c_2 = 1.43879 \times 10^4$ mK

Proper use of the "Electronics & Noise" module will help create a more realistic image that has the correct noise characteristics. The figures of merit deals with NETD because it is a common term used to quantify the content of an image with respect to a sensing system. The following section attempts to capture the imaging chain for to different sensors. One sensor produces very poor images in the long- wave infrared and the second produces high quality images in the mid-wave infrared region. Each detector has a NETD that will relate the synthetic image to the sensor it is modeling.

5 Results and Analysis

A library of image chain functions which were created using 'C' code in the AVS environment. These modules were used to model an imaging chain in two tasks. Task 1 involved degrading a DIRSIG radiance image to match an image taken through the Inframetrics scanner. Task 2 produced a degraded image to match that taken by the Kodak KIR_310 infrared camera. The results of these tasks are provided below.

5.1 Task 1 - Simulation of Inframetrics Sensor System

The Inframetrics sensor system was simulated by cascading an image through the AVS sensor simulation module system (figure 5.1). An oversampling ratio of 3:1 was used in the creation of the synthetic DIRSIG

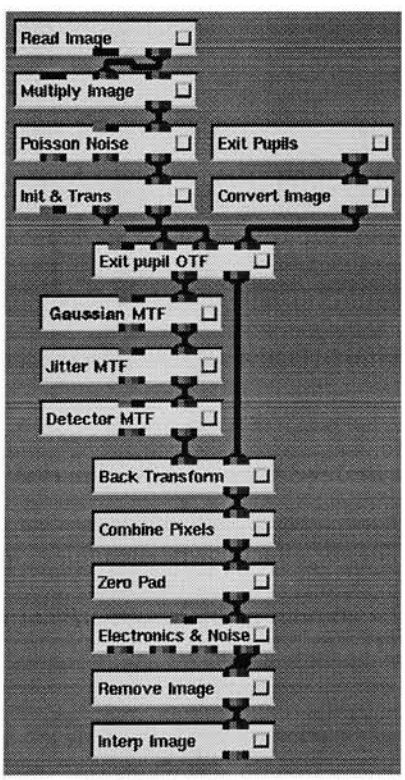

Figure 5.1: AVS network used to model the Inframetrics

512x512 image. The image was transformed into magnitude and phase images using the Fast Fourier Transform (FFT) algorithm. The image was sent through the sensor sub- system algorithm using the input settings found in Table 5.1. A bilinear interpolation of the output image was performed to get a 512x480 image which simulates Imaging Technology framegrabber board used to record the images .

Table 5.1: Input Settings for the Inframetrics Sensor System Simulation

Parameter Input	**Value**
Wavelength Region	8 - 12 μm
Focal Length	130 mm
Target Distance	402 m
Optical Aberration	0.5 mrad
Detector Element Size	600 μm
Jitter Blur Spot Size	10 mrad
Aperture Diameter	26.4 mm
D* From Curve in Appendix D	
Detector Material	HgCd
Scan Mirror Rate	16 Hz
Radiance to Voltage Gain Error	2 %
Radiance to Voltage Bias Error	2 %
Transmission of optics	0.9
Transmission of filter	0.9
X Fill Factor	95%
Y Fill Factor	95%
Amplifier SNR	4

The DIRSIG input and output images are shown in figure 5.2. The edges of the builiding in

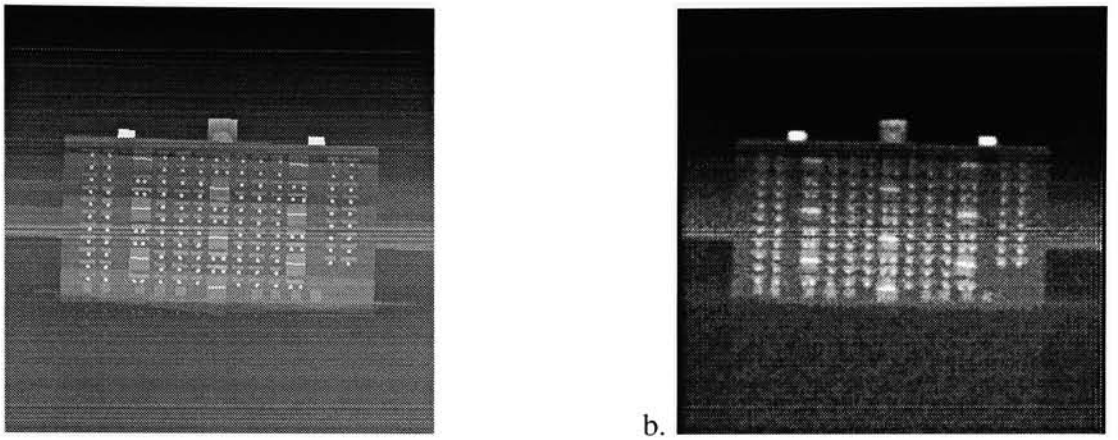

Figure 5.2: a. DIRSIG input image and b. Final Processed Image

the ouput image have been smoothed and noise has been introduced to simulate the Inframetrics. The image quality has definitely been degraded as predicted in the theory. Figure 5.3 displays the final output DIRSIG image and the actual Inframetrics image taken on May 1, 1995. The simulated image shown in figure 5.3a looks remarkably similar to the truth image 5.3b.

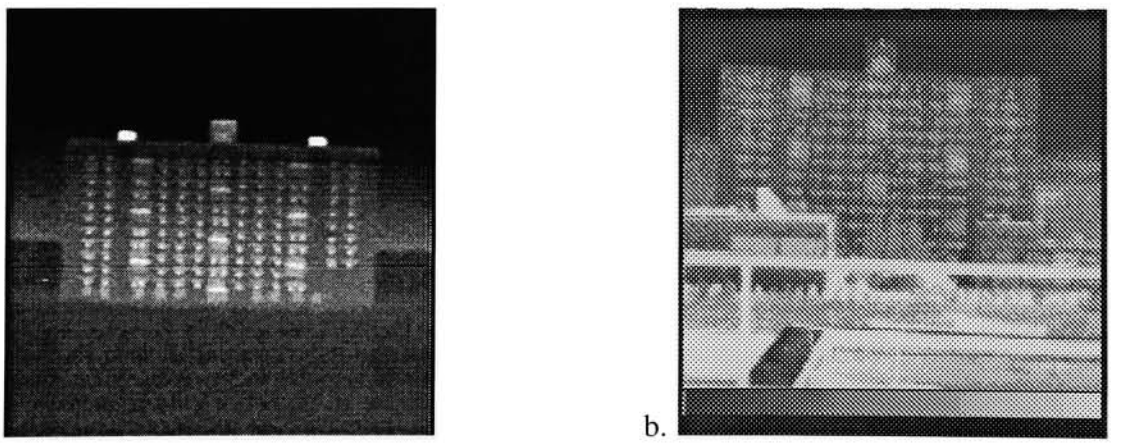

Figure 5.3: a. Final Processed Image and b. Truth Image

5.1.1 Poisson Distributed Photon Noise

The Poisson noise was added to the input signal before the sensor effects were applied. A 5 pixel standard deviation was use in the weighting function to calculate the local brighntess of which 1% was used in the Poisson noise generator (figure 5.4).

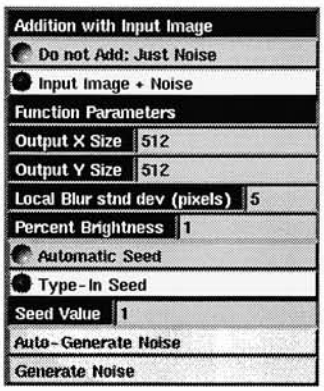

Figure 5.4: Poisson Noise Control Panel

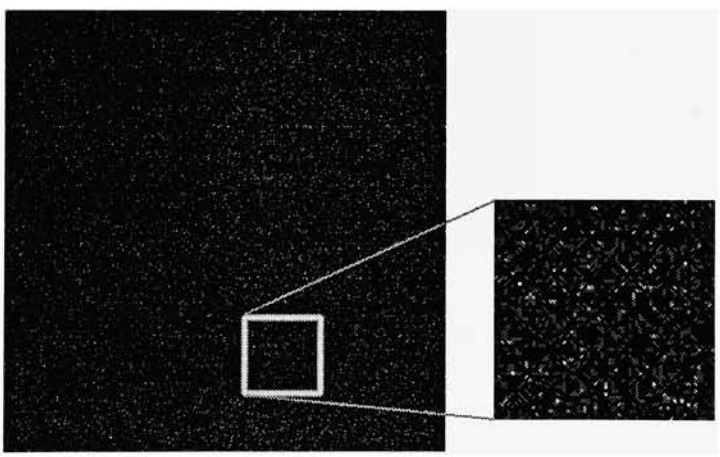

Figure 5.5: DIRSIG Poisson Noise in Simulated System

The noise image has a $\mu = 0.297 \frac{W}{m^2 sr}$ and a $\sigma = 0.544 \frac{W}{m^2 sr}$. These statistics do not describe a Poisson distribution because the noise at each pixel was calculated using a different statistics based on the local brightness of the input image.

5.1.2 Inframetrics Initialization

The simulation of the Inframetrics scanner used the input parameters shown in Table 5.1 in the "Init & Trans" module (figure 5.6).

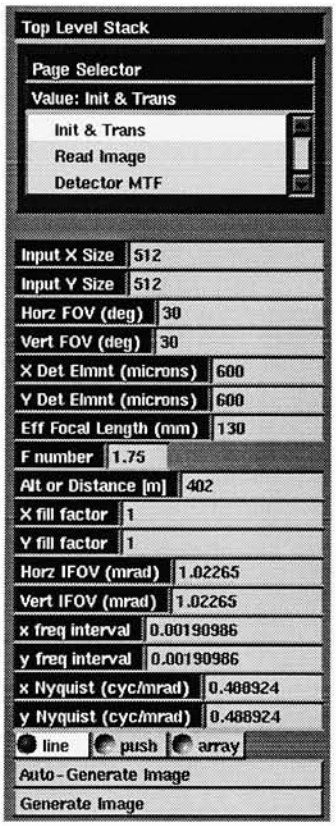

Figure 5.6: Initialization Parameters for the Inframetrics Simulation

The initialization parameters were sent automatically to each module upon the completion of this module. The input image was split into magnitude and a phase images (figure 5.7). These images were sent along the two paths in the imaging chain model.

a. 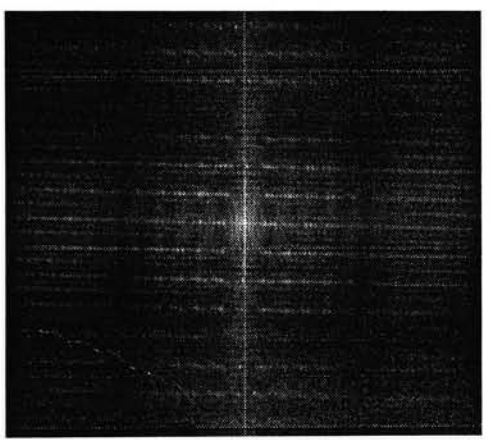 b. 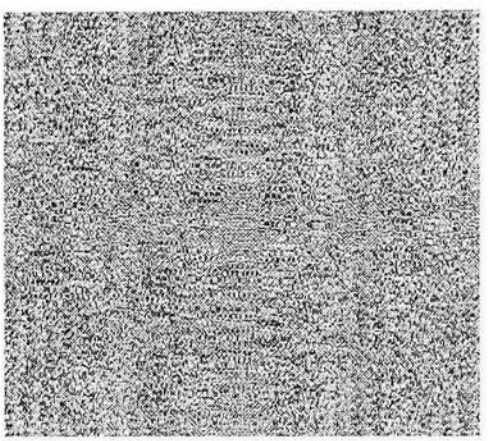

Figure 5.7: a. Magnitude Image and b. Phase Image

5.1.3 Exit Pupil MTF

A circular pupil with a diameter of 150 pixels in a 512x512 image was used in the simulation,(figure 5.8b). The exit pupil was applied in the "Exit Pupil MTF" module (figure 5.9a)

a.

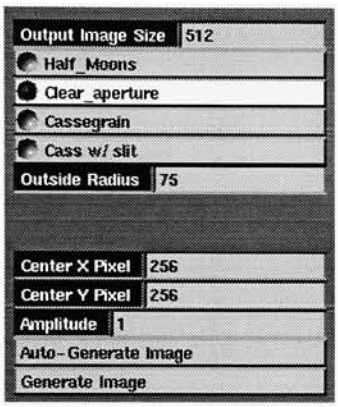

b.

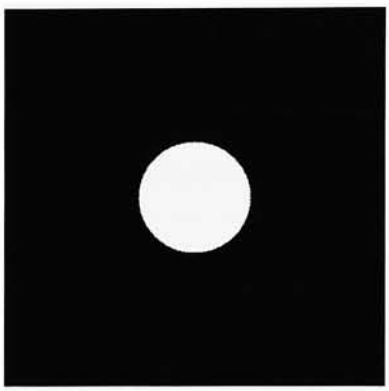

Figure 5.8: a. Exit Pupil Control panel and b. Clear Exit Pupil

a.

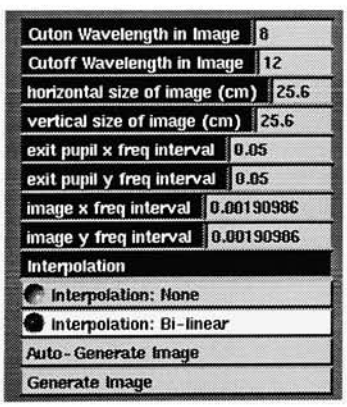

b.

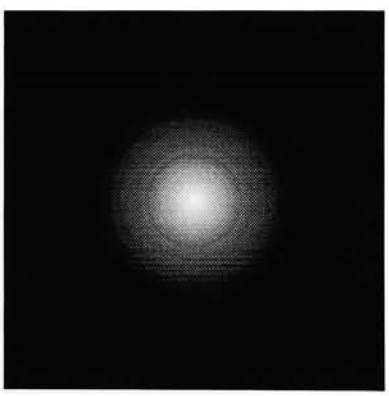

Figure 5.9: a. Autocorrelation Control Panel and b. Exit Pupil MTF

where the autocorrelation generated the MTF shown in figure 5.9b.

The autocorrelation must be scaled to the correct frequency range. Figure 5.10a is the 1-D representation of the OTF. The image must be interpolated before multiplication because only the most center portion of the image is used to modulate the input frequency image (figure 5.10b).

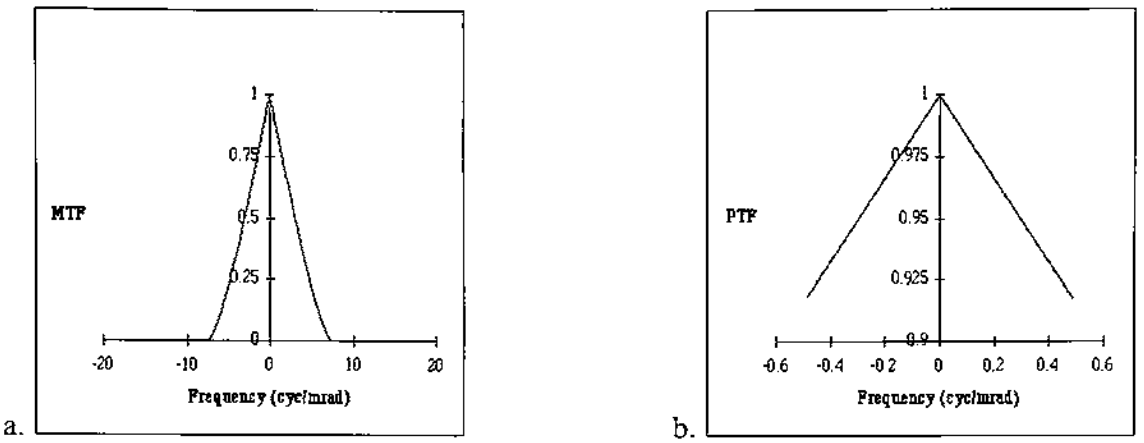

Figure 5.10: a. 1-D Exit Pupil MTF b. Interpolated 1-D Simulated Exit Pupil MTF

The interpolated MTF (figure 5.10b) suggests that the degradations due to the exit pupil are minimal as the minimum MTF value is roughly 0.918. This indicates that loss in amplitude in the chain is $\approx 8\%$ at the Nyquist frequency.

5.1.4 Gaussian Correction MTF

The Gaussian correction module followed the optics module. This module modeled the 2- D Gaussian MTF that was calculated from a 0.5 mrad PSF (figure 5.11).

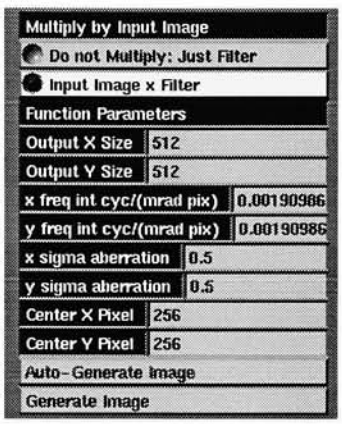

Figure 5.11: Aberration Control Panel Settings for the Inframetrics

The calculated MTF is shown in figure 5.12a. A center slice from the 2-D MTF shows only about a 70% loss in modulation at the Nyquist frequency (figure 5.12b).

a.

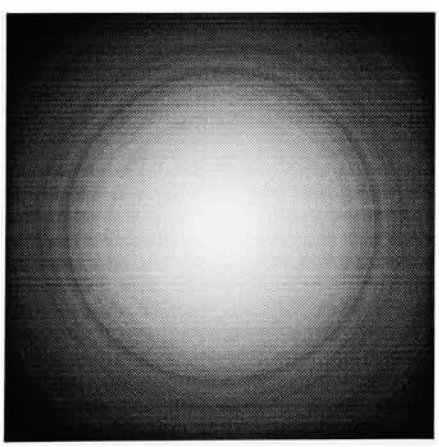

b.

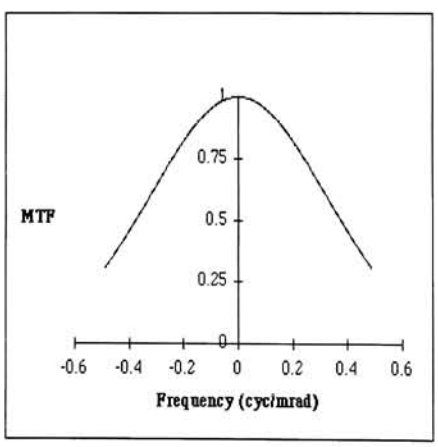

Figure 5.12: a. 2-D Gaussian MTF and b. Center Slice of the MTF

5.1.5 Jitter MTF

The motion jitter module followed the Gaussian MTF module. The PSF parameter was set to 20.0 μrad, figure 5.13 because the camera was stationary and the only vibration was from the spinning mirror.

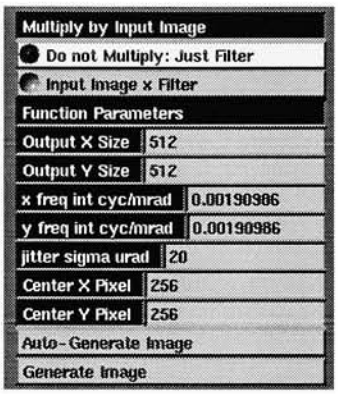

Figure 5.13: Motion Jitter Control Panel Settings for the Inframetrics

The calculated 2-D MTF due to Jitter is shown in figure 5.14a and 1-D representation is shown in figure 5.14b. The modulation from the jitter MTF is nearly unity at the Nyquist frequency and could probably be treated as negligible.

a.

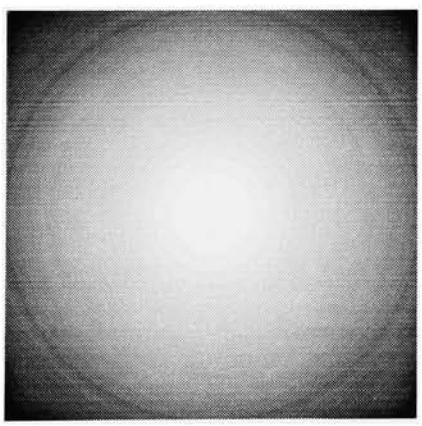

b.

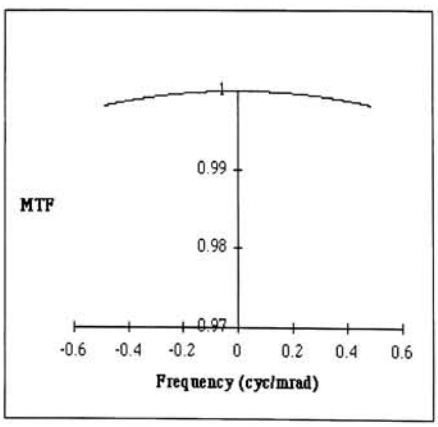

Figure 5.14: a. 2-D and b. 1-D Slice Representation for the Jitter MTF of the Simulated Inframetrics System

5.1.6 Detector Size MTF

The detector element was modeled to be a square of side 0.6mm and the effective focal length used was 130 mm. The IFOV of the detector was calculated to be 4.3846 mrad (figure 5.15).The fill factors were set to 95% in both the horizontal and vertical pitch directions. The calculated detector 2-D MTF is shown in figure 5.16a. The center slice of the MTF is shown in figure 5.16b.

Do not Multiply: Just Filter	
Input Image x Filter	
Function Parameters	
Output X Size	512
Output Y Size	512
x freq int cyc/mrad	0.00190986
y freq int cyc/mrad	0.00190986
X Det Elmnt (microns)	600
Y Det Elmnt (microns)	600
X fill factor	0.95
Y fill factor	0.95
Eff Focal Length (mm)	130
Det Horiz IFOV mrad	4.38462
Det Vert IFOV mrad	4.38462
Det x freq width cyc/mrad	0.22807
Det y freq width cyc/mrad	0.22807
Center X Pixel	256
Center Y Pixel	256
Auto-Generate Image	
Generate Image	

Figure 5.15: Detector Control Panel Settings for the Inframetrics

a.

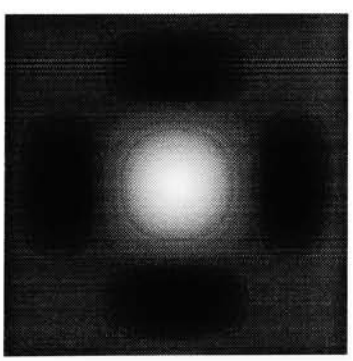

b.

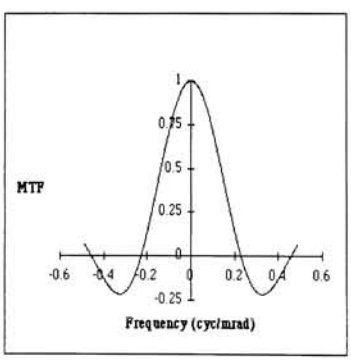

Figure 5.16: a. 2-D and b. 1-D Slice Representation for the Detector MTF of the Simulated Inframetrics System

5.1.7 Aggregation Mode

The image is reconstructed using the modified magnitude and phase values of the input image and then aggregated in a 3x3 pixel mode (figure 5.17).

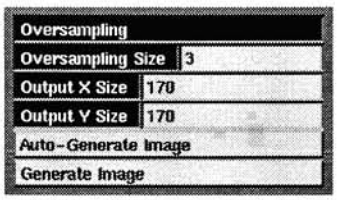

Figure 5.17: 3x3 Aggregation Mode

The images before and after aggregation are shown in figure 5.18. The image was reduced in size from 512x512 to 170x170, which was as close as possible to the actual sensor output size of 175x135 .

a. 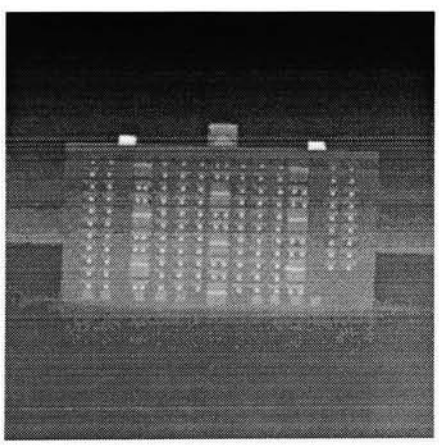

b. 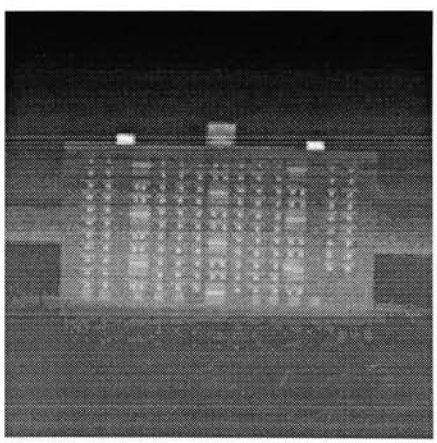

Figure 5.18: a. Before Aggregation and b. After Aggregation

5.1.8 Gaussian Distributed NER

The detector is assumed to be made of HgCdTe. The $D^*(\lambda)$ curve was used to generate the value of D^* which is used to calculate the NER used to determine the noise statistics for the detector (figure 5.19). The resulting Gaussian noise image and histogram of the noise are shown in figure 5.20.

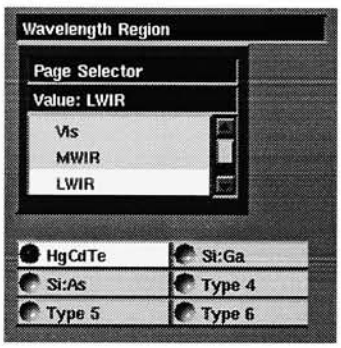

Figure 5.19: D^* Selection based on material and wavelength region

a.

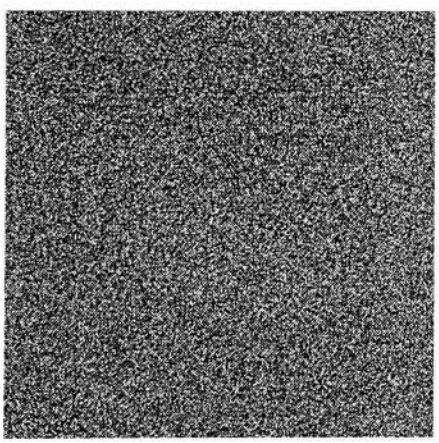

b.

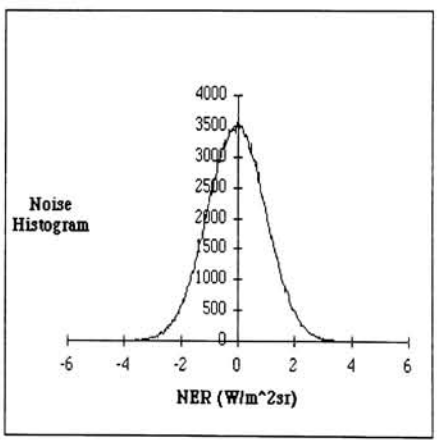

Figure 5.20: a. Gaussian Distributed NER b. Histogram of Detector Noise

5.1.9 Electronics & Noise

The "Electronics & Noise" module is the next step in the imaging chain after the aggregation of pixels to account for oversampling. The Gaussian distributed detector noise (Section 5.1.8) is a subsection of this module. The inputs for the lowpass filter are directly from the initialization module and only the the optical and filter transmissivities must be entered (figure 5.21).

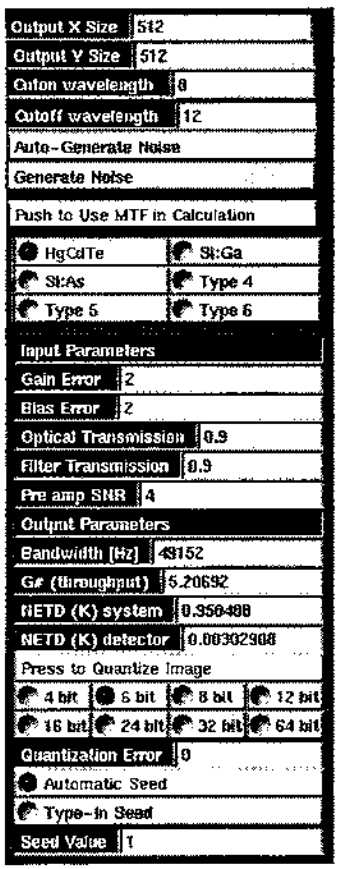

Figure 5.21: D^* Selection based on material and wavelength region

After the detector noise is added, the image was decomposed into magnitude and phase before applying the electronics section. The lowpass filter MTF and PTF are shown in figure 5.22.

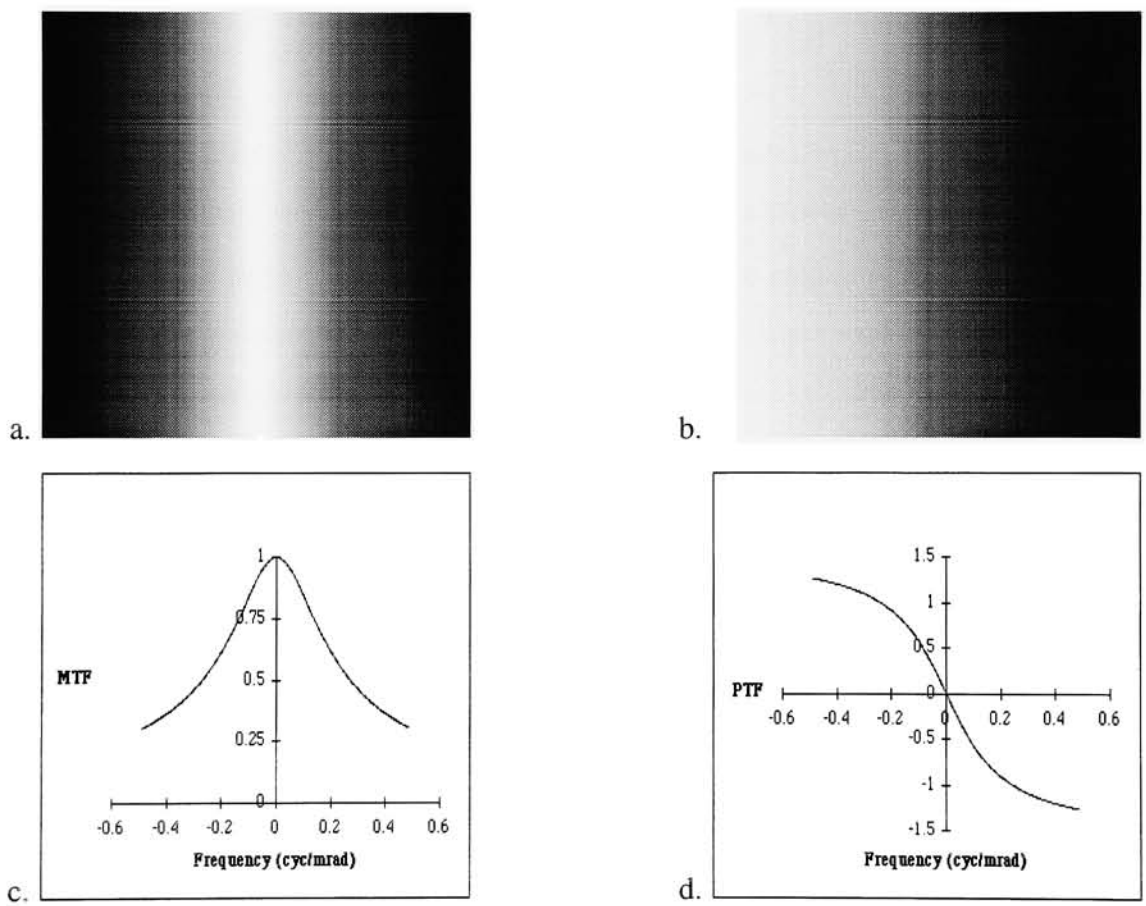

Figure 5.22: a & b Electronic MTF and PTF for the Simulated Inframetrics System

Table 5.2: Output Parameters from the Inframetrics Sensor System Simulation

Parameter Output	**Value**
Bandwidth	49152 Hz
G# (Throughput)	5.207
NETD System	0.9585 K
NETD Detector	0.0030 K
Quantization RMS Error	0.00927 $\frac{W}{m^2 sr}$

The image was reconstructed and the amplifier noise was added to the output image to model the very poor quality Inframetrics electronics package. An estimated SNR of 4 was chosen to simulate the amplifier. The amplifier and detector noise were combined to produce a total system noise expressed in noise equivalent temperature difference (NETD). The output parameters from the sensor simulation are found in table 5.2.

These parameters were extracted directly from the electronics control panel.

5.1.10 Quantization and Quantization Error

The output image was quantized to 6 bits within the dynamic range of the image. The image was not converted to digital counts because of the convenience of using the quantized floating-point values. The quantization error was $0.00927 \frac{W}{m^2 sr}$. The quantized and non-quantized output images are shown in figure 5.23. The quantization error image which is the difference of the images is shown in figure 5.24.

a. 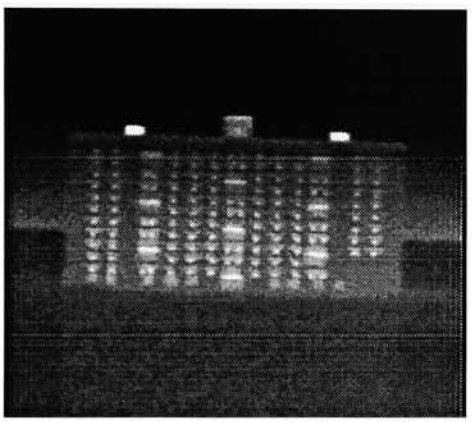 b. 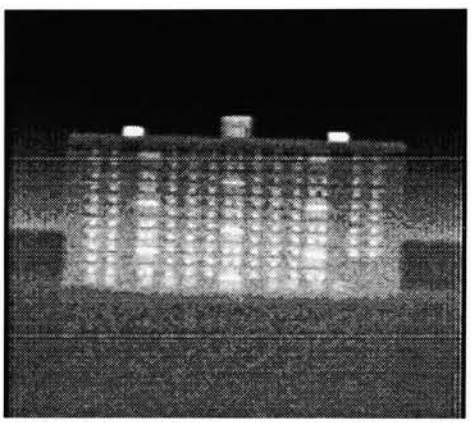

Figure 5.23: a. Quantized to 2^6 levels b. Non-quantized Image

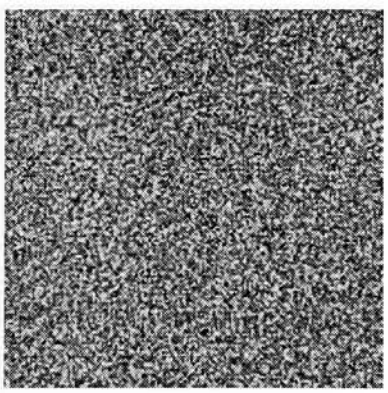

Figure 5.24: Quantization Error Image

The magnitudes of the input and output images of the DIRSIG sensor system are shown in figure 5.25. Notice the attenuation of the higher frequencies in the output image.

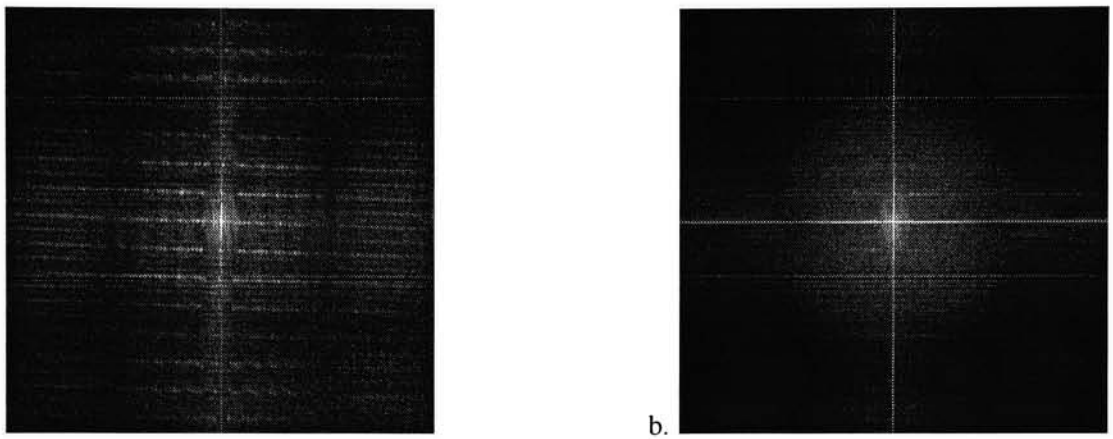

Figure 5.25: a. Transform of Input and b. Transform of Output

The 1-D horizontal slices of the MTFs of the Inframetrics sensor simulation are plotted in figure 5.26a. The vertical slices of the MTFs of the same system are shown in figure 5.26b. The "Total MTF" curves were calculated by multiplying the individual component MTFs before aggregation of pixels.

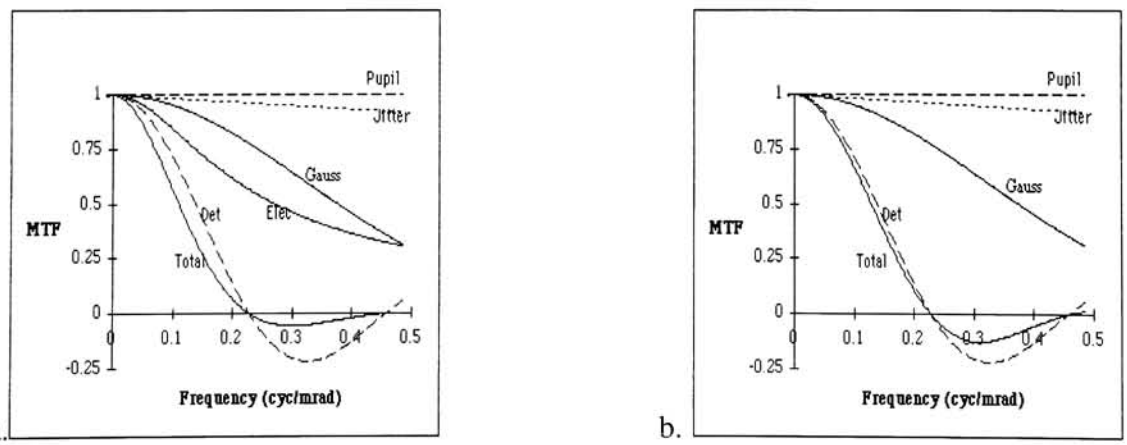

Figure 5.26: a. Horizontal MTFs and b. Vertical MTFs

Notice how the vertical and horizontal curves differ in figure 5.27. The horizontal composite MTF attenuates the higher frequencies "earlier" than the vertical MTF which indicates more bluring in the horizontal direction.

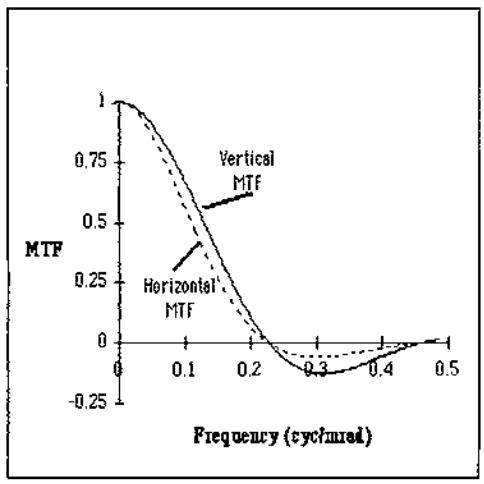

Figure 5.27: Horizontal and Vertical MTF

5.2 Task 2 - Simulation of Kodak KIR_310 Sensor System

The Kodak KIR_310 sensor system was simulated by cascading an image through the AVS sensor simulation module system (figure 5.28).

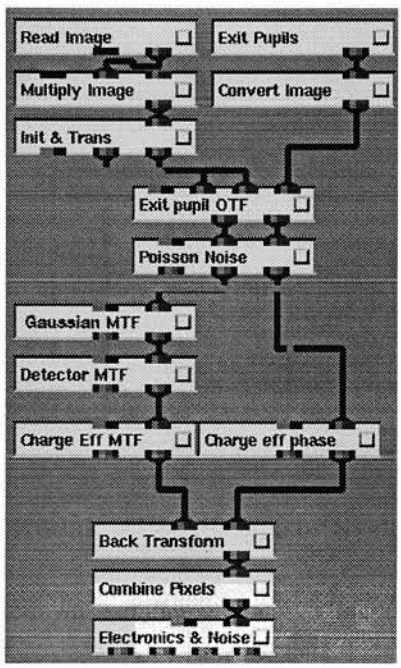

Figure 5.28: Sensor Sub-system Algorithm for KIR_310

The Kodak staring array created an image where the output is 640x486, but the final image image output is interpolated down to 512x480 by the Imaging Technology framegrabber board.

The sensor acquisition was simulated by creating a DIRSIG image using an oversampling ratio of 1.6:1 in the horizontal and 2.1:1 in the vertical direction. The 1024x1024 image was processed through the imaging chain and aggregated to 512x512 and then interpolated to 512x486. The input settings in Table 5.3 were used to process the image. The image was interpolated using a bilinear interpolation routine to get the 512x486 output size.

The processing chain was difficult to model because of the limitations on image size due to memory constraints in the hardware and the limitations of having a 2^m pixel size for the FFT.

Table 5.3: Input Settings for the Kodak KIR_310 Sensor System Simulation

Parameter Input	**Value**
Wavelength Region	3 - 5 μm
Focal Length	200 mm
Target Distance	402 m
Optical Aberration	0.1 mrad
Detector Element Size	25 μm
Aperture Diameter	90 mm
D* (Manual Setting)	3.0×10^{13}
Detector Material	PtSi
Transmission of optics	0.9
Transmission of filter	0.9
Radiance to Voltage Gain Error	1.0 %
Radiance to Voltage Bias Error	1.0 %
X Fill Factor	95%
Y Fill Factor	95%
Amplifier SNR	100

This set of images show the simulated input and modified output from the simulated system (figure 5.29). The final output DIRSIG image and the actual Kodak KIR 310 image taken on May 1, 1995 are shown in Figure 5.30.

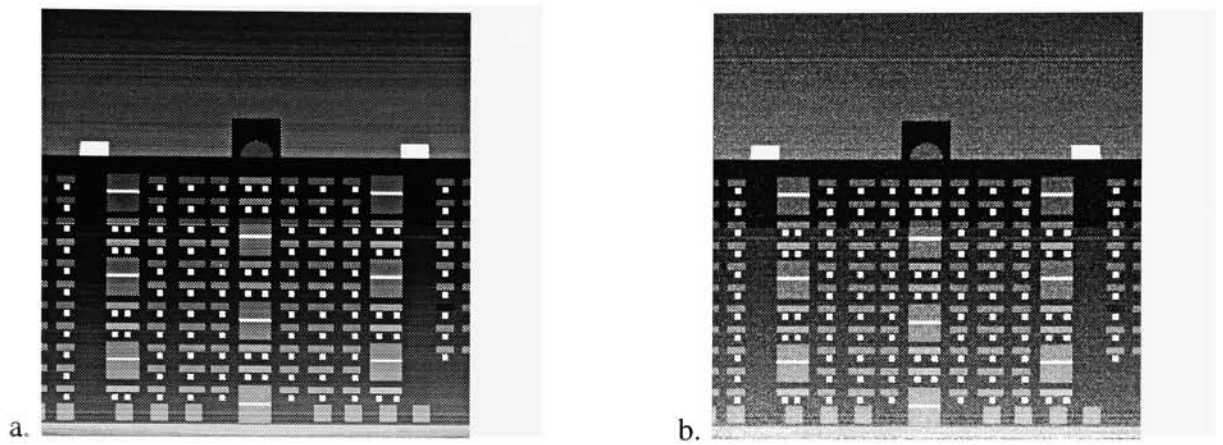

Figure 5.29: a. DIRSIG input image and b. Final Processed Image

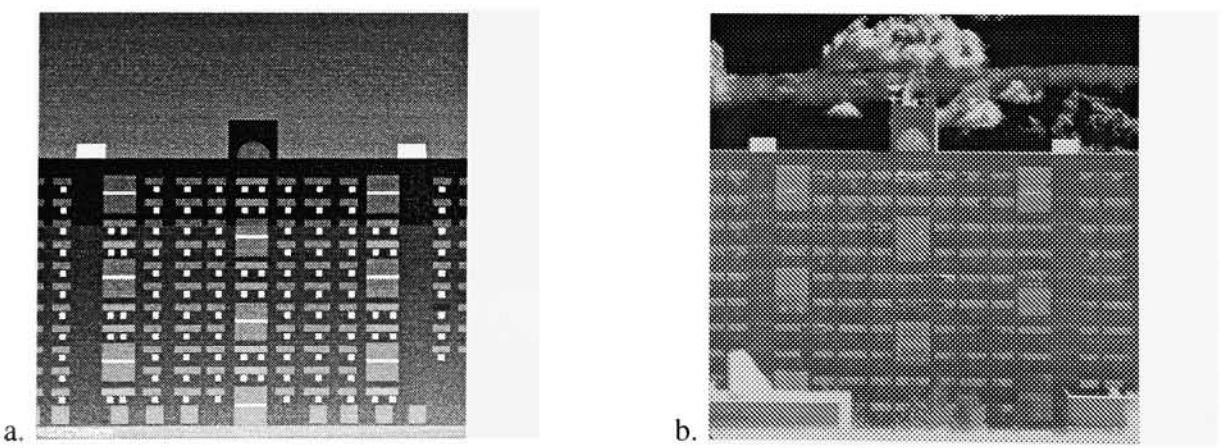

Figure 5.30: a. Final Processed Image and b. Truth Image

5.2.1 Poisson Photon Noise

The Poisson noise image encountered after the optics sub-system stage is shown in figure 5.32b.

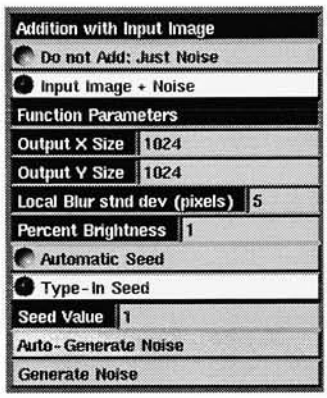

Figure 5.31: Poisson Noise Control Panel

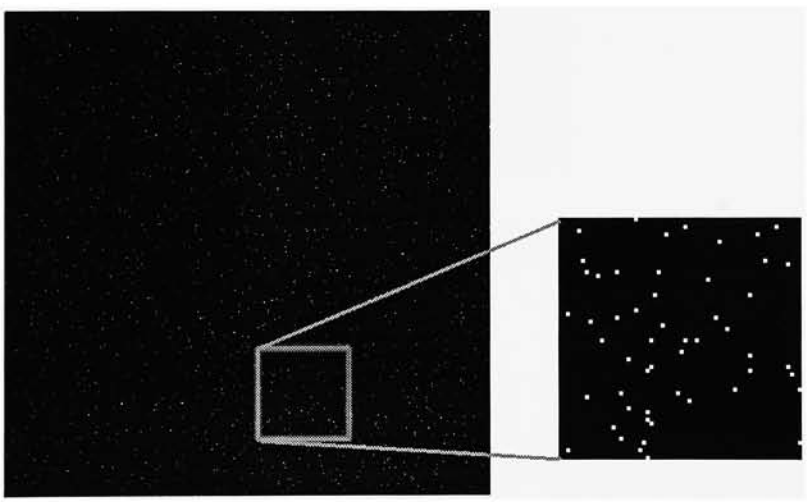

Figure 5.32: DIRSIG Poisson Noise in Simulated System

The NER variance and mean were calculated to be $0.00084 \frac{W}{cm^2 sr}$ and $0.0034 \frac{W}{cm^2 sr}$ respectively.

5.2.2 Kodak KIR_310 Initialization

The simulation of the Kodak array used the input parameters shown in Table 5.3 in the "Init & Trans" module (figure 5.33). The input image was split into magnitude and a phase images (figure 5.34).

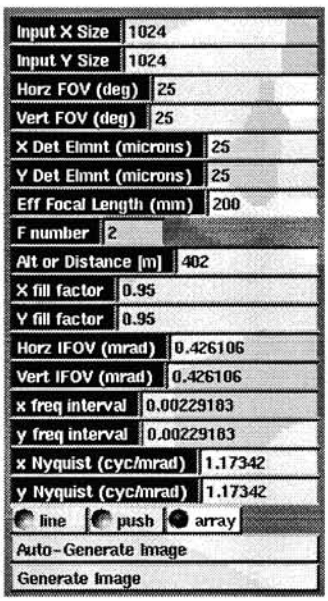

Figure 5.33: Initialization Parameters for the Kodak KIR_310 Simulation

a. 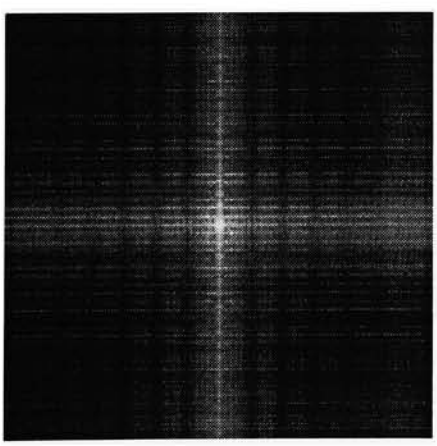

b. 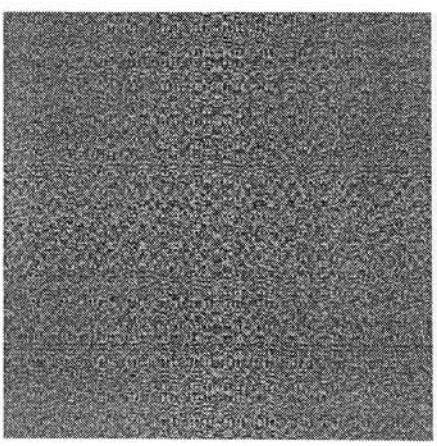

Figure 5.34: a. Magnitude Image and b. Phase Image

5.2.3 Exit Pupil MTF

A circular pupil 180 pixels in diameter in a 1024x 1024 image was used in the simulation (figure 5.35b).

a.

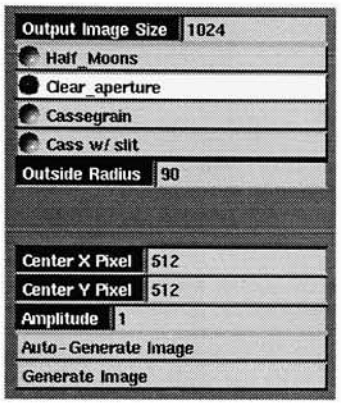

b.

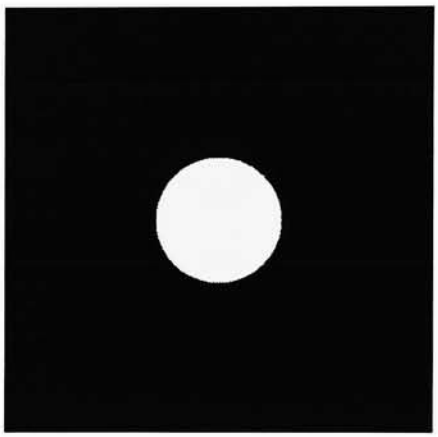

Figure 5.35: a. Exit Pupil Control panel and b. Clear Exit Pupil

The exit pupil was used in the "Exit Pupil MTF" module to calculate the MTF (figure 5.36a). The resulting MTF is shown in figure 5.36b.

a.

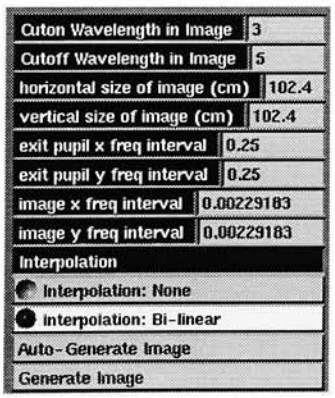

b.

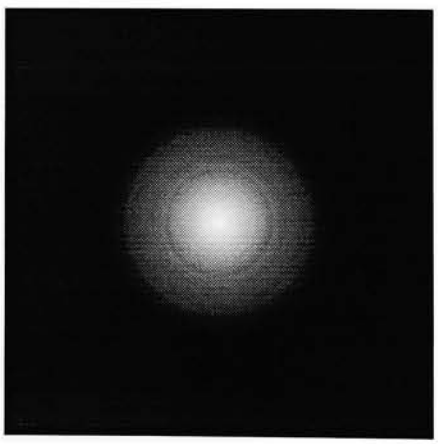

Figure 5.36: a. Autocorrelation Control Panel and b. Exit Pupil MTF

The output from the module needs to be scaled to the correct frequency intervals for multiplication. Figure 5.37a is the 1-D representation of the exit pupil OTF output. The interpolated 1-D slice used in the image chain is shown in figure 5.37b

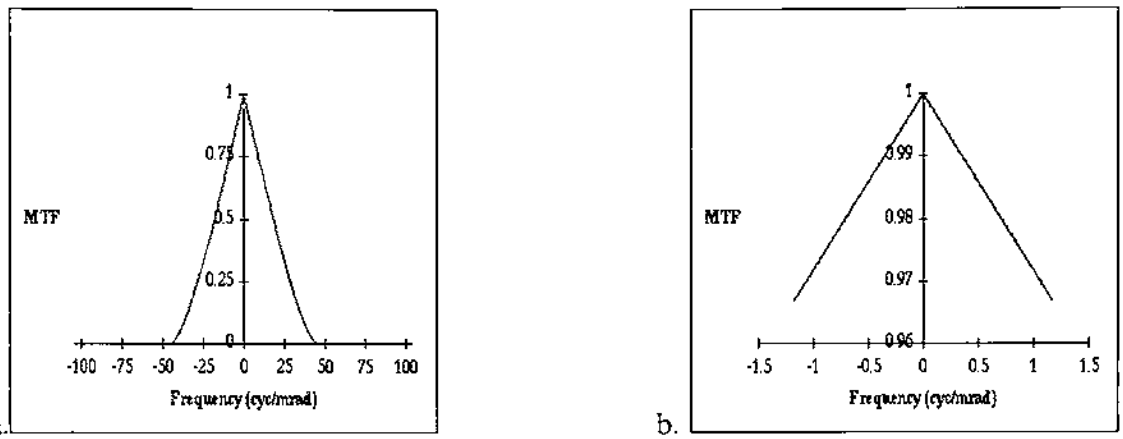

Figure 5.37: a. 1-D Exit Pupil MTF b. Interpolated 1-D Simulated Exit Pupil MTF

The 1-D interpolated values suggests that the degradations from the exit pupil itself are minimal as the minimum MTF value is roughly 0.967 (figure 5.37b). This indicates that loss from this step in the chain is $\approx 3\%$ at the Nyquist frequency.

5.2.4 Gaussian Correction MTF

The Gaussian correction module followed the optics module. This module modeled the 2- D Gaussian MTF that was calculated from a 0.1 mrad PSF (figure 5.38). The calculated 2-D Gaussian cor-

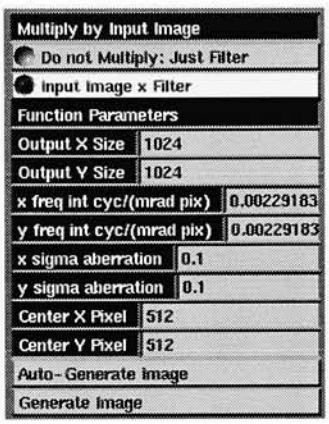

Figure 5.38: Gaussian Correction Panel Settings for the Kodak KIR_310

rection MTF is shown in figure 5.39a. The 1-D MTF representation shows a 24% loss in amplitude at the Nyquist frequency (figure 5.39b).

a.

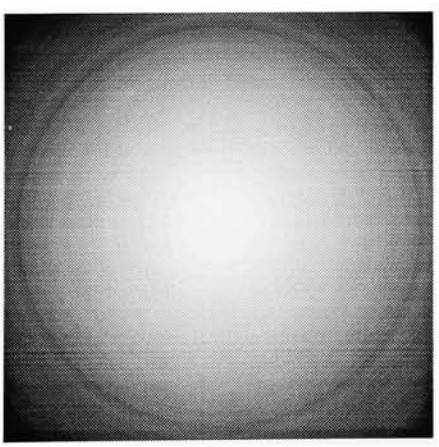

b.

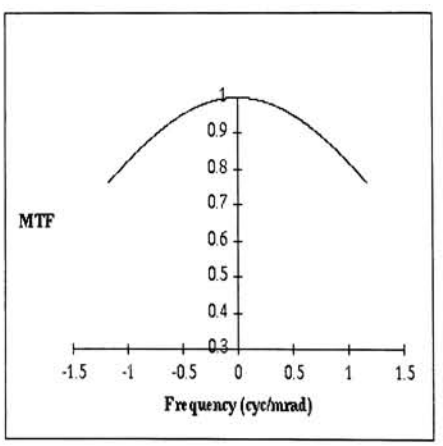

Figure 5.39: a. 2-D and b. 1-D Slice Representation for the Simulated Optical aberration MTF

5.2.5 Detector Size MTF

The detector element was $25\mu m$ square with a system effective focal length of 200 mm. The IFOV of the detector was calculated to be 0.1186 mrad (figure 5.40).

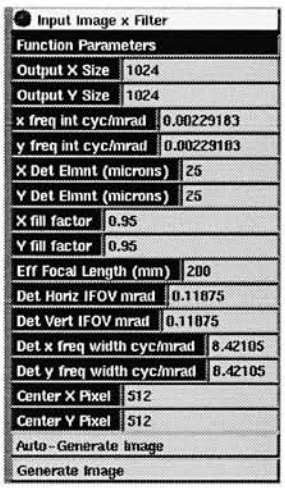

Figure 5.40: Detector Control Panel Settings for the Kodak KIR_310

The fill factors were set to 95% in both the horizontal and vertical pitch directions.

a.

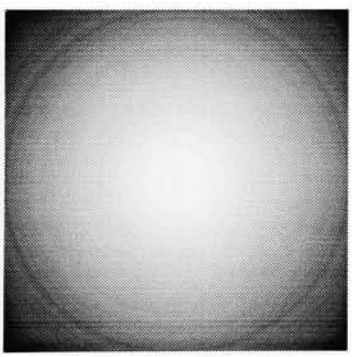

b.

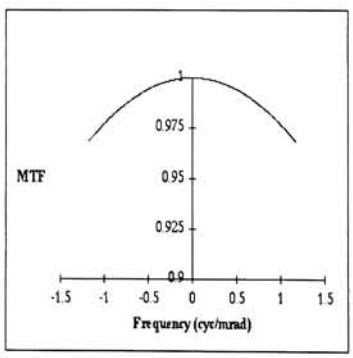

Figure 5.41: a. 2-D and b. 1-D Slice Representation for the Detector MTF of the Simulated Kodak System

The calculated detector MTF is shown in figure 5.41a. The 1-D representation is shown in figure 5.41b.

5.2.6 Charge Transfer Efficiency MTF & PTF

The CTE MTF and PTF were applied just after the detector MTF and before the aggregation of the pixels. The actual array size of 640 elements was used to calculate both the MTF and the PTF (figure 5.42). The CTE used in each module was .99999 per pixel. The calculated charge transfer efficiency MTF 2-D and 1-D slice representation are shown in figure 5.43.

a.

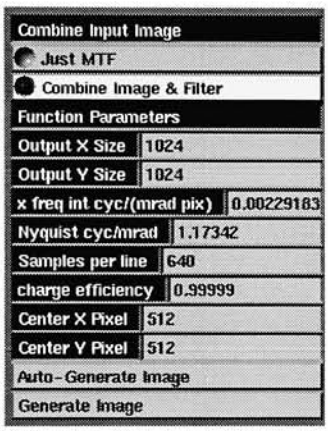

b.

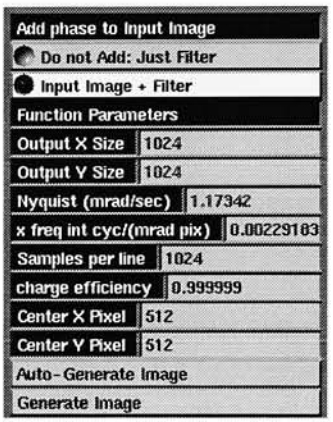

Figure 5.42: CTE MTF & PTF Control Panels

a.

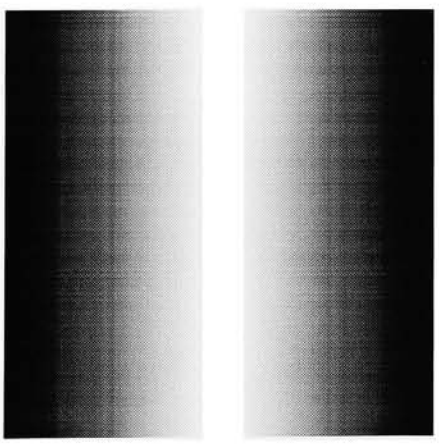

b.

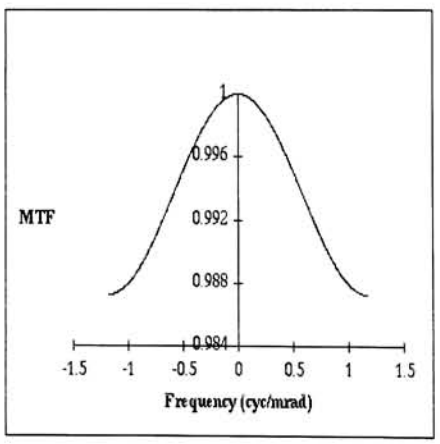

Figure 5.43: a. 2-D and b. 1-D CTE MTF for the Simulated Kodak System

The calculated charge transfer efficiency PTF images are shown in figure 5.44.

a. 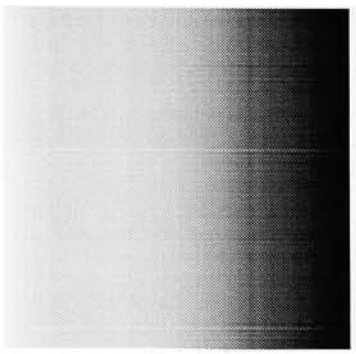

b. 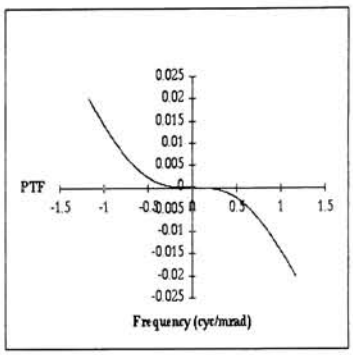

Figure 5.44: a. 2-D and b. 1-D CTE PTF for the Simulated Kodak System

5.2.7 Aggregation Mode

The image was aggregated to an image size of 512x512 from 1024x1024 using a 2x2 aggregation mode (figure 5.46).

a. 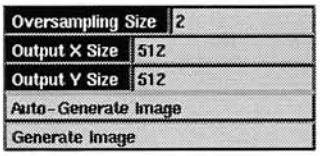

Figure 5.45: a. 2x2 Aggregation Mode

a. 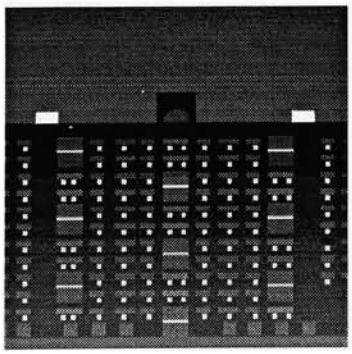

b. 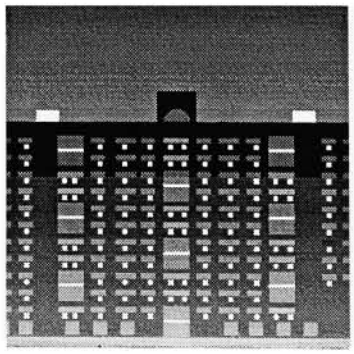

Figure 5.46: a. Before Aggregation and b. After Aggregation

5.2.8 Gaussian Distributed NER

The Gaussian distributed noise from the detector is based upon the detector material PtSi. A manual entry of the D^* was used to generate the noise equivalent radiance variance, NER, was determined for the image (figure 5.47).

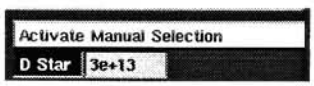

Figure 5.47: D^* Manual selection for the D^*

The resulting image representing the Gaussian noise is shown in figure 5.48

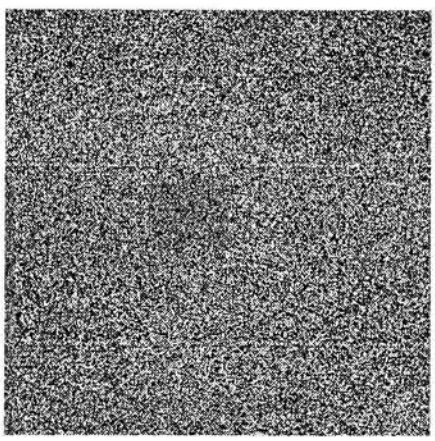

Figure 5.48: Gaussian Distributed NER

5.2.9 Electronics & Noise

The "Electronics & Noise" module is the next step in the imaging chain after the aggregation of pixels to account for oversampling. The detector noise discussed in the Gaussian noise (Section 5.2.8) is calculated in this module. The inputs come directly from the initialization module and only the optical and filter transmissivities need to be entered (figure 5.49).

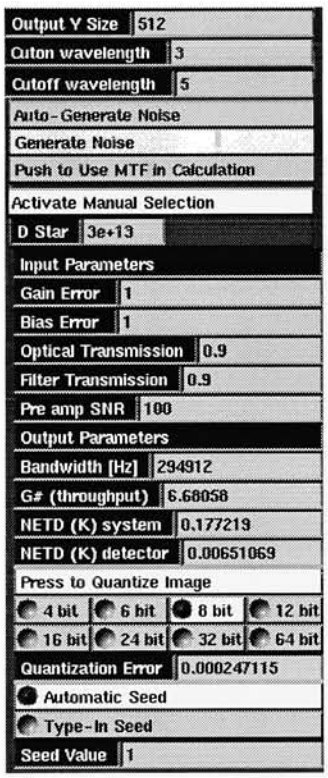

Figure 5.49: D^* Selection based on material and wavelength region

An amplifier gain and bias error due to the radiance to voltage conversion was applied along with an amplifier noise to the output image to model the very high quality Kodak electronics package. A SNR of 100 was used to simulate the amplifier. The amplifier and detector noise were combined together to get a total system noise expressed in noise equivalent temperature difference NETD. The output parameters from the sensor simulation are found in Table 5.4.

Table 5.4: Output Parameters from the Kodak Sensor System Simulation

Parameter Output	**Value**
Bandwidth	294912 Hz
G# (Throughput)	6.68
NETD System	0.177219 K
NETD Detector	0.0065K
Quantization RMS Error	0.0002 $\frac{W}{m^2 sr}$

These parameters are outputs taken from the control panel.

5.2.10 Quantization and Quantization Error

The output image was quantized to 2^6 levels within the dynamic range of the image. The quantization error was $0.0002\frac{W}{m^2 sr}$. The quantized and non- quantized output images are shown in figures 5.50a and b. The quantization error image is shown in figure 5.51.

a. 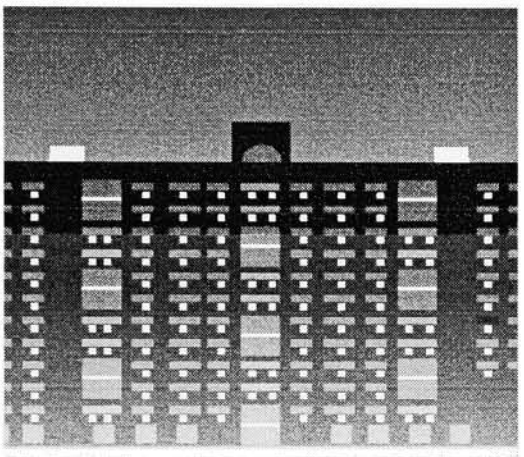 b. 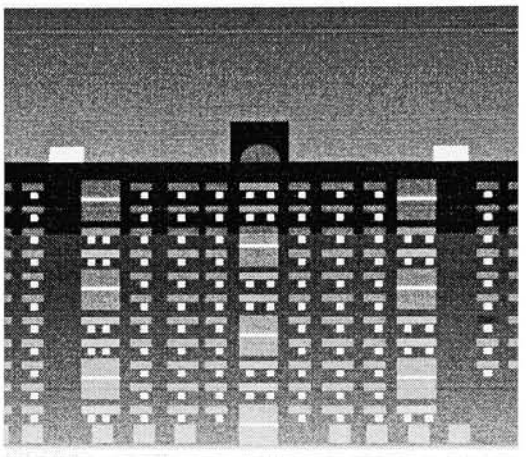

Figure 5.50: a. Quantized to 2^6 levels b. non-quantized image

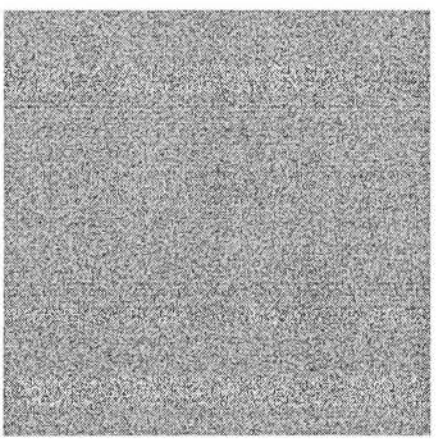

Figure 5.51: Quantization Error Image

The magnitudes of the input and output images of the DIRSIG sensor system are shown in figure 5.52. Notice the attenuation of the higher frequencies in the output image.

a. 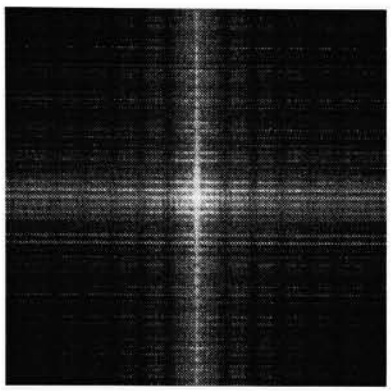 b. 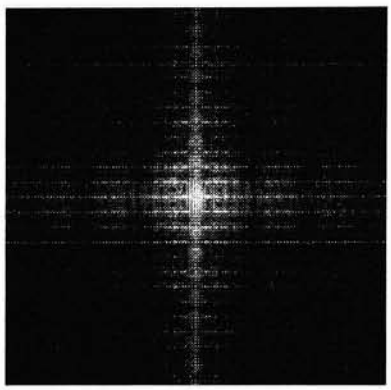

Figure 5.52: a. Transform of Input and b. Transform of Output

The 1-D horizontal slices of the MTFs of the Inframetrics sensor simulation are plotted in figure 5.26a. The vertical slices of the MTFs of the same system are shown in figure 5.26b. The "Total MTF" curves were calculated by multiplying the individual component MTFs before aggregation of pixels.

a. 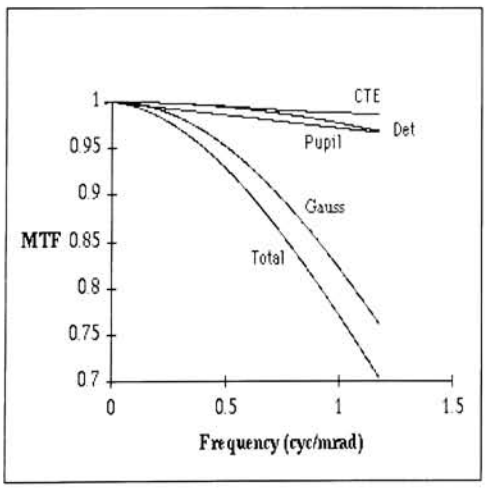

b. 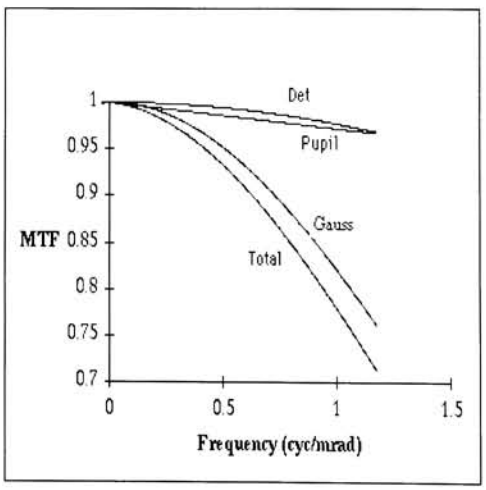

Figure 5.53: a. Horizontal MTFs and b. Vertical MTFs

Notice how the vertical and horizontal MTFS are nearly identical (figure 5.27). The horizontal composite MTF attenuates the higher frequencies slightly "earlier" than the vertical MTF indicating a stronger blur in the horizontal direction. The MTF over the entire image is approximately the same, which is the desired result.

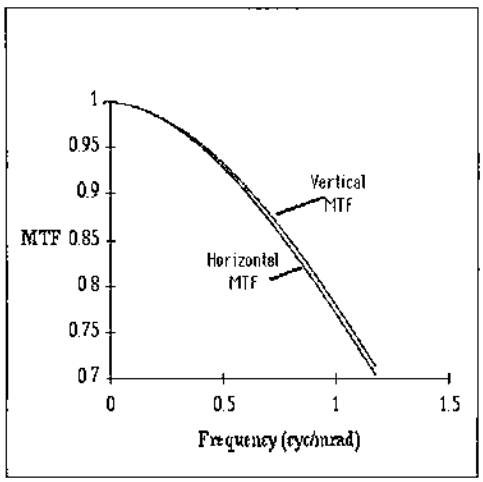

Figure 5.54: Horizontal and Vertical MTF

5.3 Task 3 - Combination of New Camera and Sensor Models

The new sensor model was used on a DIRSIG image with the Salacain Camera Model (Salacain, 1995). The results are shown in figure 5.55. The added improvements to the DIRSIG model further enhance the capabilities of DIRSIG to model the realistic environment.

a. 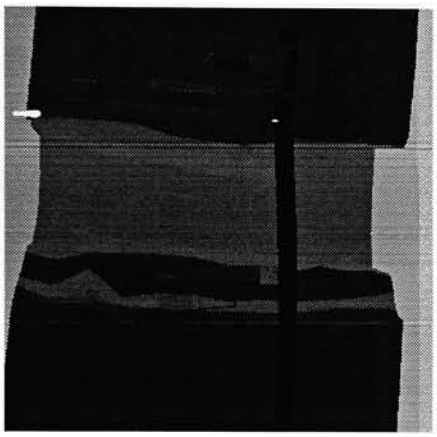 b. 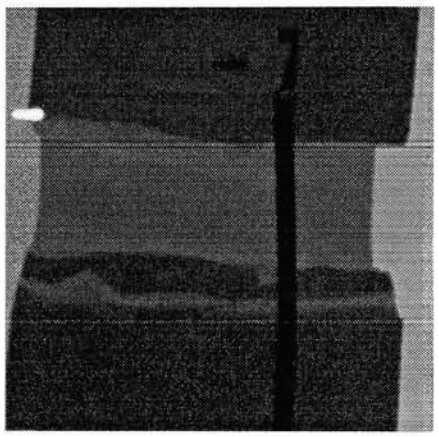

Figure 5.55: a. new DIRSIG image b. Enhanced Sensor applied to DIRSIG model

5.4 Analytical Results

An MTF was calculated from the RIT dormitory image for both the actual and the synthetic systems. A line sample across a uniform surface was used to gather the line spread function (LSF). The Fourier Transform of the derivative of the LSF was used as the system OTF (equations 5.67 thru 5.69). The normalized system MTF was calculated from the magnitude of the OTF (equation 5.70).

$$LSF(x) = \{data_1, data_2, \ldots, data_{64}\} \tag{5.67}$$

$$f(x) = \frac{d}{dx}\left(LSF(x)\right) \tag{5.68}$$

$$OTF(\xi) = F\{f(x)\} \tag{5.69}$$

$$MTF(\xi) = \frac{|OTF(\xi)|}{max[|OTF(\xi)|]} \tag{5.70}$$

MTFs were calculated in the horizontal and vertical directions and should be different for both the linescanner and the staring array camera.

The comparison of the actual MTF (dotted line) and thecalculated MTF (solid line) for the Inframetrics simulation in the horizontal and vertical directions (figures 5.56 and 5.57).

All calculations were performed in MathCad and can be found in Appendix B.

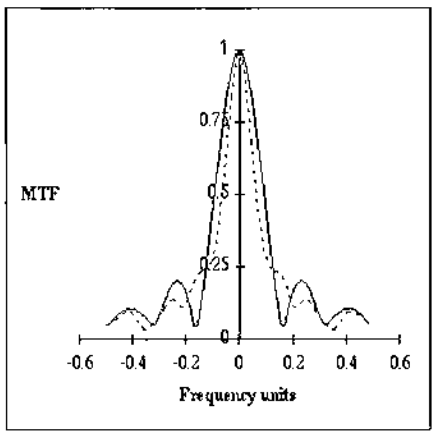

Figure 5.56: Comparison of Actual (dotted) and Synthetic System Horizontal MTFs

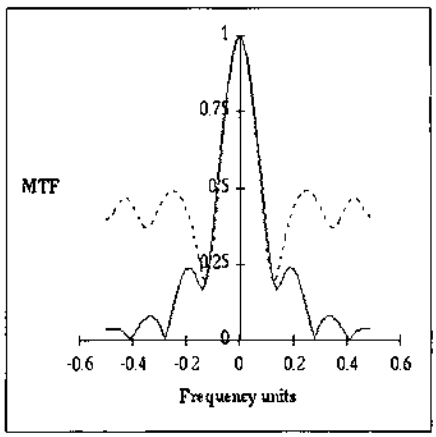

Figure 5.57: Comparison of Actual (dotted) and Synthetic System Vertical MTFs

The synthetic and real MTFs for the Inframetrics linescanner show reasonable similarities that indicate that the simulation worked properly. There are some discrepanices between the two curves. One possible explanation is that the final image and the output image were both interpolated by a factor close to three. The results that are being observed may be just due to the interpolation of the last step in the simulation and also due to the framegrabber board.

The comparison of the actual MTF (dotted line) and the calculated MTF (solid line) for the Kodak KIR_310 simulation in each the horizontal and vertical directions.

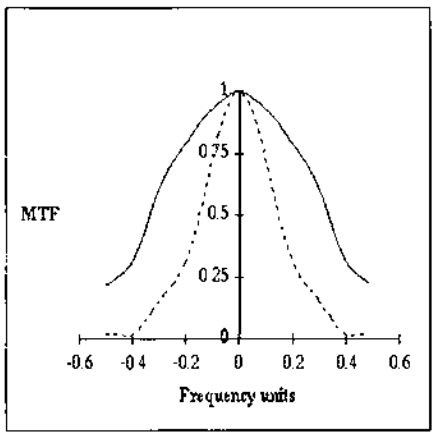

Figure 5.58: Comparison of Actual (dotted) and Synthetic System Horizontal MTFs

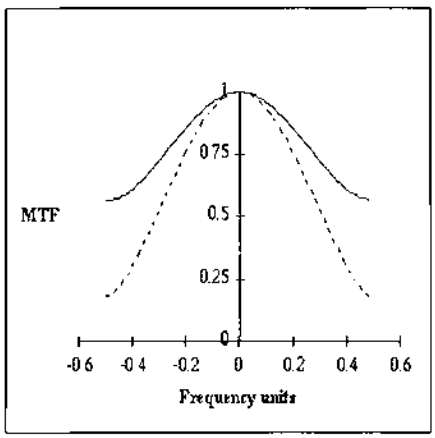

Figure 5.59: Comparison of Actual (dotted) and Synthetic System Vertical MTFs

The MTFs of the Kodak KIR_310 array simulation do not agree as well the as those for the Inframetrics MTFs. The synthetic MTFs in both the horizontal and vertical directions are consistent with the imaging chain MTF (figures 5.58 and 5.59). The vertical MTF for the synthetic and real images do not agree as well as the horozontal MTFs. The MTF for the real image (dotted) shows a significant curve that may be the result of the interpolation from the framegrabber board. The MTFs in the horizontal direction agree better, though they have a large separation over the entire frequency region.

Overall, the new enhanced sensor model simulated the performance of the Inframetrics and Kodak sensors very well. The sensor model was effective in simulating the "poor" quality of the Inframetrics sensor. The output image was dominated by noise, which reflects the inadequate capability of the sensor to accurately make sensor temperature readings. Also, the Kodak sensor performance was simulated by the sensor model. The noise did not dominate the sensor's performance.

The Kodak sensor did have a much smaller detector pitch size (25 μm versus 600 μm) and contributes only to the type of MTF that is applied to the integrated radiance image.

Full-size images showing the simulation results and the simulated imaging chains can be found in Appendix A.

6 Conclusions

The AVS environment turned out to be a very advantageous platform for simulating sensor packages. The simulation successfully modeled two sensor systems presented in the thesis. The Inframetrics sensor simulation image appeared to be degraded as much as the real system. The MTFs from the synthetic and the real image were similar, suggesting that the synthetic degradation was modeled well. A significant consideration in the Inframetrics simulation was to sufficiently model the noise content in the scene. The HgCd detector was very noisy and had a strong MTF, blurring the image significantly. The amplifier was poor and the noise content seen in the input image was very evident. In addition, the Inframetrics sensor system did not exhibit good image quality. The Kodak KIR_310 system offered a greater challenge in terms of modeling the MTFs and PTFs accurately. The noise for this system was very low and the applied noise was severely suppressed to get the same image content.

The model can easily mimic various image chains or create futuristic configurations for engineering studies. This modeling capability is important in reverse engineering and demonstrating the fundamentals. The model works well with linear sensors, but breaks down when non-linear relationships are encountered. This is because all relationships presented in the thesis are based on linear systems.

In addition to modeling sensor systems, the DIRSIG AVS sensor package can be useful in parametric studies where certain aspects of an imaging chain can be isolated and varied to provide a better understanding of the overall process. One such study could involve the study of motion MTFs to determine the limiting blur speed for a platform for pattern recognition.

Upgrading the system is very feasible. The actual code is available for updating new modules. Another advantage is that once a configuration is established, the network can be saved for future use or modification.

The goals of the thesis were accomplished. A sensor modeling package was successfully de-

signed and built and two very different sensor systems were successfully modeled. The sensor modeling package added another building block to the DIRSIG modeling chain, making it a more viable synthetic image generation system.

7 Recommendations

The problems that exist with the sensor model mostly deal with the size of the image. The simulation works best on images up to 512x512. This is because the AVS model copies each image into shared memory as it is passed bewtween modules. This results in multiple copies of the same image throughout the chain. The 1024x1024 images passed through the simulation take up most of the shared memory in AVS. This results in the inability of the simulation to pass the working images to the entire imaging chain. This is a software problem that can be remedied with the allocation of more shared memory so that large images can be processed. The sensor system could be ported from AVS and to an X environment , but the advantages of AVS would be lost. Some further investigation should be conducted to determine whether the simulation should reside in AVS.

The current constraint requiring images to have size of 2^n pixels problem for the current FFT algorithm could be alleviated by introducing a prime factor FFT.

Appendix A

Full Size Images from the Thesis

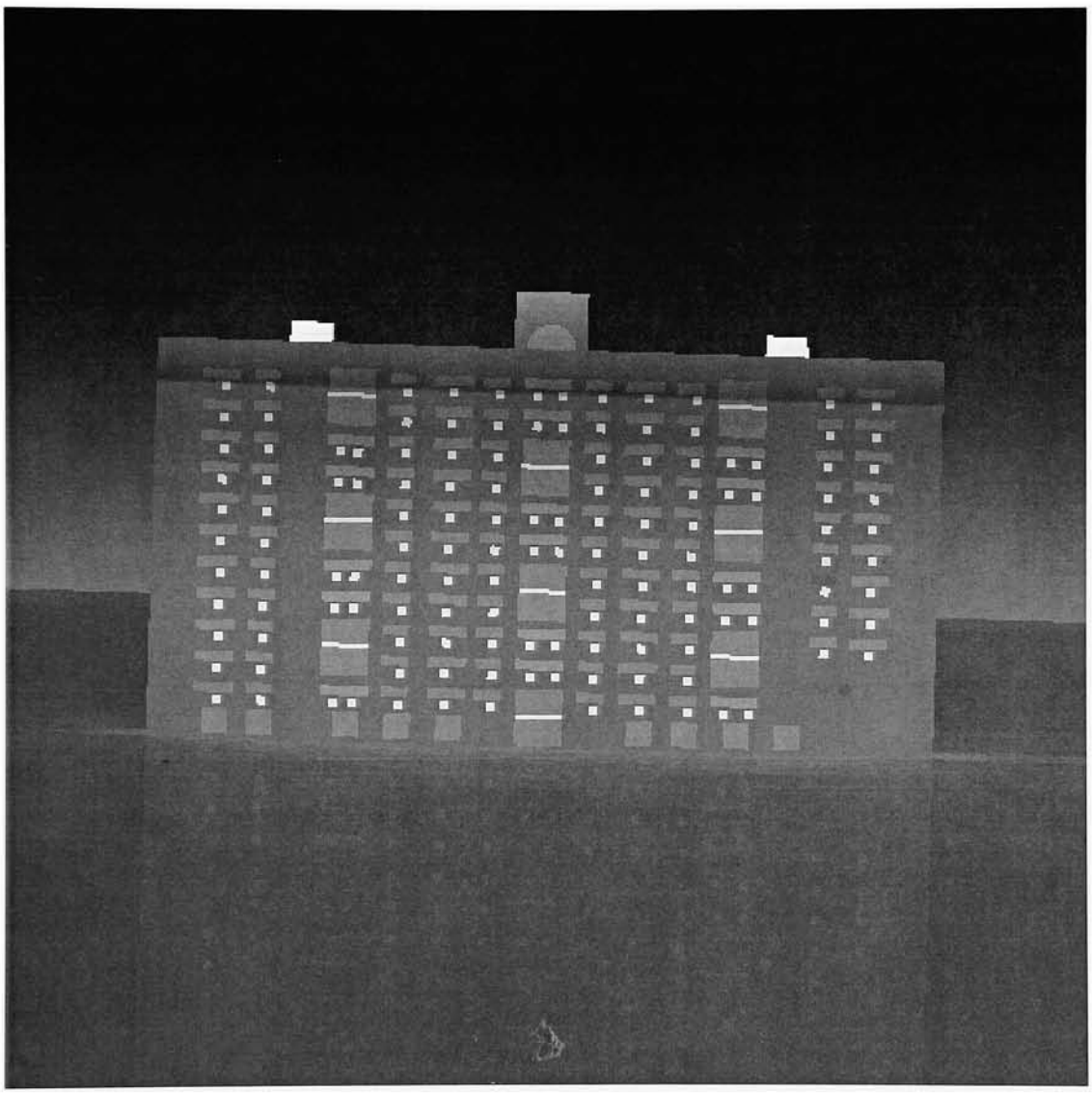

Figure A.1: Input Image for the Inframetrics Simulation

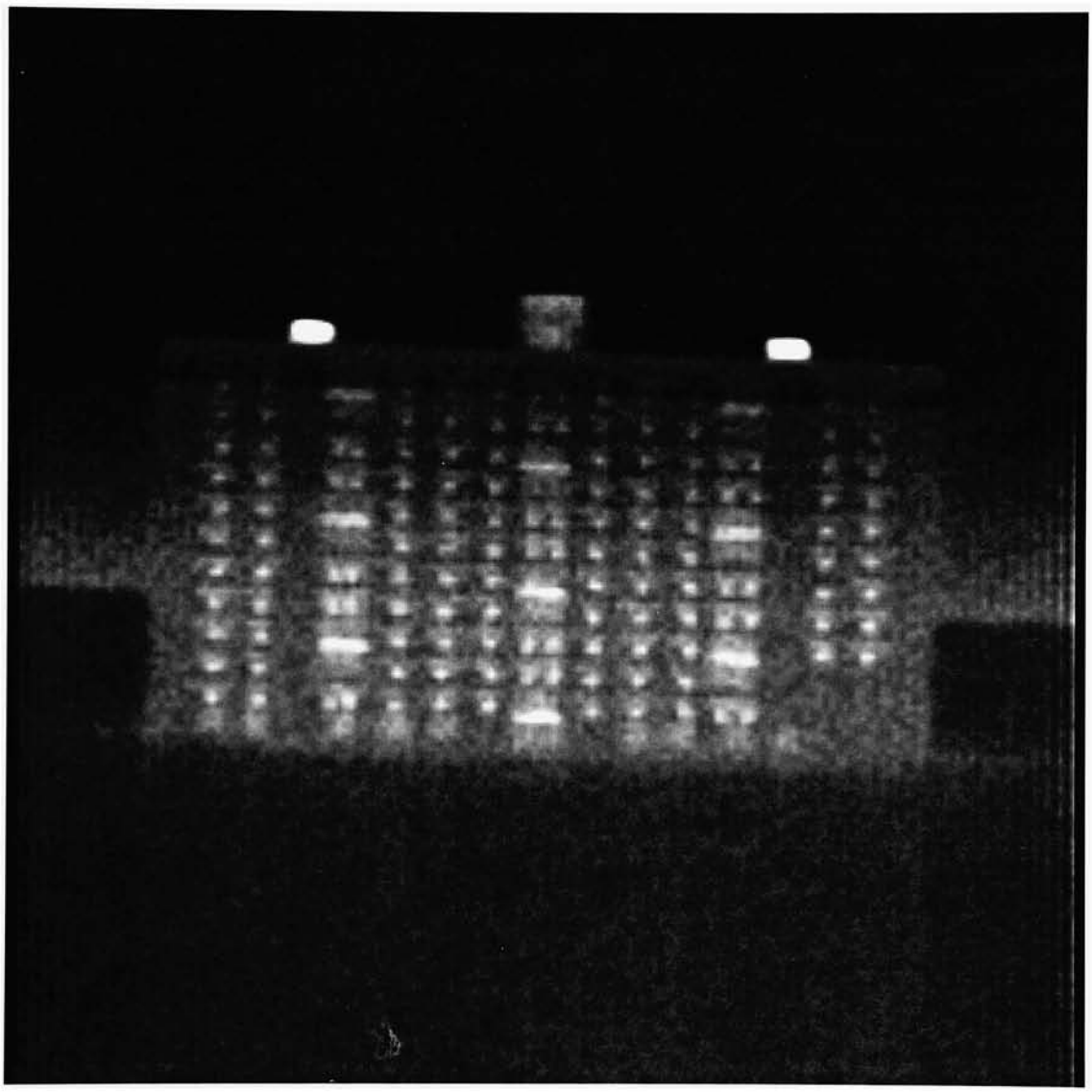

Figure A.2: Output Image from the Inframetrics Simulation

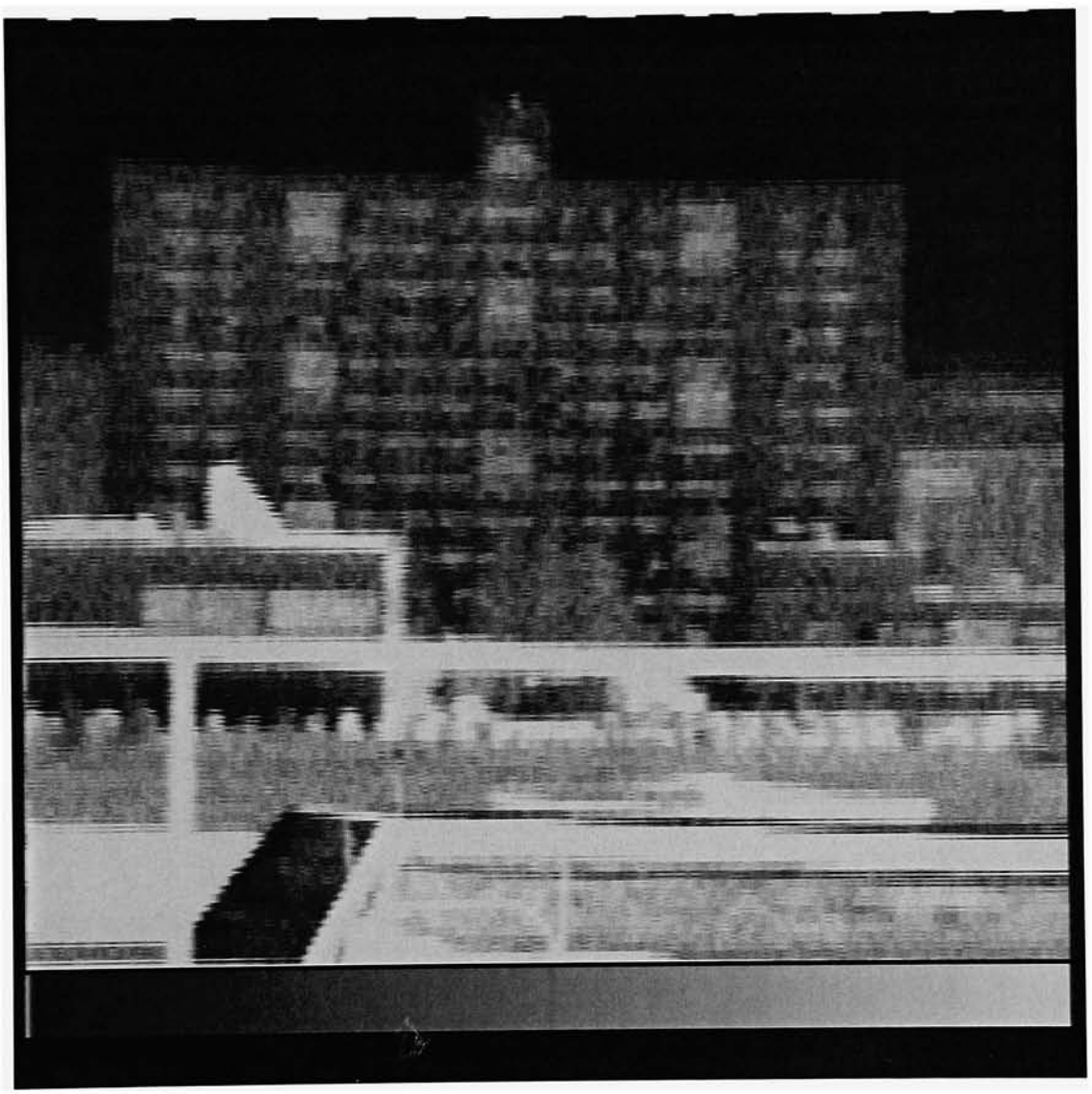

Figure A.3: Truth Image from the Inframetrics Sensor

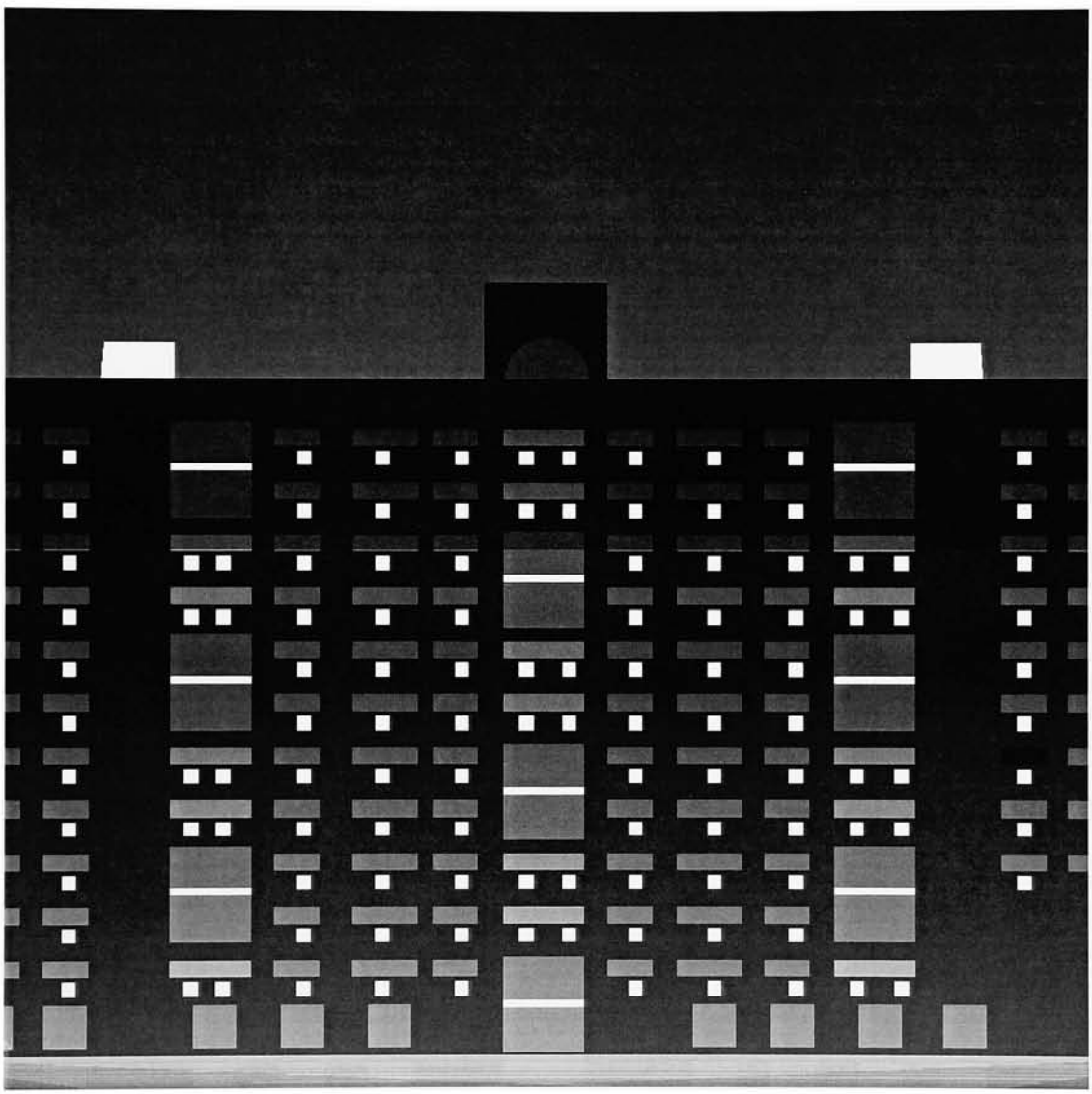

Figure A.4: Input Image for the Kodak KIR_310 Simulation

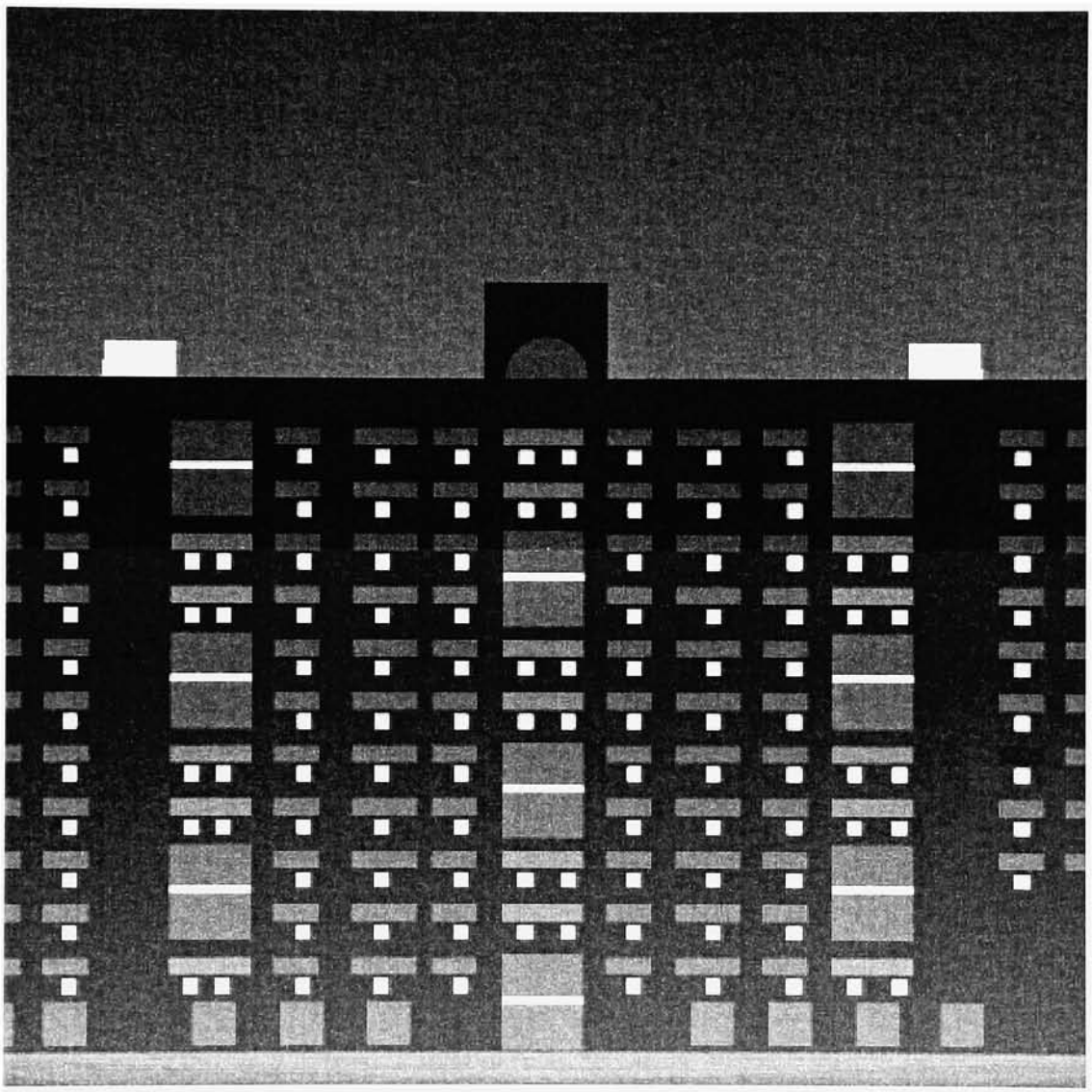

Figure A.5: Output Image from the Kodak KIR_310 Simulation

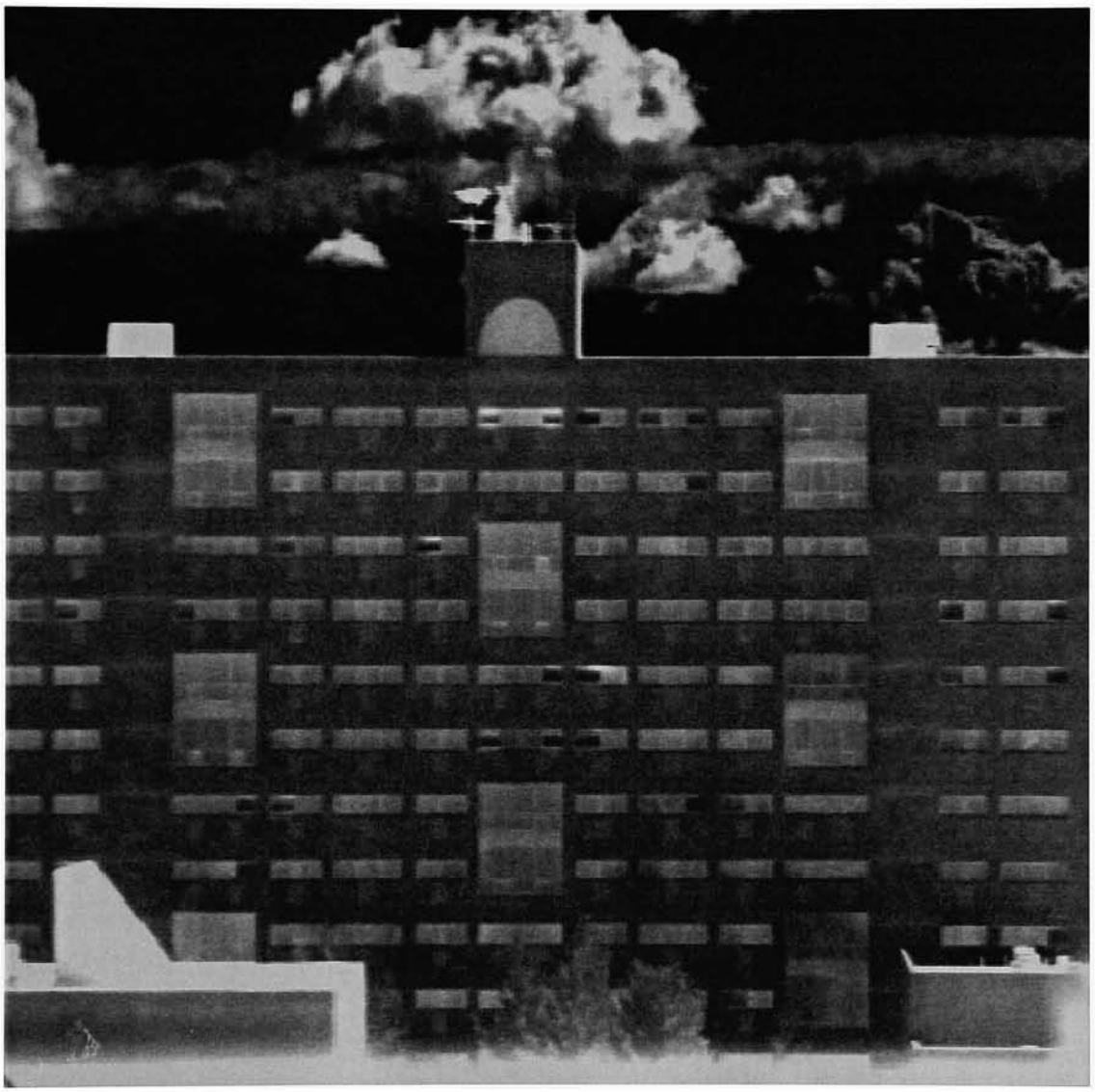

Figure A.6: Truth Image from the Kodak KIR_310 Sensor

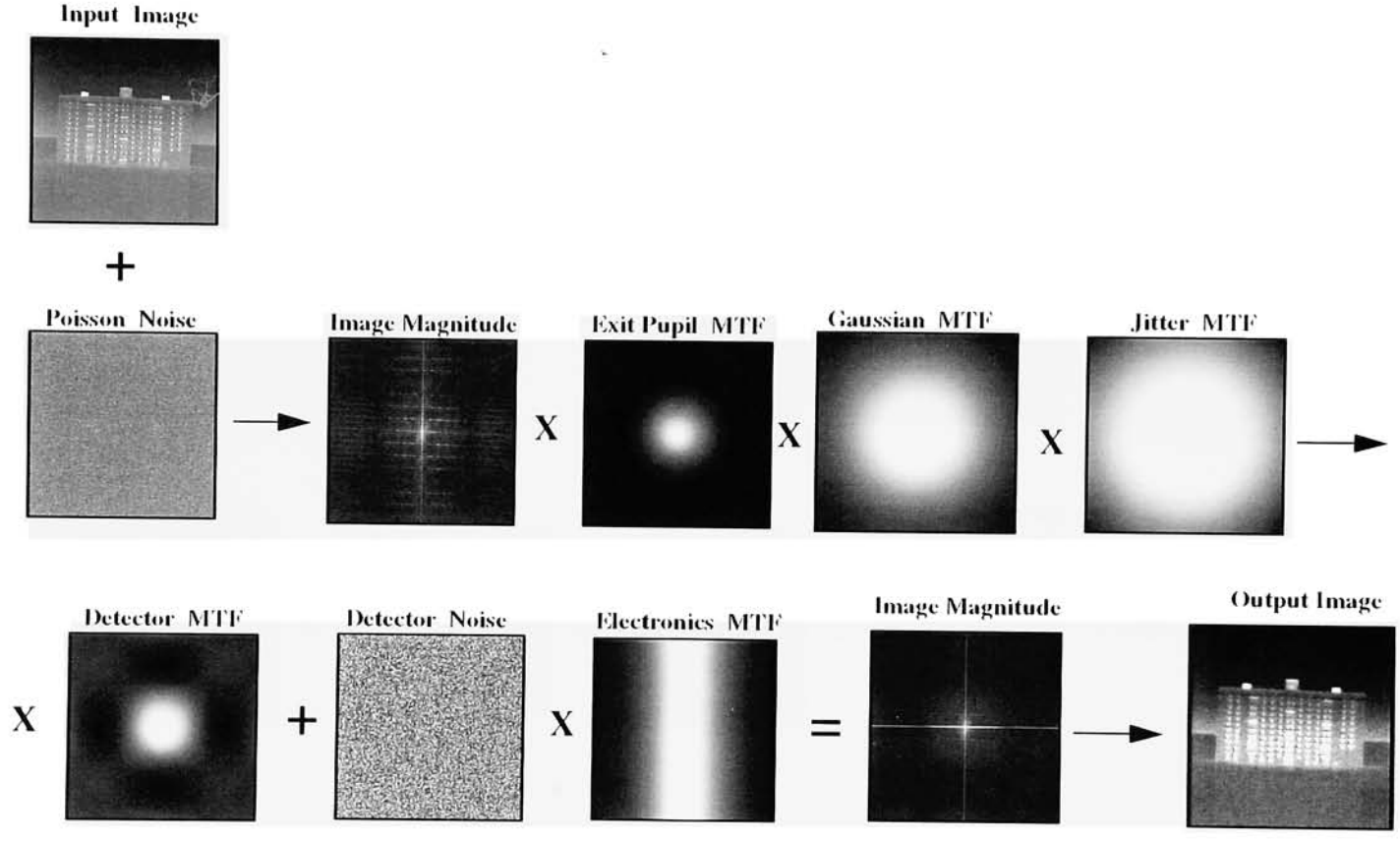

Figure A.7: Imaging Chain for the Inframetrics Simulation

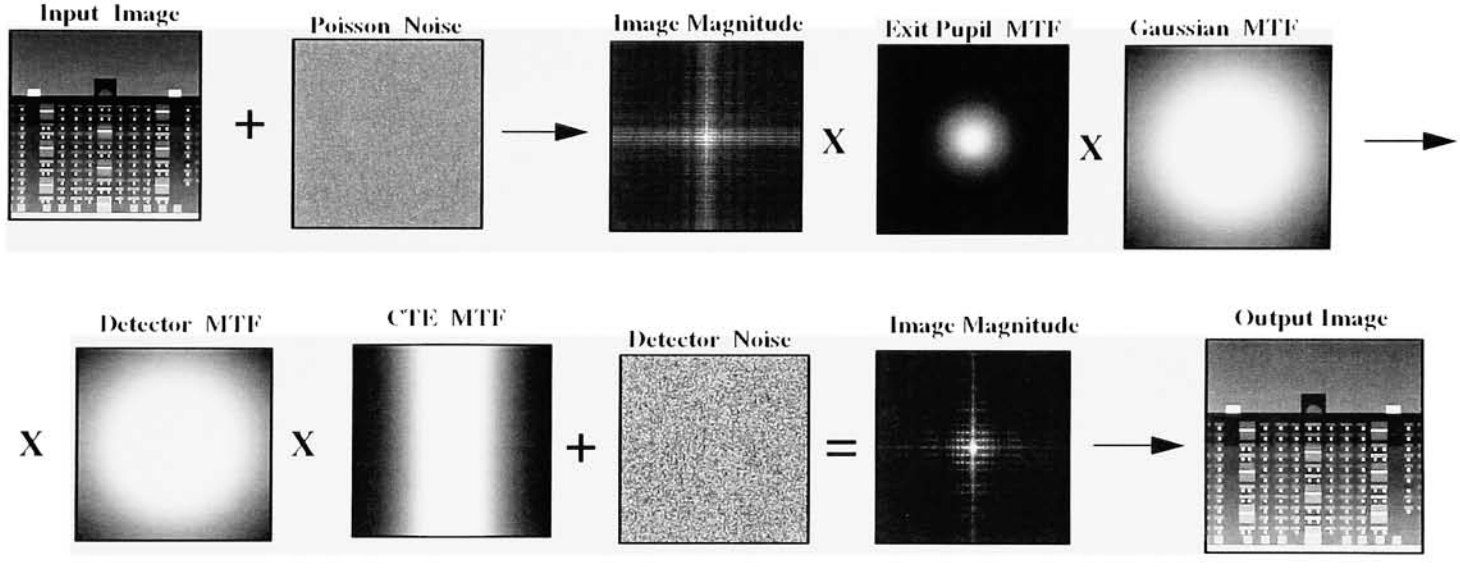

Figure: A.8 Imaging Chain for the Kodak KIR_310 Simulation

Appendix B

Calculation of the MTF via the LSF

Horizontal MTF Calculation for Actual Image from the Inframetrics Linescanner

Read in Data

M1 := READPRN(real1_h) M2 := READPRN(real2_h) M3 := READPRN(real3_h)

Index nn := 0.. rows(M1) n := 0.. rows(M1) - 2

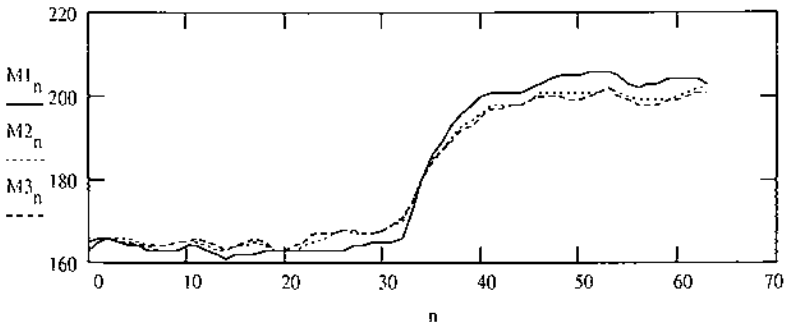

n1 := 40.. rows(M1) n2 := 42.. rows(M2) n3 := 48.. rows(M3)

n1a := 0.. 31 n2a := 0.. 30 n3a := 0.. 30

$M1_{n1} := 200$ $M1_{n1a} := 165$ $M2_{n2} := 200$ $M2_{n2a} := 168$ $M3_{n3} := 200$ $M3_{n3a} := 168$

$$L_{nn} := \frac{M1_{nn} + M2_{nn} + M3_{nn}}{3}$$

Line Spread Function Clipped at Ends

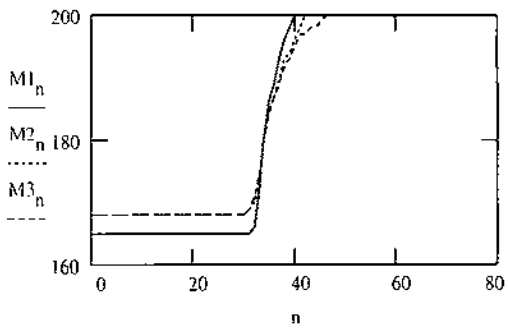

Average value of Line Spread

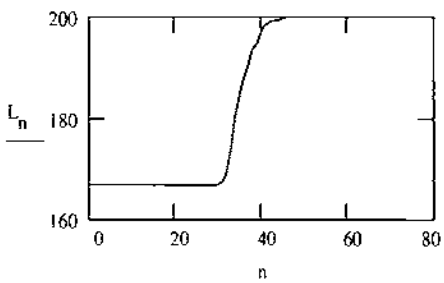

Calculate derivative of input data to calculate the line spread function (LSF)

$D1_n := M1_n - M1_{n+1}$ rows(D1) = 64

$D2_n := M2_n - M2_{n+1}$ rows(D2) = 64

$D3_n := M3_n - M3_{n+1}$ rows(D2) = 64

"Beer-can" the data

$S1_n := (-1)^n \cdot D1_n$ $S2_n := (-1)^n \cdot D2_n$ $S3_n := (-1)^n \cdot D3_n$

Calculate the Fourier Transform of the line spread function to get the Optical Transform Function (OTF)

S1_OTF := cfft(S1)
s1 := 0.. rows(S1_OTF) - 1
$OTF1_{s1} := (-1)^{s1} \cdot S1\_OTF_{s1}$

S2_OTF := cfft(S2)
s2 := 0.. rows(S2_OTF) - 1
$OTF2_{s2} := (-1)^{s2} \cdot S2\_OTF_{s2}$

S3_OTF := cfft(S3)
s3 := 0.. rows(S3_OTF) - 1
$OTF3_{s3} := (-1)^{s3} \cdot S3\_OTF_{s3}$

Compute Modulus

$$Mod1_{s1} := \sqrt{Re\left(OTF1_{s1}\right)^2 + Im\left(OTF1_{s1}\right)^2}$$

$$Mod2_{s2} := \sqrt{Re\left(OTF2_{s2}\right)^2 + Im\left(OTF2_{s2}\right)^2}$$

$$Mod3_{s3} := \sqrt{Re\left(OTF3_{s3}\right)^2 + Im\left(OTF3_{s3}\right)^2}$$

Normalize Modulus to get MTF

$$MTF1_{s1} := \frac{Mod1_{s1}}{max(Mod1)}$$

$$MTF2_{s2} := \frac{Mod2_{s2}}{max(Mod2)}$$

$$MTF3_{s3} := \frac{Mod3_{s3}}{max(Mod3)}$$

All the MTFs

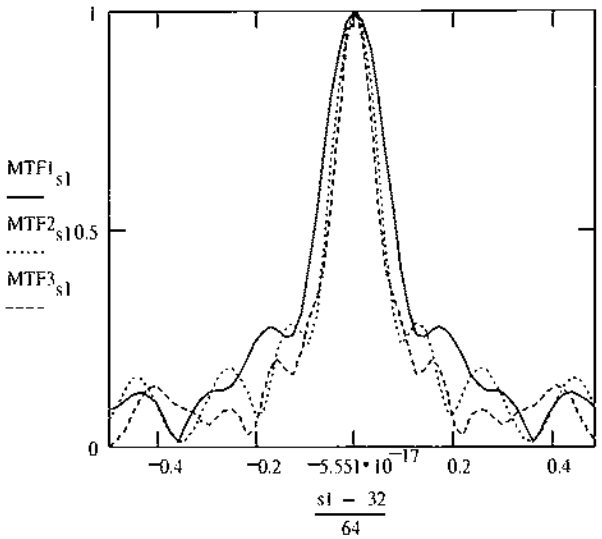

Average MTF

$$AvgMTF_{s1} := \frac{MTF1_{s1} + MTF2_{s1} + MTF3_{s1}}{3}$$

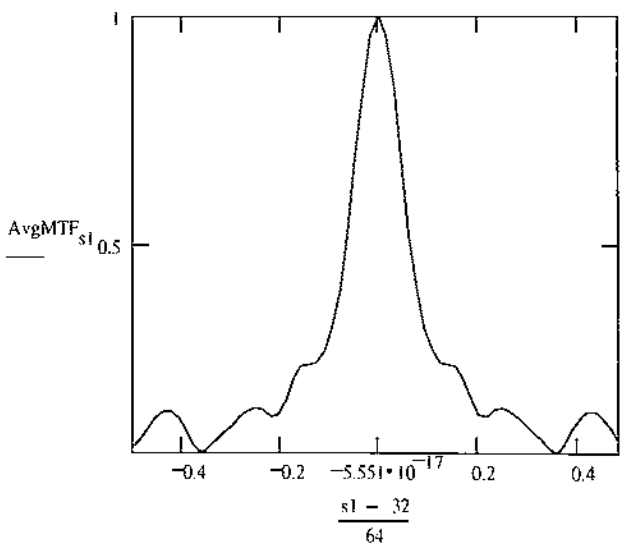

Vertical MTF Calculation for Actual Image from the Inframetrics Linescanner

Read in Data

M1 := READPRN(real1_v) M2 := READPRN(real2_v) M3 := READPRN(real3_v)

Index n := 0.. rows(M1) - 2 nn := 0.. rows(M1)

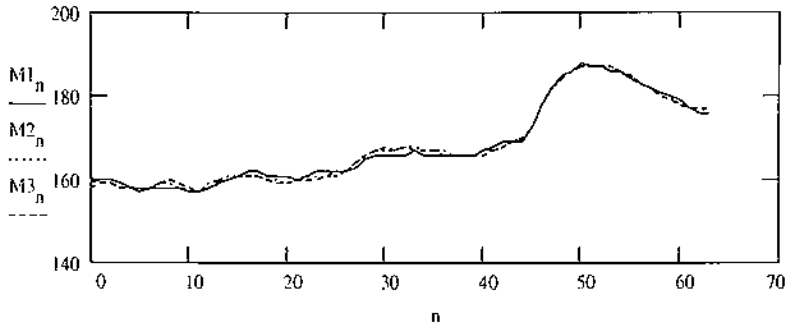

n1 := 50.. rows(M1) n2 := 50.. rows(M2) n3 := 50.. rows(M3)

n1a := 0.. 42 n2a := 0.. 42 n3a := 0.. 42

$M1_{n1} := 200$ $M1_{n1a} := 168$ $M2_{n2} := 200$ $M2_{n2a} := 168$ $M3_{n3} := 200$ $M3_{n3a} := 168$

$$L_{nn} := \frac{M1_{nn} + M2_{nn} + M3_{nn}}{3}$$

Line Spread Function Clipped at Ends

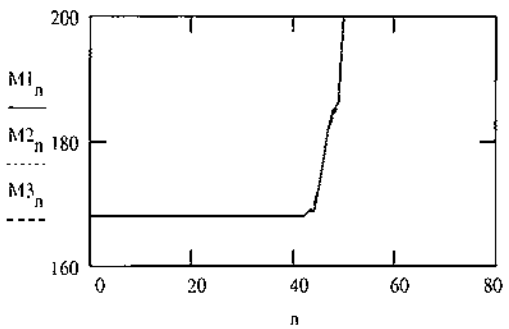

Average value of Line Spread

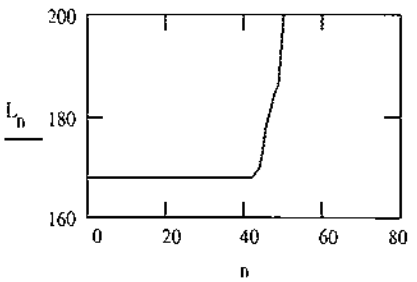

Calculate derivative of input data to calculate the line spread function (LSF)

$D1_n := M1_n - M1_{n+1}$ $D2_n := M2_n - M2_{n+1}$ $D3_n := M3_n - M3_{n+1}$

rows(D1) = 64 rows(D2) = 64 rows(D3) = 64

"Beer-can" the data

$S1_n := (-1)^n \cdot D1_n$ $S2_n := (-1)^n \cdot D2_n$ $S3_n := (-1)^n \cdot D3_n$

Calculate the Fourier Transform of the line spread function to get the Optical Transform Function (OTF)

S1_OTF := cfft(S1) S2_OTF := cfft(S2) S3_OTF := cfft(S3)

s1 := 0.. rows(S1_OTF) - 1 s2 := 0.. rows(S2_OTF) - 1 s3 := 0.. rows(S3_OTF) - 1

$OTF1_{s1} := (-1)^{s1} \cdot S1\_OTF_{s1}$ $OTF2_{s2} := (-1)^{s2} \cdot S2\_OTF_{s2}$ $OTF3_{s3} := (-1)^{s3} \cdot S3\_OTF_{s3}$

Compute Modulus

$$Mod1_{s1} := \sqrt{Re\left(OTF1_{s1}\right)^2 + Im\left(OTF1_{s1}\right)^2}$$

$$Mod2_{s2} := \sqrt{Re\left(OTF2_{s2}\right)^2 + Im\left(OTF2_{s2}\right)^2}$$

$$Mod3_{s3} := \sqrt{Re\left(OTF3_{s3}\right)^2 + Im\left(OTF3_{s3}\right)^2}$$

Normalize Modulus to get MTF

$$MTF1_{s1} := \frac{Mod1_{s1}}{\max(Mod1)}$$

$$MTF2_{s2} := \frac{Mod2_{s2}}{\max(Mod2)}$$

$$MTF3_{s3} := \frac{Mod3_{s3}}{\max(Mod3)}$$

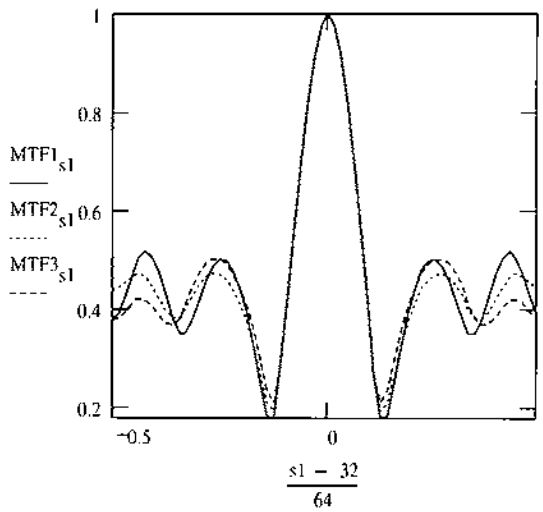

$$AvgMTF_{s1} := \frac{MTF1_{s1} + MTF2_{s1} + MTF3_{s1}}{3}$$

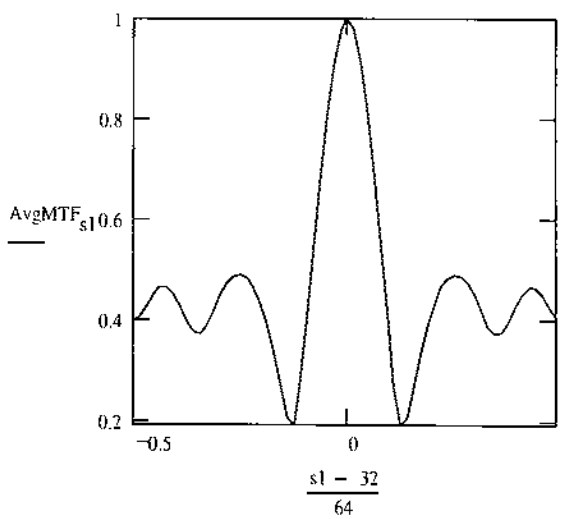

Horizontal MTF Calculation for Synthetic Image from the Inframetrics Linescanner

Read in Data

M1 := READPRN(syn1_h) M2 := READPRN(syn2_h) M3 := READPRN(syn3_h)

Index nn := 0.. rows(M1) n := 0.. rows(M1) - 2

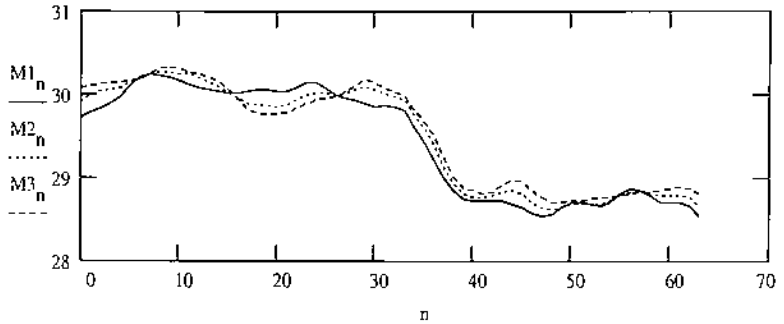

n1 := 40.. rows(M1)
n1a := 0.. 29
$M1_{n1} := 28.738$ $M1_{n1a} := 29.903$

n2 := 39.. rows(M2)
n2a := 0.. 32
$M2_{n2} := 28.778$ $M2_{n2a} := 30.094$

n3 := 39.. rows(M3)
n3a := 0.. 33
$M3_{n3} := 28.844$ $M3_{n3a} := 30.178$

$$L_{nn} := \frac{M1_{nn} + M2_{nn} + M3_{nn}}{3}$$

Line Spread Function Clipped at Ends

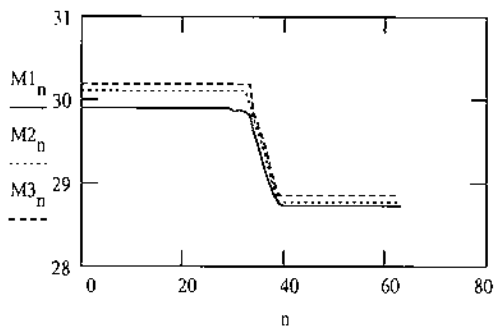

Average value of Line Spread

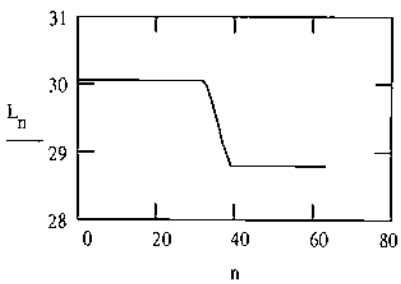

Calculate derivative of input data to calculate the line spread function (LSF)

$D1_n := M1_n - M1_{n+1}$ rows(D1) = 64

$D2_n := M2_n - M2_{n+1}$ rows(D2) = 64

$D3_n := M3_n - M3_{n+1}$ rows(D1) = 64

"Beer-can" the data

$S1_n := (-1)^n \cdot D1_n$ $S2_n := (-1)^n \cdot D2_n$ $S3_n := (-1)^n \cdot D3_n$

Calculate the Fourier Transform of the line spread function to get the Optical Transform Function (OTF)

S1_OTF := cfft(S1)
s1 := 0.. rows(S1_OTF) - 1
$OTF1_{s1} := (-1)^{s1} \cdot S1\_OTF_{s1}$

S2_OTF := cfft(S2)
s2 := 0.. rows(S2_OTF) - 1
$OTF2_{s2} := (-1)^{s2} \cdot S2\_OTF_{s2}$

S3_OTF := cfft(S3)
s3 := 0.. rows(S3_OTF) - 1
$OTF3_{s3} := (-1)^{s3} \cdot S3\_OTF_{s3}$

Compute Modulus

$$Mod1_{s1} := \sqrt{Re\left(OTF1_{s1}\right)^2 + Im\left(OTF1_{s1}\right)^2}$$

$$Mod2_{s2} := \sqrt{Re\left(OTF2_{s2}\right)^2 + Im\left(OTF2_{s2}\right)^2}$$

$$Mod3_{s3} := \sqrt{Re\left(OTF3_{s3}\right)^2 + Im\left(OTF3_{s3}\right)^2}$$

Normalize Modulus to get MTF

$$MTF1_{s1} := \frac{Mod1_{s1}}{max(Mod1)}$$

$$MTF2_{s2} := \frac{Mod2_{s2}}{max(Mod2)}$$

$$MTF3_{s3} := \frac{Mod3_{s3}}{max(Mod3)}$$

All The MTFs

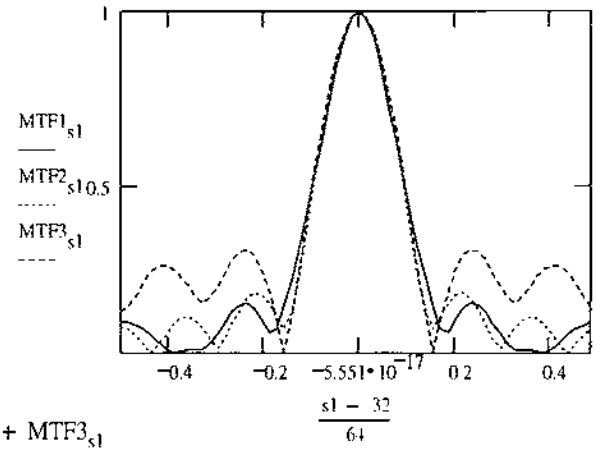

$$AvgMTF_{s1} := \frac{MTF1_{s1} + MTF2_{s1} + MTF3_{s1}}{3}$$

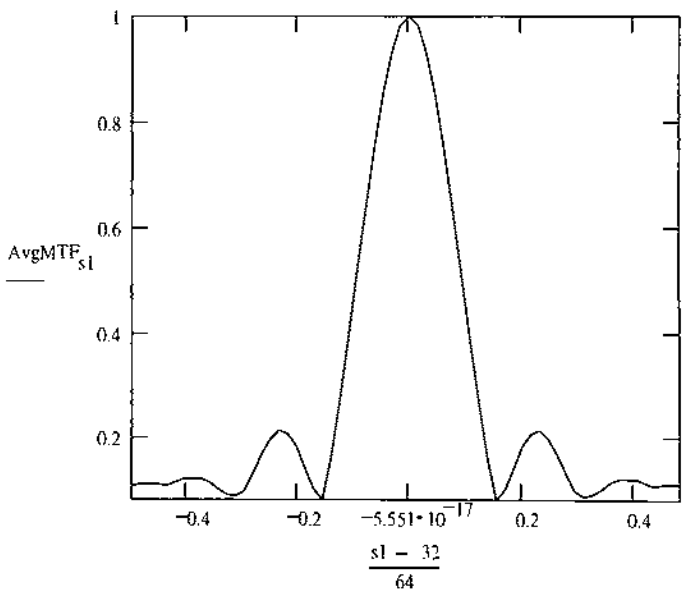

Vertical MTF Calculation for Synthetic Image from the Inframetrics Linescanner

Read in Data

M1 := READPRN(syn1_v) M2 := READPRN(syn2_v) M3 := READPRN(syn3_v)

Index $n := 0..\text{rows}(M1) - 2$ $nn := 0..\text{rows}(M1)$

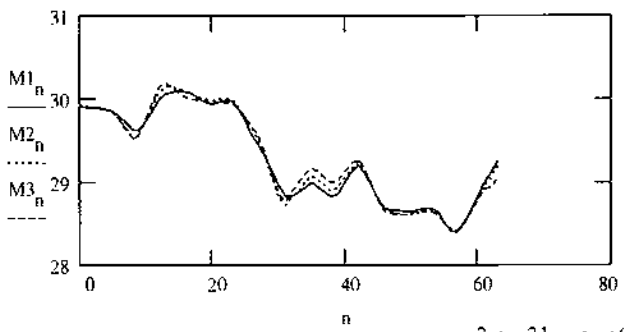

$n1 := 31..\text{rows}(M1)$ $n2 := 31..\text{rows}(M2)$ $n3 := 31..\text{rows}(M3)$

$n1a := 0..21$ $n2a := 0..21$ $n3a := 0..21$

$M1_{n1} := 28.838$ $M1_{n1a} := 29.958$ $M2_{n2} := 28.727$ $M2_{n2a} := 29.99$ $M3_{n3} := 28.779$ $M3_{n3a} := 29.966$

$$L_{nn} := \frac{M1_{nn} + M2_{nn} + M3_{nn}}{3}$$

Line Spread Function Clipped at Ends

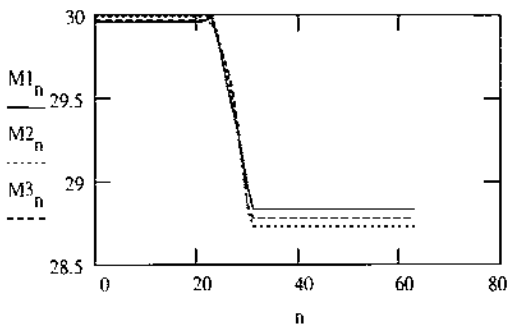

Average value of Line Spread

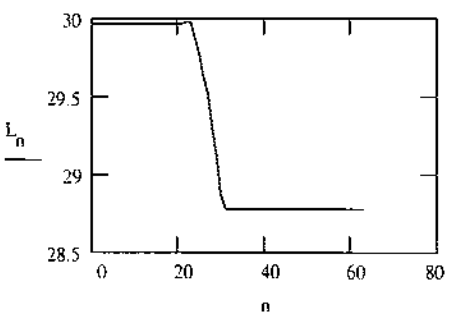

Calculate derivative of input data to calculate the line spread function (LSF)

$D1_n := M1_n - M1_{n+1}$ $D2_n := M2_n - M2_{n+1}$ $D3_n := M3_n - M3_{n+1}$

rows(D1) = 64 rows(D2) = 64 rows(D3) = 64

"Beer-can" the data

$S1_n := (-1)^n \cdot D1_n$ $S2_n := (-1)^n \cdot D2_n$ $S3_n := (-1)^n \cdot D3_n$

Calculate the Fourier Transform of the line spread function to get the Optical Transform Function (OTF)

S1_OTF := cfft(S1) S2_OTF := cfft(S2) S3_OTF := cfft(S3)

$s1 := 0..\text{rows}(S1\_OTF) - 1$ $s2 := 0..\text{rows}(S2\_OTF) - 1$ $s3 := 0..\text{rows}(S3\_OTF) - 1$

$OTF1_{s1} := (-1)^{s1} \cdot S1\_OTF_{s1}$ $OTF2_{s2} := (-1)^{s2} \cdot S2\_OTF_{s2}$ $OTF3_{s3} := (-1)^{s3} \cdot S3\_OTF_{s3}$

Compute Modulus

$$Mod1_{s1} := \sqrt{Re(OTF1_{s1})^2 + Im(OTF1_{s1})^2}$$

$$Mod2_{s2} := \sqrt{Re(OTF2_{s2})^2 + Im(OTF2_{s2})^2}$$

$$Mod3_{s3} := \sqrt{Re(OTF3_{s3})^2 + Im(OTF3_{s3})^2}$$

Normalize Modulus to get MTF

$$MTF1_{s1} := \frac{Mod1_{s1}}{max(Mod1)}$$

$$MTF2_{s2} := \frac{Mod2_{s2}}{max(Mod2)}$$

$$MTF3_{s3} := \frac{Mod3_{s3}}{max(Mod3)}$$

All The MTFs

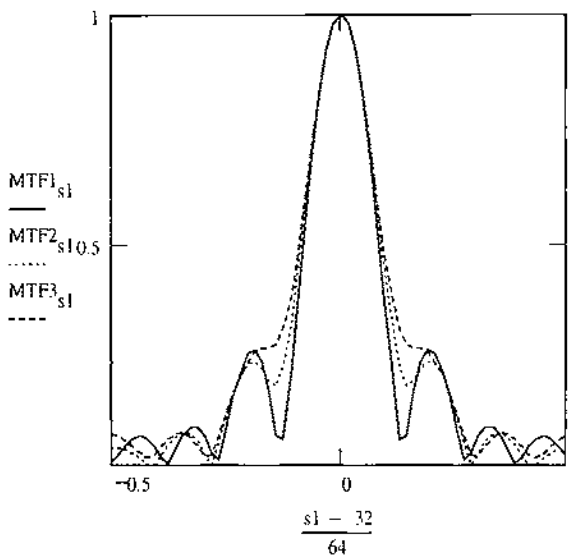

$$AvgMTF_{s1} := \frac{MTF1_{s1} + MTF2_{s1} + MTF3_{s1}}{3}$$

Average MTF

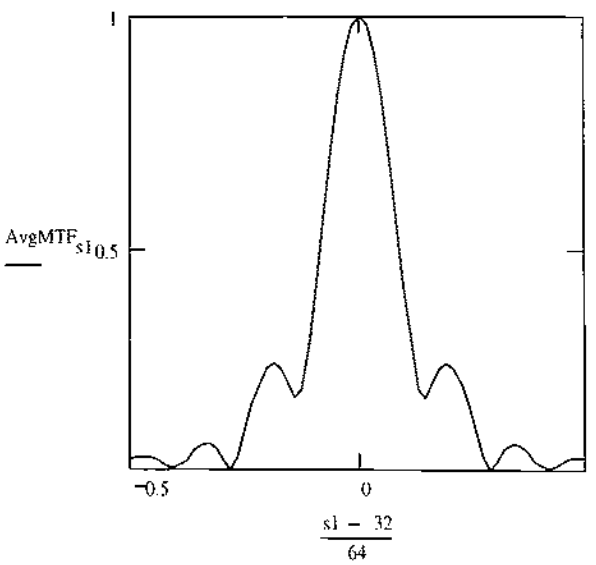

Read in Data

M1 := READPRN(kdreal1_h) M2 := READPRN(kdreal2_h) M3 := READPRN(kdreal3_h)

Index

n := 0.. rows(M1) - 2

nn := 0.. rows(M1)

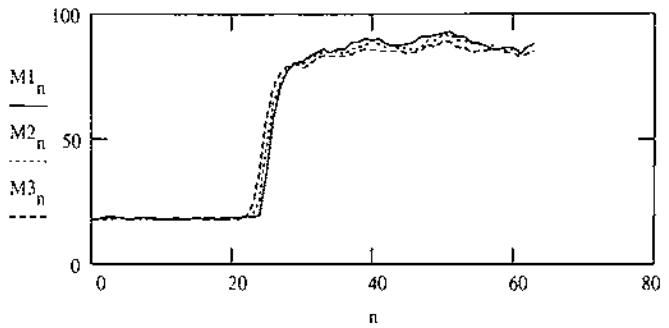

n1 := 30.. rows(M1)

n1a := 0.. 23

$M1_{n1} := 81.333$ $M1_{n1a} := 18.667$

n2 := 30.. rows(M2)

n2a := 0.. 22

$M2_{n2} := 80$

$M2_{n2a} := 19$

n3 := 31.. rows(M3)

n3a := 0.. 23

$M3_{n3} := 78.667$ $M3_{n3a} := 18.667$

$$L_{nn} := \frac{M1_{nn} + M2_{nn} + M3_{nn}}{3}$$

Line Spread Function Clipped at Ends

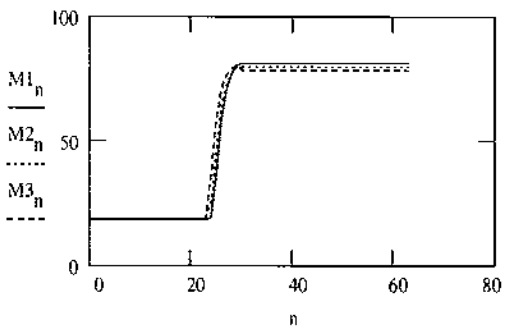

Average value of Line Spread

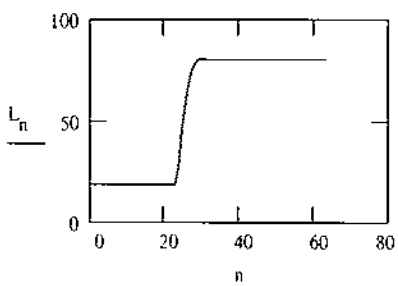

Calculate derivative of input data to calculate the line spread function (LSF)

$D1_n := M1_n - M1_{n+1}$ $D2_n := M2_n - M2_{n+1}$ $D3_n := M3_n - M3_{n+1}$

rows(D1) = 64 rows(D2) = 64 rows(D3) = 64

"Beer-can" the data

$S1_n := (-1)^n \cdot D1_n$ $S2_n := (-1)^n \cdot D2_n$ $S3_n := (-1)^n \cdot D3_n$

Calculate the Fourier Transform of the line spread function to get the Optical Transform Function (OTF)

S1_OTF := cfft(S1)

s1 := 0.. rows(S1_OTF) - 1

$OTF1_{s1} := (-1)^{s1} \cdot S1\_OTF_{s1}$

S2_OTF := cfft(S2)

s2 := 0.. rows(S2_OTF) - 1

$OTF2_{s2} := (-1)^{s2} \cdot S2\_OTF_{s2}$

S3_OTF := cfft(S3)

s3 := 0.. rows(S3_OTF) - 1

$OTF3_{s3} := (-1)^{s3} \cdot S3\_OTF_{s3}$

Compute Modulus

$$Mod1_{s1} := \sqrt{Re(OTF1_{s1})^2 + Im(OTF1_{s1})^2}$$

$$Mod2_{s2} := \sqrt{Re(OTF2_{s2})^2 + Im(OTF2_{s2})^2}$$

$$Mod3_{s3} := \sqrt{Re(OTF3_{s3})^2 + Im(OTF3_{s3})^2}$$

Normalize Modulus to get MTF

$$MTF1_{s1} := \frac{Mod1_{s1}}{max(Mod1)}$$

$$MTF2_{s2} := \frac{Mod2_{s2}}{max(Mod2)}$$

$$MTF3_{s3} := \frac{Mod3_{s3}}{max(Mod3)}$$

All the MTFs

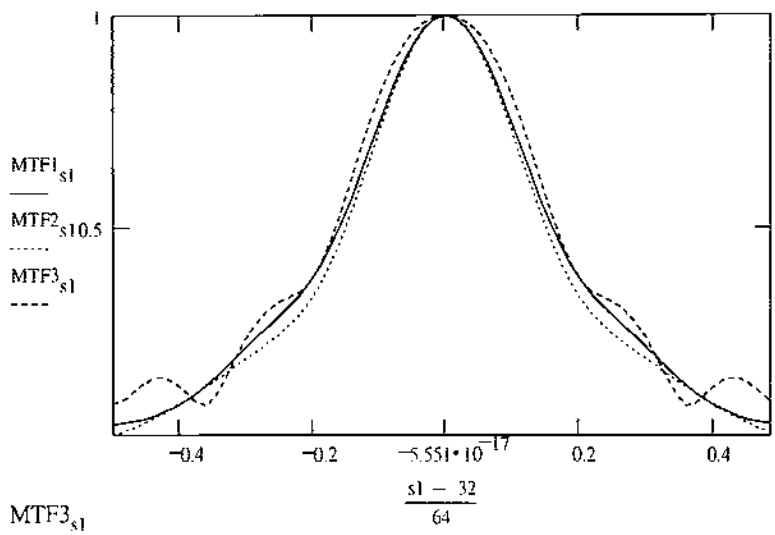

Average MTFs

$$AvgMTF_{s1} := \frac{MTF1_{s1} + MTF2_{s1} + MTF3_{s1}}{3}$$

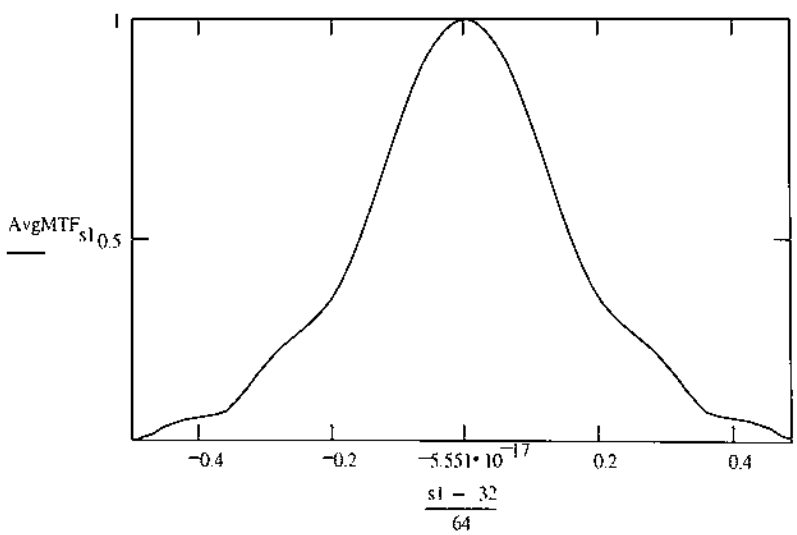

Vertical MTF Calculation for Actual Image from the Kodak_310 Camera

Read in Data

M1 := READPRN(kdreal1_v) M2 := READPRN(kdreal2_v) M3 := READPRN(kdreal3_v)

Index

n := 0.. rows(M1) - 2 nn := 0.. rows(M1)

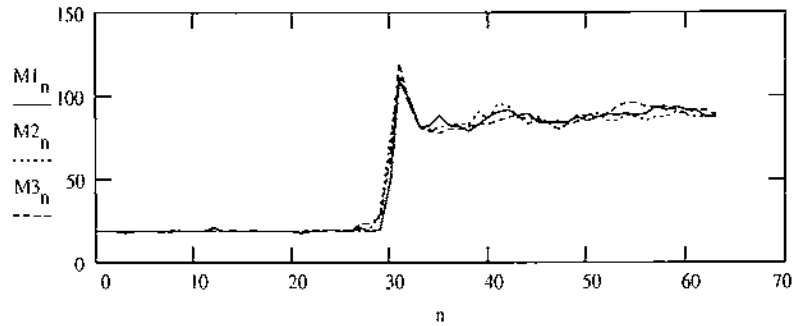

n1 := 31.. rows(M1)
n1a := 0.. 28
$M1_{n1} := 109.667$ $M1_{n1a} := 18.667$

n2 := 31.. rows(M2)
n2a := 0.. 28
$M2_{n2} := 112.667$ $M2_{n2a} := 20$

n3 := 31.. rows(M3)
n3a := 0.. 28
$M3_{n3} := 119.667$
$M3_{n3a} := 24$

$$L_{nn} := \frac{M1_{nn} + M2_{nn} + M3_{nn}}{3}$$

Line Spread Function Clipped at Ends

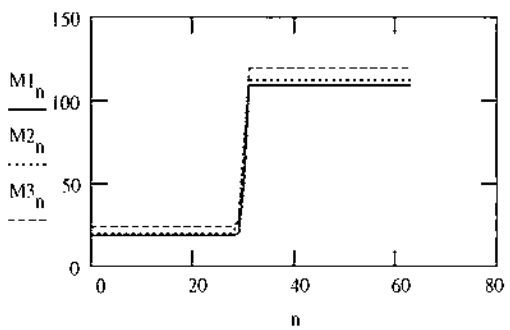

Average value of Line Spread

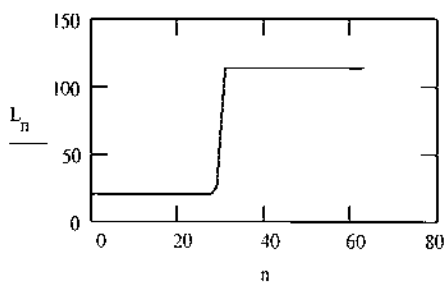

Calculate derivative of input data to calculate the line spread function (LSF)

$D1_n := M1_n - M1_{n+1}$ $D2_n := M2_n - M2_{n+1}$ $D3_n := M3_n - M3_{n+1}$

rows(D1) = 64 rows(D2) = 64 rows(D3) = 64

"Beer-can" the data

$S1_n := (-1)^n \cdot D1_n$ $S2_n := (-1)^n \cdot D2_n$ $S3_n := (-1)^n \cdot D3_n$

Calculate the Fourier Transform of the line spread function to get the Optical Transform Function (OTF)

S1_OTF := cfft(S1)
s1 := 0.. rows(S1_OTF) - 1

S2_OTF := cfft(S2)
s2 := 0.. rows(S2_OTF) - 1

S3_OTF := cfft(S3)
s3 := 0.. rows(S3_OTF) - 1

$OTF1_{s1} := (-1)^{s1} \cdot S1\_OTF_{s1}$ $OTF2_{s2} := (-1)^{s2} \cdot S2\_OTF_{s2}$ $OTF3_{s3} := (-1)^{s3} \cdot S3\_OTF_{s3}$

Compute Modulus

$$Mod1_{s1} := \sqrt{Re(OTF1_{s1})^2 + Im(OTF1_{s1})^2}$$

$$Mod2_{s2} := \sqrt{Re(OTF2_{s2})^2 + Im(OTF2_{s2})^2}$$

$$Mod3_{s3} := \sqrt{Re(OTF3_{s3})^2 + Im(OTF3_{s3})^2}$$

Normalize Modulus to get MTF

$$MTF1_{s1} := \frac{Mod1_{s1}}{max(Mod1)}$$

$$MTF2_{s2} := \frac{Mod2_{s2}}{max(Mod2)}$$

$$MTF3_{s3} := \frac{Mod3_{s3}}{max(Mod3)}$$

All the MTFs

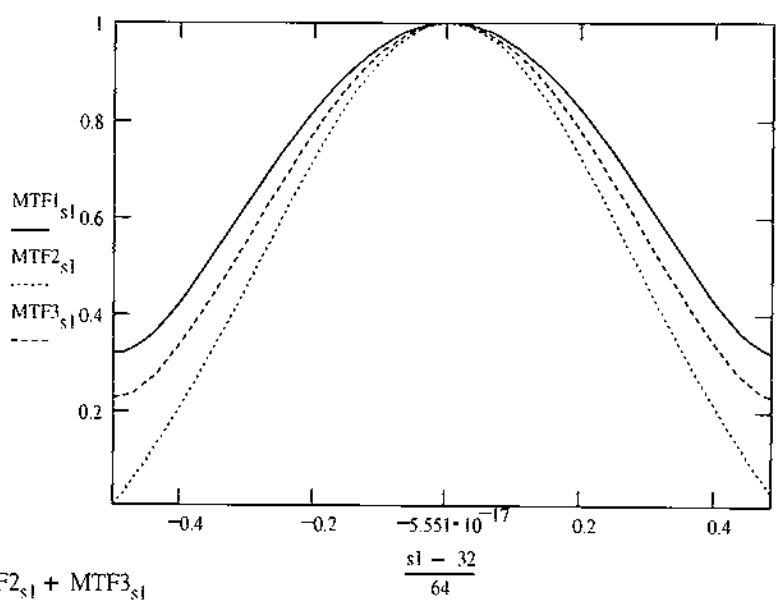

Average MTfs

$$AvgMTF_{s1} := \frac{MTF1_{s1} + MTF2_{s1} + MTF3_{s1}}{3}$$

WRITEPRN(realavgv2) := $AvgMTF_{\square}$

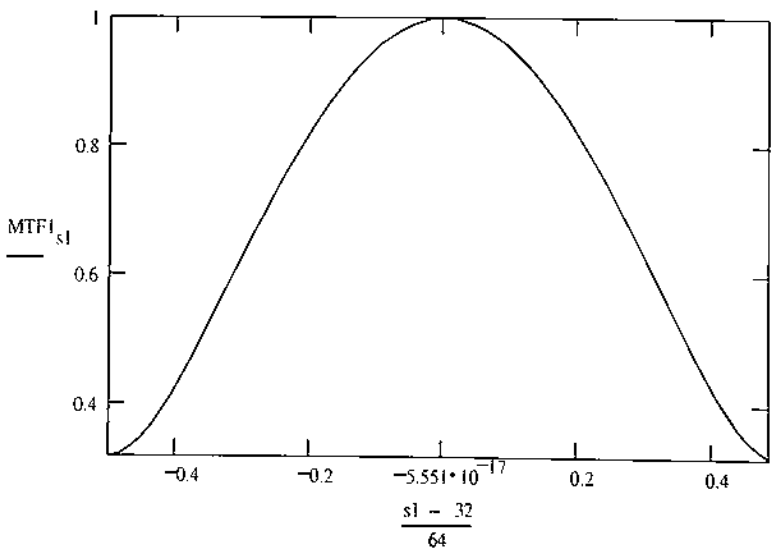

Horizontal MTF Calculation for Synthetic Image from the Kodak_310 Camera

Read in Data

M1 := READPRN(kdsyn1_h) M2 := READPRN(kdsyn2_h) M3 := READPRN(kdsyn3_h)

Index n := 0.. rows(M1) − 2

nn := 0.. rows(M1)

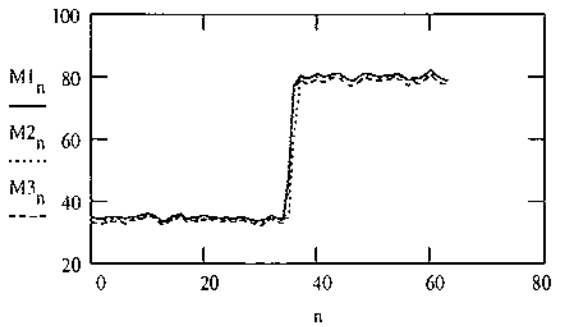

n1 := 42.. rows(M1) n2 := 42.. rows(M2) n3 := 42.. rows(M3)

n1a := 0.. 33 n2a := 0.. 34 n3a := 0.. 34

$M1_{n1} := 80.8$ $M1_{n1a} := 34.6$ $M2_{n2} := 79.677$ $M2_{n2a} := 33.969$ $M3_{n3} := 79.154$ $M3_{n3a} := 32.646$

$$L_{nn} := \frac{M1_{nn} + M2_{nn} + M3_{nn}}{3}$$

Line Spread Function Clipped at Ends

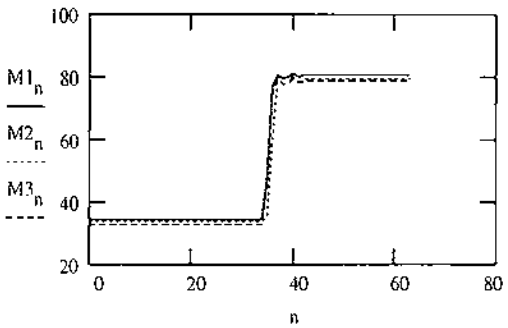

Average value of Line Spread

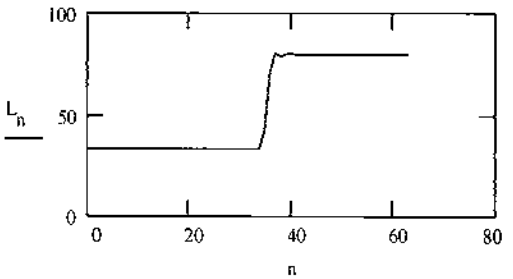

Calculate derivative of input data to calculate the line spread function (LSF)

$D1_n := M1_n - M1_{n+1}$ $D2_n := M2_n - M2_{n+1}$ $D3_n := M3_n - M3_{n+1}$

rows(D1) = 64 rows(D2) = 64 rows(D1) = 64

"Beer-can" the data

$S1_n := (-1)^n \cdot D1_n$ $S2_n := (-1)^n \cdot D2_n$ $S3_n := (-1)^n \cdot D3_n$

Calculate the Fourier Transform of the line spread function to get the Optical Transform Function (OTF)

S1_OTF := cfft(S1) S2_OTF := cfft(S2) S3_OTF := cfft(S3)

s1 := 0.. rows(S1_OTF) − 1 s2 := 0.. rows(S2_OTF) − 1 s3 := 0.. rows(S3_OTF) − 1

$OTF1_{s1} := (-1)^{s1} \cdot S1\_OTF_{s1}$ $OTF2_{s1} := (-1)^{s1} \cdot S2\_OTF_{s1}$ $OTF3_{s1} := (-1)^{s1} \cdot S3\_OTF_{s1}$

Compute Modulus

$$Mod1_{s1} := \sqrt{Re\left(OTF1_{s1}\right)^2 + Im\left(OTF1_{s1}\right)^2}$$

$$Mod2_{s2} := \sqrt{Re\left(OTF2_{s2}\right)^2 + Im\left(OTF2_{s2}\right)^2}$$

$$Mod3_{s3} := \sqrt{Re\left(OTF3_{s3}\right)^2 + Im\left(OTF3_{s3}\right)^2}$$

Normalize Modulus to get MTF

$$MTF1_{s1} := \frac{Mod1_{s1}}{max(Mod1)}$$

$$MTF2_{s2} := \frac{Mod2_{s2}}{max(Mod2)}$$

$$MTF3_{s3} := \frac{Mod3_{s3}}{max(Mod3)}$$

All MTFs

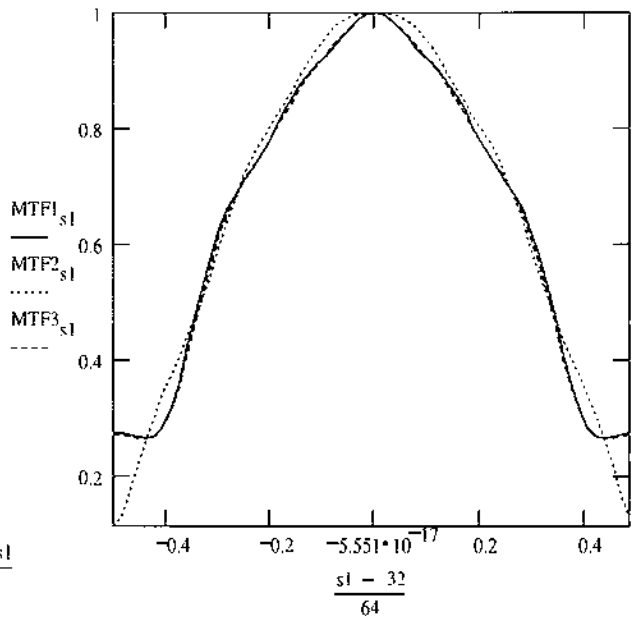

Average MTF

$$AvgMTF_{s1} := \frac{MTF1_{s1} + MTF2_{s1} + MTF3_{s1}}{3}$$

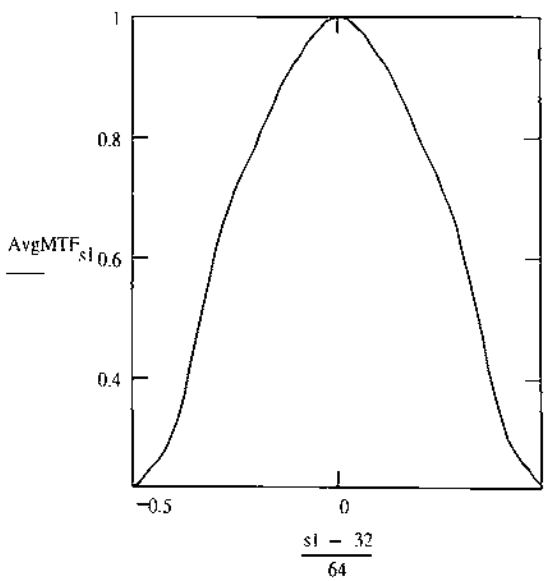

Vertical MTF Calculation for Synthetic Image from the Kodak_310 Camera

Read in Data

M1 := READPRN(kdsyn1_v) M2 := READPRN(kdsyn2_v) M3 := READPRN(kdsyn3_v)

Index

n := 0.. rows(M1) - 2

nn := 0.. rows(M1)

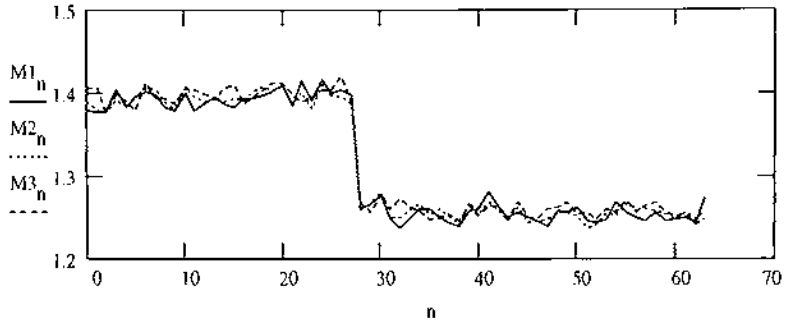

n1 := 29.. rows(M1) n2 := 29.. rows(M2) n3 := 29.. rows(M3)

n1a := 0.. 26 n2a := 0.. 26 n3a := 0.. 26

$M1_{n1} := 1.256$ $M1_{n1a} := 1.424$ $M2_{n2} := 1.252$ $M2_{n2a} := 1.414$ $M3_{n3} := 1.257$ $M3_{n3a} := 1.421$

$$L_{nn} := \frac{M1_{nn} + M2_{nn} + M3_{nn}}{3}$$

Line Spread Function Clipped at Ends

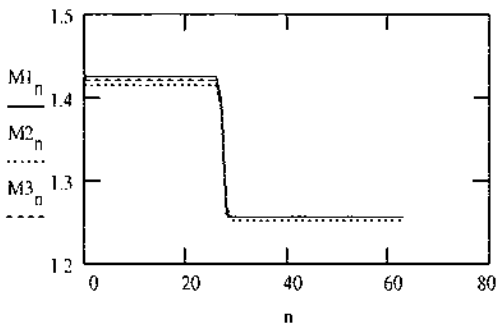

Average value of Line Spread

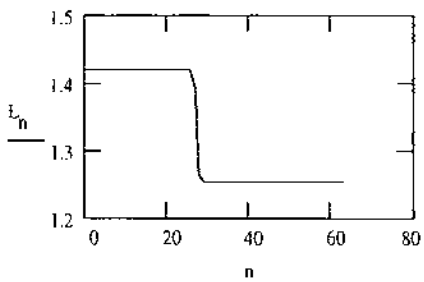

Calculate derivative of input data to calculate the line spread function (LSF)

$D1_n := M1_n - M1_{n+1}$ $D2_n := M2_n - M2_{n+1}$ $D3_n := M3_n - M3_{n+1}$

rows(D1) = 64 rows(D2) = 64 rows(D1) = 64

"Beer-can" the data

$S1_n := (-1)^n \cdot D1_n$ $S2_n := (-1)^n \cdot D2_n$ $S3_n := (-1)^n \cdot D3_n$

Calculate the Fourier Transform of the line spread function to get the Optical Transform Function (OTF)

S1_OTF := cfft(S1) S2_OTF := cfft(S2) S3_OTF := cfft(S3)

s1 := 0.. rows(S1_OTF) - 1 s2 := 0.. rows(S2_OTF) - 1 s3 := 0.. rows(S3_OTF) - 1

$OTF1_{s1} := (-1)^{s1} \cdot S1\_OTF_{s1}$ $OTF2_{s2} := (-1)^{s2} \cdot S2\_OTF_{s2}$ $OTF3_{s3} := (-1)^{s3} \cdot S3\_OTF_{s3}$

Compute Modulus

$$Mod1_{s1} := \sqrt{Re(OTF1_{s1})^2 + Im(OTF1_{s1})^2}$$

$$Mod2_{s2} := \sqrt{Re(OTF2_{s2})^2 + Im(OTF2_{s2})^2}$$

$$Mod3_{s3} := \sqrt{Re(OTF3_{s3})^2 + Im(OTF3_{s3})^2}$$

Normalize Modulus to get MTF

$$MTF1_{s1} := \frac{Mod1_{s1}}{max(Mod1)}$$

$$MTF2_{s2} := \frac{Mod2_{s2}}{max(Mod2)}$$

$$MTF3_{s3} := \frac{Mod3_{s3}}{max(Mod3)}$$

All the MTFs

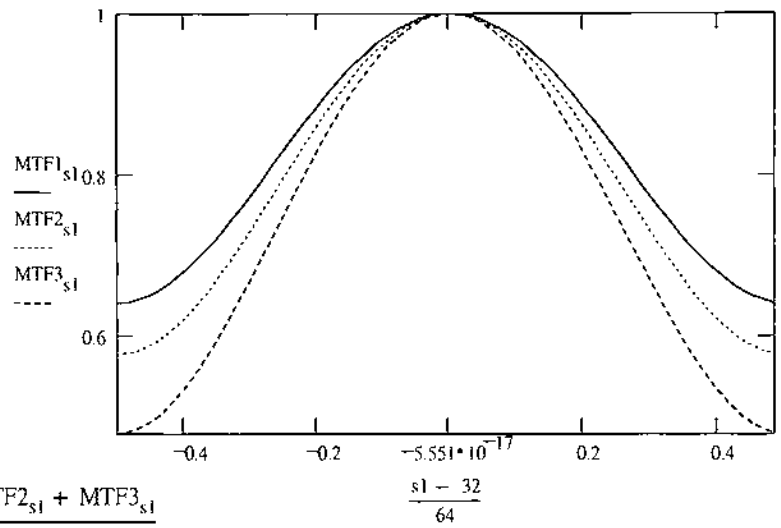

Average MTFs

$$AvgMTF_{s1} := \frac{MTF1_{s1} + MTF2_{s1} + MTF3_{s1}}{3}$$

$$WRITEPRN(synavgv2) := AvgMTF_{s1}$$

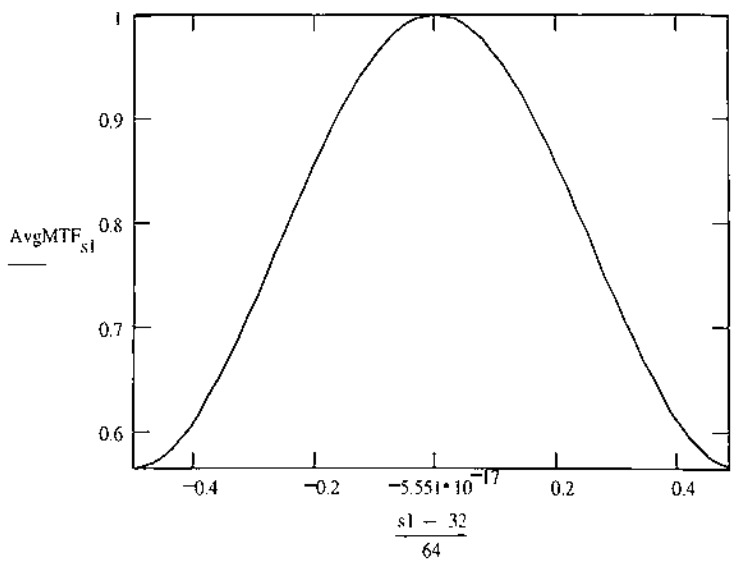

Appendix C

Whitaker-Shannon Sampling Theorem

The Whitaker-Shannon sampling theorem states that adequate sampling requires that the sampling rate must be smaller than the inverse of twice the largest frequency. This frequency is referred to as the Nyquist frequency, ξ_{Nyq}

$$\Delta x < \frac{1}{2\xi_{Nyq}} \tag{C.71}$$

If the sampling rate is high (i.e. Δx is small), then it is called oversampling. Undersampling is the terminology that describes a system that has not been sampled properly. When this occurs, signal aliasing (higher frequencies masquerading as lower frequencies) becomes evident in the reconstructed signal. Often many are confused and quote the number of samples taken, when they should be quoting the sampling interval in reference to the Nyquist criteria.

Appendix D

D^* and QE Curves for Calculating Noise Equivalent Radiance

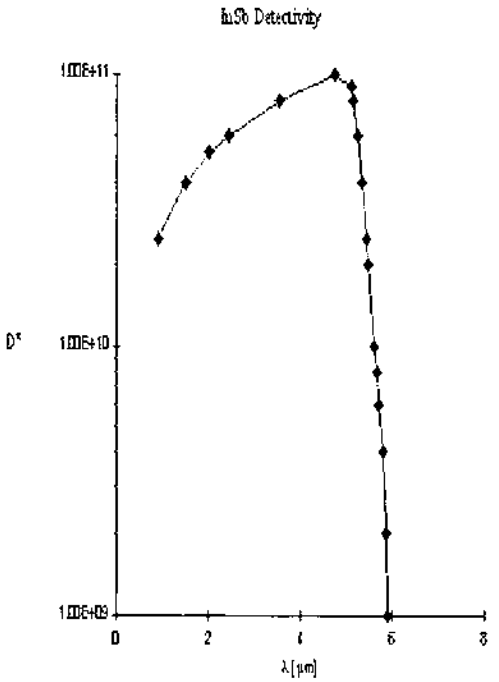

Figure D.1: D^* Curve for InSb

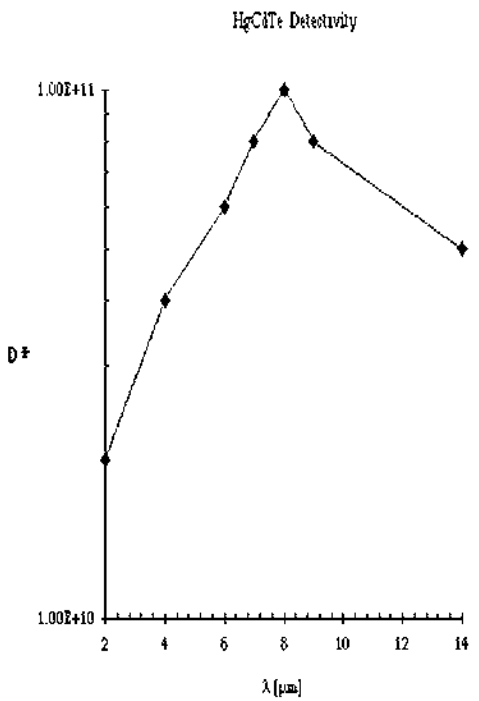

Figure D.2: D^* Curve for HgCdTe

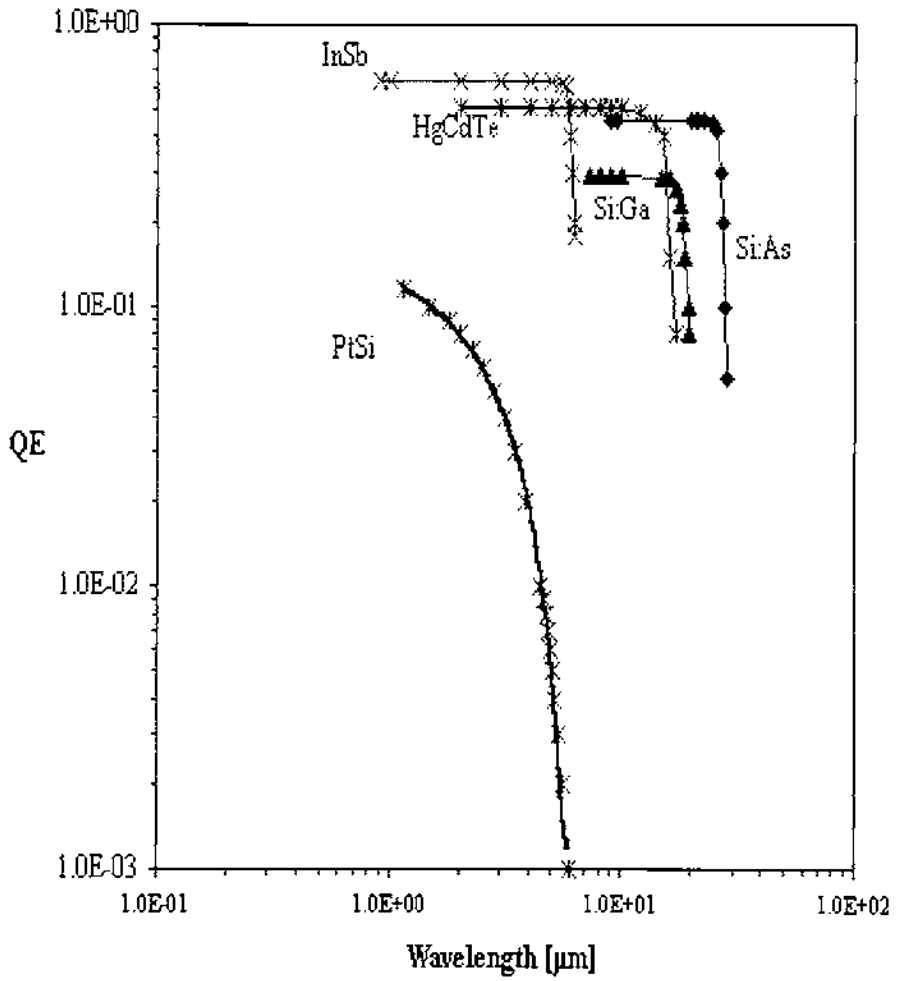

Figure D.3: Quantum Efficiency Curves

Appendix E

Obscuration in Exit Pupil

This is the analytical form of the diffraction limited optical MTF that accounts for an obscuration. This can be used to compare results using the autocorrelation method.

$$
\begin{aligned}
MTF_{opt} &= \left[\frac{A+B+C}{1-R}\right] \\
A &= \frac{2}{\pi}\left\{a\cos\left[\frac{\nu}{\nu_{co}}\right] - \frac{\nu}{\nu_{co}}\sin\left[a\cos\left[\frac{\nu}{\nu_{co}}\right]\right]\right\} && \text{if } 0 < \frac{\nu}{\nu_{co}} < 1 \\
B &= \frac{2R^2}{\pi}\cdot\left\{a\cos\left[\frac{\nu}{\nu_{co}}\right] - \frac{\nu}{\nu_{co}}\sin\left[a\cos\left[\frac{\nu}{\nu_{co}}\right]\right]\right\} && \text{if } 0 < \frac{\nu}{\nu_{co}}\frac{1}{R} < 1 \\
C &= -2R^2 && \text{if } 0 < \frac{\nu}{\nu_{co}} < \frac{1-R}{2} \\
C &= \frac{2R}{\pi}\sin a + \frac{1+R^2}{\pi}a - \frac{2(1-R^2)}{\pi}\tan^{-1}\left[\left[\frac{1+R}{1-R}\right]\tan\left(\frac{a}{2}\right)\right] - 2R^2 && \text{if } \frac{1-R}{2} < \frac{\nu}{\nu_{co}} < \frac{1+R}{2} \\
a &= \cos^{-1}\left[\frac{1+R-4X^2}{2R}\right] && \text{where } X = \frac{\nu}{\nu_{co}} \\
R &= \frac{\text{Obscuration Diameter}}{\text{Aperture Diamter}}
\end{aligned}
$$

where,

ν is the radial frequency

ν_{co} is the radial cutoff frequency.

Appendix F

Image Acquistion Setup & Target

The image acquistion setup is shown in figure F.1 below. The two infrared sensors were placed at the same vantage points on top of the RIT's Center for Imaging Science's Carlson Building. Figure F.2 depicts the the NTID dormitory which was used as the target for the thesis.

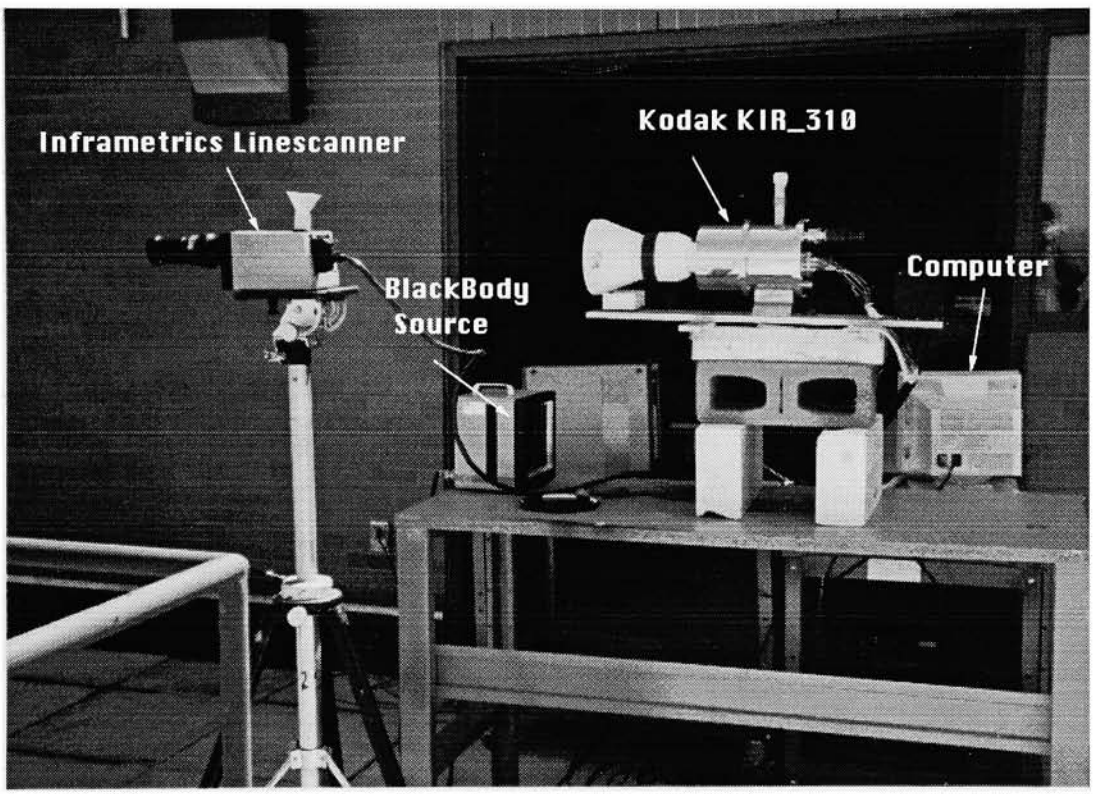

Figure F.1: Inframetrics and Kodak KIR_310 Image Acquistion Setup

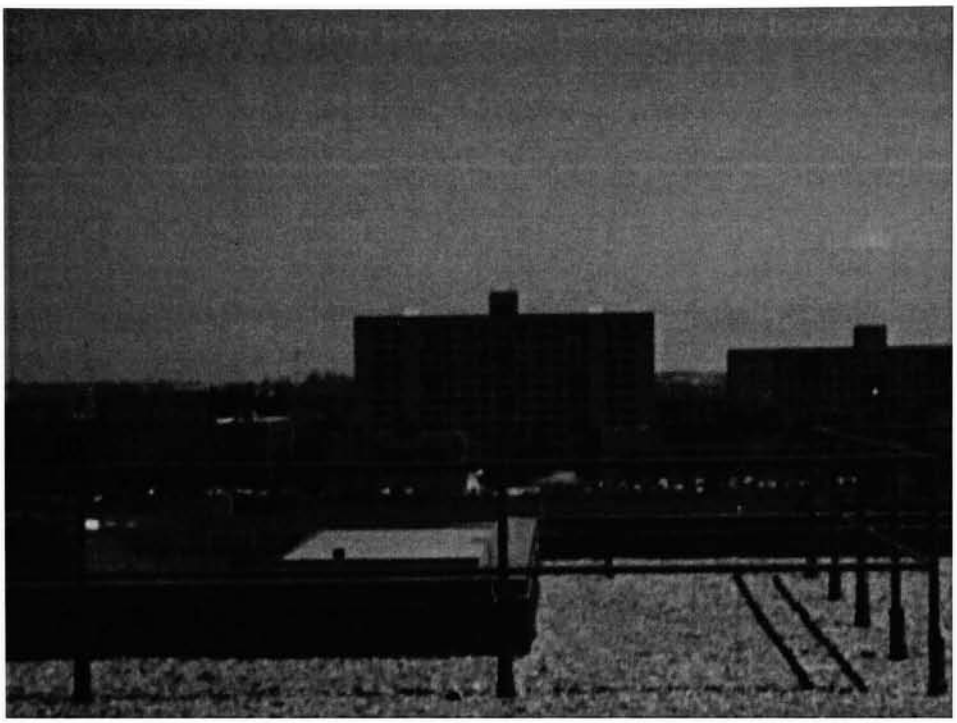

Figure F.2: RIT NTID Dormitory in the Visible Spectrum

References

[1] Ballik, E.A. and Wan, W., "Development and Analysis of a simple Model for an IR Sensor", *Proceedings of the SPIE, Infrared Imaging Systems: Design, Analysis, Modeling and Testing II*, Vol. 1488, Orlando, FL, 1991.

[2] Blouke, M. M., Burgett, C. B., and Williams, R. L., "Sensitivity Limits for Extrinsic and Intrinsic Infrared Detectors", *Infrared Physics*, Vol. 13, 1973.

[3] Bradley, D. J. Et. al., "Computer Simulation of Staring Array Thermal Imagers", *Proceedings of the SPIE, Infrared Imaging Systems: Design, Analysis, Modeling and Testing II*, Vol. 1488, Orlando, FL, 1991.

[4] Cohen, G. et. al., "Improved Electro-Optical Target Detection in a Natural Fractal Environment", *Proceedings of the SPIE,8th Meeting on Optical Engineering in Israel*, Vol. 1971, Israel, 1992.

[5] D'Agostino, John and Webb, Curtis, "3-D Analysis Framework and Measurement Methodology for Imaging System Noise", *Proceedings of the SPIE, Infrared Imaging Systems: Design, Analysis, Modeling and Testing II*, Vol. 1488, Orlando, FL, 1991.

[6] Dereniak, Euace L., and Brown, F. Gerald, "NETD Calculations Using the Radiation Slide Rule", *Infrared Physics*, Vol. 15, 1975.

[7] Driggers, Ronald G. et. al., "Comparison of Two Frame Noise Calculations for Infrared Linescanners", *Optical Engineering*, Vol. 29, July 1990.

[8] Dudzik, Michael C., "Fundamentals of Electro-Optical Imaging Systems Analysis", *The Infrared & Electro-Optical Systems Handbook.*, Vol. 4, 1993.

[9] Emmons, R. B., Hawkins, S. R., and Cuff, K. F., "Infrared Detectors: An Overview", *Optical Engineering*, Vol. 14, 1975.

[10] Emmons, R. B., "Thermal Imaging System Performance Estimates", *Infrared Physics*, Vol. 17, 1977.

[11] Fraedrich, Douglas, S., "Performance Improvement of an IR Imaging System Using Sub-System MTF Analysis", *Proceedings of the SPIE, Infrared Imaging Systems: Design, Analysis, Modeling and Testing*, Vol. 1309, Orlando, FL, 1990.

[12] Frieden, B. R., Probability, Statistical Optics, and Data Testing 2nd ed, New York, Springer-Verlag, 1991.

[13] Friedman, Melvin and et. al., "Standard Night Vision Thermal Modeling Parameters", *Proceedings of the SPIE, Infrared Imaging Systems: Design, Analysis, Modeling and Testing III*, Vol. 1689, Orlando, FL, 1992.

[14] Gaskill, Linear Systems, Fourier Transforms and Optics, New York, John Wiley & Sons, 1979.

[15] Gonzalez, Rafael C. and Woods, Richard E., Digital Image Processing, New York, Addison-Wesley Publishing Company, 1992.

[16] Hadar, O., Dror, I., and Kopeika, N.S., "Real-Time Numerical Calculation of Optical Transfer Function for Image Motion and Vibration. Part 1: Experimental Verification", *Proceedings of the SPIE, 8th Meeting on Optical Engineering in Israel*, Vol. 1971, Israel, 1992.

[17] Hoover, Carl Jr. and Webb, Curtis, "What is an MRT? and how do I get one?", *Proceedings of the SPIE, Infrared Imaging Systems: Design, Analysis, Modeling and Testing II*, Vol. 1488, Orlando, FL, 1991.

[18] Horger, John D., "NVSIM: UNIX-based Thermal Imaging System Simulator", *Proceedings of the SPIE, Infrared Imaging Systems: Design, Analysis, Modeling and Testing IV*, Vol. 1969, Orlando, FL, 1993.

[19] Jaggi, S., "ATTIRE: Analytical Tools for Thermal Infrared Engineering - A Thermal Sensor Simulation Package", *Proceedings of the SPIE, Infrared Imaging Systems: Design, Analysis, Modeling and Testing III*, Vol. 1689, Orlando, FL, 1992.

[20] Kaufman, Y.J., "Solution of the Equation of Radiative Transfer for Remote Sensing Over Nonuniform Surface Reflectivity", *Journal of Geophysical Research*, Vol. 87, No. C6, 1982.

[21] Kennedy, Howard V., "Modeling Second Generation Thermal Imaging Systems", *Proceedings of the SPIE, Infrared Imaging Systems: Design, Analysis, Modeling and Testing*, Vol. 1309, Orlando, FL, 1990.

[22] Kennedy, Howard V., "Recognition Criteria for Two-Dimensional Minimum Resolvable Temperature Difference (MRTD)", *Proceedings of the SPIE, Infrared Imaging Systems: Design, Analysis, Modeling and Testing II*, Vol. 1488, Orlando, FL, 1991a.

[23] Kennedy, Howard V., "Miscellaneous Modulation Transfer Function (MTF) Effects Relating to Sample Summing", *Proceedings of the SPIE, Infrared Imaging Systems: Design, Analysis, Modeling and Testing II*, Vol. 1488, Orlando, FL, 1991b.

[24] Kennedy, Howard V., "Modeling Noise in Thermal Imaging Systems", *Proceedings of the SPIE, Infrared Imaging Systems: Design, Analysis, Modeling and Testing IV*, Vol. 1969, Orlando, FL, 1993.

[25] Konopka,W. et. al., "Transient Radiometric Measurements with a PtSi IR Camera", *Proceedings of the SPIE, Infrared Imaging Systems: Design, Analysis, Modeling and Testing II*, Vol. 1488, Orlando, FL, 1991.

[26] LeBlanc, R. and Contini, "Infrared Focal Plane Array Modeling", *Proceedings of the SPIE, Infrared Imaging Systems: Design, Analysis, Modeling and Testing*, Vol. 1309, Orlando, FL, 1990.

[27] Lloyd, Thermal Imaging Systems, New York, Plenum Press, 1975.

[28] O'Neill, Edward L., "Transfer Function for an Annular Aperture", *Journal of the Optical Society of America*, Vol. 46, April 1956.

[29] Owen, Philip, "Solutions to Modeling of IR Systems for Missile Applications: MICOM Imaging IR System Performance Model-90", *Proceedings of the SPIE, Infrared Imaging Systems: Design, Analysis, Modeling and Testing II*, Vol. 1488, Orlando, FL, 1991.

[30] Pearce, W. A., "A Study of the Effects of the Atmosphere on Thematic Mapper Observation", Final Report under NASA Contract NAS5-23639 (1977).

[31] Pinsky, Howard J., "Determination of FLIR LOS Stabilization Errors", *Proceedings of the SPIE, Infrared Imaging Systems: Design, Analysis, Modeling and Testing II*, Vol. 1488, Orlando, FL, 1991.

[32] Ratches, James A., "Static Performance Model for Thermal Imaging Systems", *Optical Engineering*, Vol. 15, November/December, 1976.

[33] Rogatto, William D., "Electro-Optical Components", *The Infrared & Electro-Optical Systems Handbook.*, Vol. 3, 1993.

[34] Sadot, D. and Kopeika, N.S., "Effects of Aerosol Forward Scatter of Infrared and Visible Light on Atmospheric Coherence Diameter: Theory and Validation", *Proceedings of the SPIE, 8th Meeting on Optical Engineering in Israel*, Vol. 1971, Israel, 1992a.

[35] Sadot, D. and Kopeika, N.S., "Aerosol Scattering and Absorption Modulation Transfer Function", *Proceedings of the SPIE, 8th Meeting on Optical Engineering in Israel*, Vol. 1971, Israel, 1992b.

[36] Sadot, D. and Kopeika, N.S., "Thermal Imaging Through the Atmosphere: Atmospheric MTF Theory and Verification", *Proceedings of the SPIE, 8th Meeting on Optical Engineering in Israel*, Vol. 1971, Israel, 1992c.

[37] Salacain, Jim, Rochester Institute of Technology M.S. Thesis for Imaging Science, 1995.

[38] Sato D.L., et. al., "High Performance PTSI MWIR Camera", *Proceedings of the SPIE, Infrared Detectors and Focal Plane Arrays*, Vol. 1308, Orlando, FL, 1990.

[39] Scott, Luke B. and Condiff, Lesley R., "C2NVEO Advanced LWIR Systems Performance Model", *Proceedings of the SPIE, Infrared Imaging Systems: Design, Analysis, Modeling and Testing*, Vol. 1309, Orlando, FL, 1990.

[40] Scott, Luke and D'Agostino, John, "NVEOD FLIR92 Thermal Imaging Systems Performance Model", *Proceedings of the SPIE, Infrared Imaging Systems: Design, Analysis, Modeling and Testing III*, Vol. 1689, Orlando, FL, 1992.

[41] Scott, Luke, "Modeling Staring Thermal Systems with FLIR92", *Proceedings of the SPIE, Infrared Imaging Systems: Design, Analysis, Modeling and Testing IV*, Vol. 1969, Orlando, FL, 1993.

[42] Turon, Pierre J. and Depost, Thibault S., "LEO Thermal Imagers: Pushbroom or Whiskbroom?", *Proceedings of the SPIE, Infrared Imaging Systems: Design, Analysis, Modeling and Testing III*, Vol. 1689, Orlando, FL, 1992.

[43] Vroombout, Leo O., "Second Generation Thermal Imaging System Design Trades Modeling", *Proceedings of the SPIE, Infrared Imaging Systems: Design, Analysis, Modeling and Testing*, Vol. 1309, Orlando, FL, 1990.

[44] Watkins, Wendell R.. and Jordan, Jay B., "Characterization of atmospheric degradation of IR scene content", *Proceedings of the SPIE, 8th Meeting on Optical Engineering in Israel*, Vol. 1971, Israel, 1992.

[45] Wyatt, Clair L., Radiometric System Design, New York, MacMillan, 1987.

Thank you.